



**UNIVERSIDADE FEDERAL DE GOIÁS
PRÓ-REITORIA DE PESQUISA E PÓS-GRADUAÇÃO
PROGRAMA DE PÓS-GRADUACAO EM CIÊNCIAS
AMBIENTAIS – NÍVEL DOUTORADO**

ANTONIO ELISEU HOLDEFER

**EMPREGO DE SENSORIAMENTO REMOTO NAS ESTIMATIVAS DE
CONCENTRAÇÃO DE SEDIMENTOS EM ÁGUA**

**Goiânia
2019**



UNIVERSIDADE FEDERAL DE GOIÁS
GERÊNCIA DE CURSOS E PROGRAMAS INTERDISCIPLINARES

TERMO DE CIÊNCIA E DE AUTORIZAÇÃO (TECA) PARA DISPONIBILIZAR VERSÕES ELETRÔNICAS DE TESES

E DISSERTAÇÕES NA BIBLIOTECA DIGITAL DA UFG

Na qualidade de titular dos direitos de autor, autorizo a Universidade Federal de Goiás (UFG) a disponibilizar, gratuitamente, por meio da Biblioteca Digital de Teses e Dissertações (BDTD/UFG), regulamentada pela Resolução CEPEC nº 832/2007, sem ressarcimento dos direitos autorais, de acordo com a [Lei 9.610/98](#), o documento conforme permissões assinaladas abaixo, para fins de leitura, impressão e/ou download, a título de divulgação da produção científica brasileira, a partir desta data.

O conteúdo das Teses e Dissertações disponibilizado na BDTD/UFG é de responsabilidade exclusiva do autor. Ao encaminhar o produto final, o autor(a) e o(a) orientador(a) firmam o compromisso de que o trabalho não contém nenhuma violação de quaisquer direitos autorais ou outro direito de terceiros.

1. Identificação do material bibliográfico

☐ Dissertação ☒ Tese

2. Nome completo do autor

Antônio Eliseu Holdefer

3. Título do trabalho

EMPREGO DE SENSORIAMENTO REMOTO NAS ESTIMATIVAS DE CONCENTRAÇÃO DE SEDIMENTOS EM ÁGUA

4. Informações de acesso ao documento (este campo deve ser preenchido pelo orientador)

Concorda com a liberação total do documento ☒ SIM ☐ NÃO¹

[1] Neste caso o documento será embargado por até um ano a partir da data de defesa. Após esse período, a possível disponibilização ocorrerá apenas mediante:

a) consulta ao(a) autor(a) e ao(a) orientador(a);

b) novo Termo de Ciência e de Autorização (TECA) assinado e inserido no arquivo da tese ou dissertação.

O documento não será disponibilizado durante o período de embargo.

Casos de embargo:

- Solicitação de registro de patente;
- Submissão de artigo em revista científica;
- Publicação como capítulo de livro;
- Publicação da dissertação/tese em livro.

Obs. Este termo deverá ser assinado no SEI pelo orientador e pelo autor.



Documento assinado eletronicamente por **ANTÔNIO ELISEU HOLDEFER, Discente**, em 13/08/2020, às 23:22, conforme horário oficial de Brasília, com fundamento no art. 6º, § 1º, do [Decreto nº 8.539, de 8 de outubro de 2015](#).



Documento assinado eletronicamente por **Klebber Teodomiro Martins Formiga, Professor do Magistério Superior**, em 14/08/2020, às 10:16, conforme horário oficial de Brasília, com fundamento no art. 6º, § 1º, do [Decreto nº 8.539, de 8 de outubro de 2015](#).



A autenticidade deste documento pode ser conferida no site https://sei.ufg.br/sei/controlador_externo.php?acao=documento_conferir&id_orgao_acesso_externo=0, informando o código verificador **1488112** e o código CRC **1B7B1F07**.

Referência: Processo nº 23070.035476/2020-95

SEI nº 1488112

ANTONIO ELISEU HOLDEFER

**EMPREGO DE SENSORIAMENTO REMOTO NAS ESTIMATIVAS DE
CONCENTRAÇÃO DE SEDIMENTOS EM ÁGUA**

ORIENTADOR: Prof. Dr. Klebber Teodomiro Martins Formiga

**Tese apresentada ao Programa de Pós-Graduação em Ciências Ambientais da Universidade Federal de Goiás como parte dos requisitos para obtenção do título de Doutor em Ciências Ambientais.
Linha de pesquisa: Monitoramento e análise de recursos naturais.**

**Goiânia
2019**

Ficha de identificação da obra elaborada pelo autor, através do Programa de Geração Automática do Sistema de Bibliotecas da UFG.

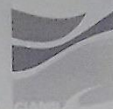
Holdefer, Antonio
EMPREGO DE SENSORIAMENTO REMOTO NAS
ESTIMATIVAS DE CONCENTRAÇÃO DE SEDIMENTOS EM ÁGUA
[manuscrito] / Antonio Holdefer. - 2019.
CX, 110 f.: il.

Orientador: Prof. Dr. Klebber Formiga.
Tese (Doutorado) - Universidade Federal de Goiás, Escola de
Engenharia Civil e Ambiental(EECA), Programa de Pós-Graduação em
Ciências Ambientais, Goiânia, 2019.

Bibliografia.
Inclui siglas, mapas, fotografias, abreviaturas, símbolos, gráfico,
tabelas, lista de figuras, lista de tabelas.

1. Imagens de satélite. 2. Concentração de sedimentos. 3. CSS. 4.
Bacias Fluviais. I. Formiga, Klebber , orient. II. Título.

CDU 502/504



SERVIÇO PÚBLICO FEDERAL
UNIVERSIDADE FEDERAL DE GOIÁS
PRÓ-REITORIA DE PÓS-GRADUAÇÃO
PROGRAMA DE PÓS-GRADUAÇÃO EM CIÊNCIAS AMBIENTAIS

ATA DA DEFESA PÚBLICA DE TESE Nº 003/2019

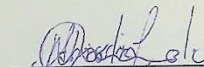
Aos vinte e quatro dias do mês de setembro do ano de dois mil e dezenove, às 14h00, reuniu-se no Centro de Documentação, informação e Memória - CDIM/UFG, Câmpus Samambaia, a Banca Examinadora composta pelos: Prof. Dr. Klebber Teodomiro Martins Formiga – EECA, o Prof. Dr. Nilson Clementino Ferreira – CIAMB, o Prof. Dr. Saulo Bruno Silveira e Souza – EECA, o Prof. Dr. Antonio Marcos de Melo Medeiros - PUC/GO e o Prof. Dr. Felipe Correa Veloso dos Santos - PUC/GO para, sob a presidência do primeiro, proceder a defesa da Tese intitulada: **"EMPREGO DE SENSORIAMENTO REMOTO NAS ESTIMATIVAS DE CONCENTRAÇÃO DE SEDIMENTOS EM ÁGUA"**, de autoria de Antônio Eliseu Holdefer, discente de Doutorado do Programa de Pós-Graduação em Ciências Ambientais (CIAMB), área de concentração em Estrutura e Dinâmica Ambiental. Foi realizada a avaliação oral no sistema de apresentação e defesa de tese de autoria do discente. Terminada a avaliação oral, a Banca Examinadora reuniu-se emitindo os seguintes pareceres mediante as justificativas e sugestões abaixo:

Membro da Banca	Parecer (Aprovado/Reprovado)	Assinatura
Dr. Klebber Teodomiro Martins Formiga		
Dr. Nilson Clementino Ferreira		
Dr. Saulo Bruno Silveira e Souza		
Dr. Felipe Correa Veloso dos Santos		
Dr. Antonio Marcos de Melo Medeiros		

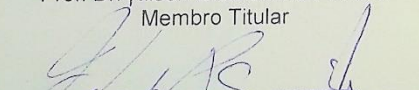
JUSTIFICATIVAS e SUGESTÕES:

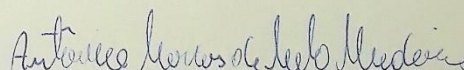
ATENDER AS SOLICITAÇÕES NO TEXTO APRESENTADO
PELA BANCA

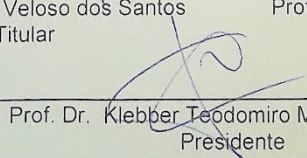
Após a avaliação, o referido discente foi considerada _____ na defesa de tese. Às _____ horas, o Prof. Dr. Klebber Teodomiro Martins Formiga, Presidente da Banca Examinadora, deu por encerrada a sessão e, para constar, lavrou-se a presente Ata.


Prof. Dr. Nilson Clementino Ferreira
Membro Titular


Prof. Dr. Saulo Bruno Silveira e Souza
Membro Titular


Prof. Dr. Felipe Correa Veloso dos Santos
Membro Titular


Prof. Dr. Antonio Marcos de Melo Medeiros
Membro Titular


Prof. Dr. Klebber Teodomiro Martins Formiga
Presidente

AGRADECIMENTOS

A Deus, toda glória por este trabalho e por ter colocado em meu caminho a realização deste doutorado. Aos meus pais Romeu Holdefer e Marlise Beatriz Holdefer por terem mantido um lar de paz. A minha esposa Monah, pelos incentivos. Ao professor Dr. Klebber Teodomiro Formiga, pela orientação e apoio no desenvolvimento desta pesquisa, como também pela amizade e oportunidade de aprendizado no âmbito do Laboratório de Hidráulica. Ao professor Dr. Laerte Guimarães Ferreira, pela acesso ao Laboratório de Processamento de Imagens e Geoprocessamento (LAPIG) e oferecimento de diversos cursos de geoprocessamentos que foram muito úteis na elaboração da presente tese. À toda equipe do Laboratório de hidráulica, por meio de sugestões e análises. À CAPES pelo oferecimento da Bolsa de Doutorado.

RESUMO

Os sedimentos em suspensão em rios e no litoral brasileiro afetam entre outros aspectos a hidrologia, geomorfologia e o funcionamento ecológico das planícies e deltas de inundação. A medição *in situ* tradicional de CSS é na maioria das vezes desafiadora em termos de tempo, custo, pessoal qualificado e em cobertura espacial. A detecção remota por satélite oferece uma maneira conveniente de cobrir vastas áreas em curtos intervalos de tempo.

O presente estudo tem por objetivo desenvolver uma abordagem no uso de imagens obtidas por sensores remotos instalados em plataformas orbitais disponíveis ao público para quantificar a concentração de sedimentos em suspensão (CSS) em rios, no litoral e em bacias hidrográficas brasileiras. Além da obtenção de tendências históricas, para melhor compreensão das variações de CSS ocorridas nas últimas três décadas.

A abordagem utilizada nos artigos resultantes desta tese fazem uso de índices derivados dos valores de reflectância das bandas espectrais das imagens via satélite de maneira a estimar o valor de CSS presente em rios, bacias hidrográficas e no litoral brasileiro, fazendo uso de valores medidos *in situ* para a calibração de tais índices. A presente tese se constitui da introdução ao tema, métodos utilizados e dos quatro artigos gerados no decorrer do doutorado, o primeiro artigo faz uma abordagem geral do estado da arte existente atualmente para a derivação de valores de CSS a partir de índices derivados dos valores de reflectância das bandas espectrais das imagens de satélite. O segundo artigo faz uso das técnicas de estimação de CSS para estudo das variações de concentração de sedimento em água ao longo do Rio Araguaia. O terceiro artigo faz uma análise temporal das variações de CSS nas bacias hidrográficas brasileiras nos últimos 32 anos. O quarto e último artigo apresenta uma nova metodologia para a análise temporal das variações de CSS ao longo da costa brasileira.

Dentre as principais inovações resultantes desta tese podemos destacar: 1) Estimação de concentração de sedimentos em suspensão CSS em todo o território nacional, juntamente com tendências históricas. 2) Utilização de imagens obtidas por sensores instalados a bordo dos satélites da série Landsat para a estimação da concentração de sedimentos em suspensão CSS para todo o litoral brasileiro, a uma distância de até 50 km da costa brasileira, também com tendências históricas.

PALAVRAS-CHAVE: Imagens de satélite, Concentração de sedimentos, SSC, Bacias fluviais

ABSTRACT

Suspended sediments in rivers and on the coastline affects the hydrological, geomorphological and ecological aspects of flood plains and deltas. Traditional SSC *in-situ* measurement is most often challenging in terms of time, cost, qualified personnel, and space coverage. Remote satellite sensing offers a convenient way to cover large areas at reasonable intervals of time.

The objective of this study is to develop an approach to the use of public accessible satellite images to quantify the concentration of suspended sediments (SSC) in Brazilian rivers, watersheds and coastline. In addition to obtaining historical trends, for a better understanding of the CSS variations that have occurred over the past three decades.

The approach used in the articles present in this thesis makes use of indexes derived from the reflectance values of the spectral bands of the satellite images in order to estimate the value of SSC present in rivers, coast and watersheds, making use of values measured *in situ* for the calibration of such values. The present thesis consists of the introduction to the topic, methods and four articles, the first article makes a general approach to the current state of the art for the derivation of SSC values through indexes derived from the reflectance values of the spectral bands of satellite images. The second article makes use of SSC estimation techniques to study the sediment concentration variations in water along the Araguaia River. The third article makes a temporal analysis of SSC variations in the Brazilian basins in the last 32 years. The fourth article presents a new methodology for the temporal analysis of the SSC variations along the entire Brazilian coastline for the last 32 years.

Among the main innovations present in this thesis we can highlight: 1) Estimation of SSC throughout the entire Brazilian territory, together with historical trends. 2) Use of LandSat family of terrestrial satellites to estimate the concentration of SSC for the entire Brazilian coast, at a distance of up to 50 km from the Brazilian coast, also with historical trends.

KEY WORDS: Satellite images, sediment concentration, SSC, river basins

Lista de Figuras

Figura 1 - Ilustração da contribuição dos raios de luz para a reflectância de irradiância.	14
Figura 2 - Ilustração raios de luz contribuindo para a reflectância de sensoriamento remoto RSR.	15
Figura 3 - Perfis de Reflectância de amostras com valores crescentes de CSS. Adaptado de Qu, (2014).	16
Figura 4 - Correlação típica entre CSS e reflectância. Adaptado de Qu (2014).	17

ARTIGO I

Figure 1 - Reflectance profiles of samples with increasing values of SSC. Adapted from Qu, (2014).	25
Figure 2 - Typical correlation between SSC and reflectance. Adapted from Qu (2014)..	26
Figure 3 - Variation of the reflectance as a function of suspended sediment concentration according to equation (2) for various wavelengths from red to near infrared.	28
Figure 4 - Spectral decomposition in Gaussian distributions for Chlorophyll (a) and the suspended sediment concentration SSC (Cheng et al., 2013)..	30

ARTIGO II

Figure 1 - Mobile Sandbanks on the Araguaia River for the city of Sao Felix do Araguaia in the years 2009 (below) and 2016 (above). Location: (Lat: -11.640674, Long: -50.663634).	45
Figure 2 - Map of the Araguaia River watershed with the sediment monitoring stations.	46
Figure 3 - Reflectance values for different SSC values in water samples. Adapted (Qu, 2014).	48
Figure 4 - Image pixel size comparison between Sentinel2 (smaller square) and Landsat8 (bigger square), showing that Sentinel2 images are more suitable for the required application	49
Figure 5 - Points of measurement and Sentinel2 path over the Araguaia River Basin...	53
Figure 6 - SSC indexes applied for the points shown in Figure 5	54
Figure 7 - Depth retrieval. Color scalebar from shallow areas to deeper areas. The black dot shows where the measurement takes place..	55
Figure 8 - NSMI index versus SSC for different sediment monitoring stations.	56
Figure 9 - Dry (left) and Rain (right) season SSC for the year 2016 in a section of the river using the NSMI index – Position (-50.64835, -11.10935)..	57
Figure 10 - The SSC in the rain and dry season for three consecutive years (2016,2017,2018) showing where the Bananal Island begins and ends.	58
Figure 11 - Hipsometry map of the Bananal Island.....	59

ARTIGO III

Figure 1 - The main Brazilian Watersheds.....	68
Figure 2 - Band average relative spectral response of Landsat 7 ETM+ (solid line), Landsat 8 OLI (dash line). Adapted from (Ke et al., 2015)... ..	68

Figure 3 - Reflectance profiles of samples with increasing values of SSC. Adapted from (Qu, 2014).	70
Figure 4 - Illustration of a mean operation applied for the pixels of the same position in an Image Collection, adapted from (Gorelick et al., 2017).	73
Figure 5 - Illustration of a mean operation applied in an Image Region adapted from (Gorelick et al., 2017).	73
Figure 6 - Illustration of Linear Regression applied to an Image Collection, adapted from (Gorelick et al., 2017).	74
Figure 7 - Acquisition points.	75
Figure 8 - SSC indexes applied for the Tocantins basin.	75
Figure 9 - NSMI index versus SSC for different sediment monitoring stations.	77
Figure 10 - SSC trend analysis.	78
Figure 11 - Mean annual estimated SSC trend analysis for all basins.	80
Figure 12 - Water area count for all basins.	81
Figure 13 - Estimation of mean SSC: (a) 1984-1989; (b) (2012-2017).	82
Figure 14 - Estimation of mean SSC difference between the five final years (2012-2017) and the five initial years (1984-1989).	83
Figure 15 - Estimation of water area difference between the five final years (2012-2017) and the five initial years (1984-1989).	83

ARTIGO IV

Figure 1 - Band average relative spectral response of Landsat 7 ETM+ (solid line), Landsat 8 OLI (dash line). Adapted from (Ke et al., 2015).	91
Figure 2 - Reflectance profiles of samples with increasing values of SSC. Adapted from (Qu, 2014).	92
Figure 3 - Illustration of a mean operation applied for the pixels of the same position in an Image Collection, adapted from (Gorelick et al., 2017).	95
Figure 4 - Illustration of a mean operation applied in an Image Region adapted from (Gorelick et al., 2017).	95
Figure 5 - Area of Acquisition.	96
Figure 6 - SSC indexes applied for the southwest coast.	97
Figure 7 - NSMI index versus SSC for different sediment monitoring stations.	98
Figure 8 - Estimation of mean SSC map: year 1984 to 1989 (Left), year 2012 to 2017 (Right).	99
Figure 9 - Estimation of mean SSC difference between the five final years (2011-2016) and (2012-2017).	100
Figure 10 - Estimation of the mean SSC value per latitude degree for five final years (2012-2017) and the five initial years (1984-1989).	101
Figure 11 - Mean SSC values per year for the different coastal regions of Brazil.	103

Lista de Tabelas

ARTIGO I

Table 1 - Compilation of some models developed empirically relating the reflectance and the suspended sediment concentration SSC (Coastal Areas). Adapted from (Qu 2014).	31
Table 2 - Compilation of some models developed empirically relating the reflectance and suspended sediment concentration (Lakes and reservoirs). Adapted from (Qu 2014).	31
Table 3 - Compilation of some models developed empirically relating the reflectance and suspended sediment concentration in rivers. Adapted from (Qu 2014).	31
Table 4. Compilation of published and empirically developed models relating the suspended sediment concentration or turbidity with the reflectance of the surface of the water. The maximum values of turbidity were converted to approximate values of SSC. In column 5 are the data obtained for the Peace-Athabasca Delta, located in northwest Alberta, Canada, these results were taken from the work of (Long & Pavelsky 2013).	32

ARTIGO II

Table 1 - Table 1. Location of sediment monitoring stations, with average flow and drainage area information.	56
--	----

ARTIGO III

Table 1 - Spectral Band range comparison for Landsat 5, 7 and 8.....	69
Table 2 - Satellite selection and Data range.	69
Table 3 - Location of sediment monitoring stations.	76

ARTIGO IV

Table 1 - Spectral Band range comparison for Landsat 5, 7 and 8.....	91
Table 2 - Satellite selection and Data range.	91
Table 3 - Location of sediment monitoring stations.	98

Lista de Siglas

SSC – *Suspended Sediment Concentration*

NSMI - *Normalized Suspended Material Index*

NDSSI - *Normalized Difference Suspended Sediment Index*

ANA - *Agência Nacional de Águas*

SUMÁRIO

1. INTRODUÇÃO	15
2. MÉTODOS	17
2.1. REFLECTÂNCIA EM SENSORIAMENTO REMOTO – VISÃO GERAL	17
3. CONCLUSÃO	21
4. REFERÊNCIAS	22

ARTIGO I - State of the art on remote sensing methods for suspended sediment concentration in inland and coastal waters.....	26
--	----

ABSTRACT	26
1. INTRODUCTION.....	26
2. METHODS	28
2.1. INGLE BAND ALGORITHMS	30
2.2. BAND RATIO ALGORITHMS	32
2.3. SPECTRAL SEPARATION ALGORITHMS	33
3. DISCUSSION	37
3.1. LIMITATIONS	37
4. CONCLUSION	38
5. REFERENCES	38

ARTIGO II - Study on remote sensing methods for suspended sediment concentration SSC in large rivers with mobile sandbanks. The case of the Araguaia river - Brazil.....	46
--	----

ABSTRACT	46
1. INTRODUCTION	47
2. AREA OF STUDY	50
3. METHODS	51
3.1 NSMI INDEX	53
3.2 NDSSI INDEX	54
3.3 BAND RATIO GREEN/BLUE	54
3.4 SPECTRALLY-BASED DEPTH RETRIEVAL	55
3.5 ACQUISITION POINTS	56
4. RESULTS	57
4.1 COMPARISON OF INDEXES	57

4.2 WATER DEPTH RETRIEVAL	58
4.3 CALIBRATION	59
4.4 SSC MEASUREMENTS	60
5. A GEOLOGICAL EXPLANATION.....	63
6. DISCUSSION.....	64
7. CONCLUSION.....	65
REFERENCES	66

ARTIGO III - Temporal Analysis of Suspended Concentration for Over 30 Years in the Main Brazilian Watersheds	69
--	----

ABSTRACT	69
1. INTRODUCTION.....	70
2. MATERIALS AND METHODS	72
2.1. SSC INDEXES	73
2.1.1. NSMI.....	74
2.1.2. NDSSI	75
2.1.3. BAND RATIO GREEN/BLUE	75
2.2. METHODOLOGY	76
3. RESULTS	79
3.1. CALIBRATION.....	79
3.2. SSC TREND ANALYSIS	81
3.3. CHARTS	83
3.4. MAPS	86
4. CONCLUSION.....	88
5. REFERENCES.....	88

ARTIGO IV - Temporal Analysis of Suspended Concentration for Over 30 Years in the Brazilian Coastline.....	92
--	----

ABSTRACT	92
1. INTRODUCTION.....	92
2. MATERIALS AND METHODS	94
2.1. SSC INDEXES	95
2.1.1. NSMI.....	97
2.1.2. NDSSI	97
2.1.3. BAND RATIO GREEN/BLUE	98
2.2. METHODOLOGY	98
3. RESULTS	100
3.1. CALIBRATION.....	101
3.2. MAPS	103
4. CONCLUSION.....	108
5. REFERENCES.....	108

1. INTRODUÇÃO

Os sedimentos em suspensão em água são definidos na prática como sendo toda a matéria inorgânica que permanece em um filtro com tamanho de poro de 0,7 μm (Eisma, 1993; Kirk, 1994).

A suspensão, transporte e deposição de sedimentos figura entre os processos geomorfológicos mais importantes na modelagem da paisagem física e regulação de sistemas (Knighton, 1998). Os sedimentos em suspensão são uma parte natural do ambiente hidrológico, tendo importância fundamental na estruturação do ambiente aquático, criando habitats para a vida aquática, assim como transportando nutrientes fundamentais (Dean et al., 2016; Koiter et al., 2013).

Os sedimentos são particularmente críticos em ambientes inundáveis e em deltas de rios, onde a maior parte das características da paisagem são transformadas pelo movimento de sedimentos em água (Gomez et al., 1995).

Apesar de estar relacionado a aspectos fundamentais da vida aquática, os sedimentos em suspensão também estão muitas vezes associados a diversos problemas ecológicos, tais como transporte de poluentes através de adsorção, inundações, assoreamentos de reservatórios, etc (Bilotta et al., 2008; Horowitz, 2009).

Portanto, a observação dos aspectos espaciais e padrões temporais no transporte de sedimentos são úteis na compreensão das transformações e da função desses ambientes e como eles podem responder às futuras perturbações naturais e antropogênicas, criando-se estratégias de gerenciamento de recursos hídricos que contabilizem a correta quantidade de sedimentos transportados.

Num sentido básico, o transporte de sedimentos através da bacia hidrográfica é facilmente compreendido, sendo originado nas erosões presentes em terra e posteriormente movimentados até as correntes de água e finalmente transportados na forma de sedimentos em suspensão.

Entretanto apesar de décadas de estudos, as dinâmicas, interações espaciais e temporais e todos os fatores que interferem no transporte de sedimentos em suspensão ainda não estão totalmente compreendidos.

O problema das variações temporais e espaciais significativas encontradas nos processos hidrológicos é frequentemente encontrado pelos pesquisadores na modelagem de ciclos hidrológicos (Chen et al., 2005).

Os pesquisadores têm cada vez mais verificado a natureza estocástica e variável de cada estágio desse processo básico (Phillips, 2003). De fato essa complexidade faz a estimativa dos valores do transporte de sedimentos e sedimentação muito desafiadores (Gao et al., 2008).

A concentração de sedimentos em suspensão (CSS), que descreve a quantidade de material suspenso na mistura água-sedimento, é uma medida padrão para o transporte de sedimentos nos rios. Uma grande variedade de métodos de coleta de dados *in situ* foram desenvolvidos para medir o CSS. Mais comumente, uma amostra de água é coletada em campo e filtrada para extrair a matéria sólida em suspensão. O material filtrado é depois secado, pesado e dividido pelo volume da amostra para obter o valor de CSS, na maioria das vezes em (mg/L).

Outros métodos, mais sofisticados, exploram mudanças nas propriedades ópticas ou acústicas da água associado a variações de CSS (Wren et al., 2000). Os métodos baseados em coletas *in situ* fornecem medidas de CSS mais precisas e de locais mais bem específicos, mas as variações espaciais raramente são capturadas e a resolução temporal é geralmente limitada (Curran et al., 1988; Miller et al., 2004).

Devido à grande variabilidade espaço-temporal, o monitoramento de variáveis hidrológicas requer dados em intervalos de tempo relativamente pequenos. Para o fluxo, o problema da variabilidade temporal é resolvido usando a curva chave que é usada para monitorar o fluxo em um ponto específico. Para cargas de sedimentos, são utilizados turbidímetros, ou equipamentos equivalentes, a fim de relacionar os valores de turbidez com a carga de sedimentos. No entanto, a variabilidade espacial das cargas de sedimentos é maior do que as de fluxo, e ainda assim as estações de monitoramento de sedimentos são muito mais escassas em número. Então, para preencher esta lacuna, as técnicas de sensoriamento remoto foram e são usadas.

Com o lançamento do satélite Landsat-1 em julho de 1972, cientistas e engenheiros ganharam uma valiosa nova fonte de observações orbitais para estudar os sistemas hidrológicos e processos que são muito difíceis ou mesmo impossíveis de monitorar a partir de métodos *in situ* tradicionais (Pietroniro e Prowse, 2002). Vários estudos posteriores analisaram o progresso na aplicação de técnicas de sensoriamento remoto em estudos hidrológicos e manejo de recursos hídricos (Salomonson 1983; Kite & Pietroniro 1996; Pietroniro & Prowse 2002; Chen et al., 2005).

Em estudos utilizando-se o sensoriamento remoto, o CSS é estimado pelas propriedades ópticas das partículas em suspensão, assumindo, direta ou indiretamente,

uma relação constante entre a massa das partículas e sua dispersão ou absorção óptica. Sabe-se que essa relação entre a massa de partículas e as propriedades ópticas varia de acordo com o tamanho e a composição das partículas (Babin et al., 2003), criando um limite essencial na generalidade e precisão dos algoritmos de sensoriamento remoto para estimar o valor de CSS.

A maioria das técnicas de detecção remota de CSS constroem relações empíricas entre reflectância e medições *in situ* coletadas em campo (Curran et al., 1988; Schmugge et al., 2002). A sensibilidade às variações de CSS são geralmente mais altas nas porção vermelha do espectro (620 - 740 nm) (Schiebe et al., 1992), embora uma combinação de bandas visíveis e de infravermelho-próximo frequentemente produz uma relação de reflectâncias mais robusta para o CSS (Stumpf et al., 1989).

Nesta tese, optou-se por utilizar o termo CSS, equivalentemente SSC em inglês, em todo o texto, pois esse é o termo mais comumente encontrado na literatura em geral para descrever o transporte e a concentração de sedimentos presentes nos corpos d'água e que apenas diferem ligeiramente dos demais termos utilizados.

Finalmente, a detecção remota por satélite oferece uma opção alternativa para rastrear variações espaciais e temporais de CSS. Isto é especialmente útil em sistemas hidrológicos remotos, de grande extensão ou em ambientes de alta complexidade onde o monitoramento *in situ* é insuficiente ou impraticável.

2. MÉTODOS

2.1. REFLECTÂNCIA EM SENSORIAMENTO REMOTO – VISÃO GERAL

A reflectância da irradiância espectral (ou razão de irradiância), $R(z, \lambda)$, é definida como a razão entre as irradiâncias incidentes e refletidas, tal como definido pela Equação 1 e ilustrado pela Figura 1.

$$R(z, \lambda) = \frac{E_i(z, \lambda)}{E_r(z, \lambda)} \quad (1)$$

$R(z, \lambda)$ é portanto uma medida do quanto da irradiação incidente é refletida para cima em qualquer direção, conforme medido por um coletor com resposta cosenoidal.

Conforme está ilustrado na Figura 1. A profundidade z pode ser qualquer profundidade dentro da coluna de água, ou no ar logo acima da superfície da água.

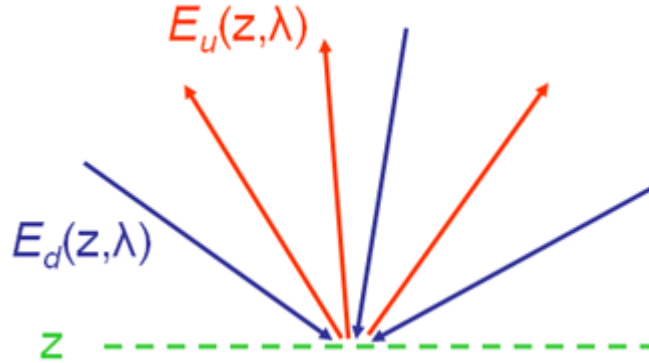


Figura 1 - Ilustração da contribuição dos raios de luz para a reflectância de irradiância.

A reflectância de irradiação tem a virtude de poder ser medida por um único detector de irradiação não calibrado. A irradiância incidente pode ser medida, e então o detector pode ser virado "para baixo" para medir a irradiância refletida. O fator de calibração necessário para converter as unidades de detecção (voltagem, corrente ou contagem digital) para unidades de irradiação ($\text{W.m}^{-2}.\text{nm}^{-1}$) se cancelam ao se efetuar o quociente.

Por outro lado a reflectância de sensoriamento remoto R_{SR} é definida como:

$$R_{SR}(\theta, \Phi, \lambda) = \frac{L_w(\theta, \Phi, \lambda)}{E_d(\lambda)} \quad (2)$$

A reflectância de sensoriamento remoto é uma medida de quanto da radiação incidente na superfície da água em qualquer direção é eventualmente retornada através da superfície em um pequeno ângulo sólido $\Delta\Omega$ centrado em uma direção particular (θ, Φ) como ilustrado na Figura 2.

Embora a reflectância de sensoriamento remoto R_{SR} seja frequentemente calculada para as direções de visualização do nadir somente, na detecção remota real geralmente é uma direção fora do nadir que está sendo observada por um sensor remoto no ar ou por um satélite.

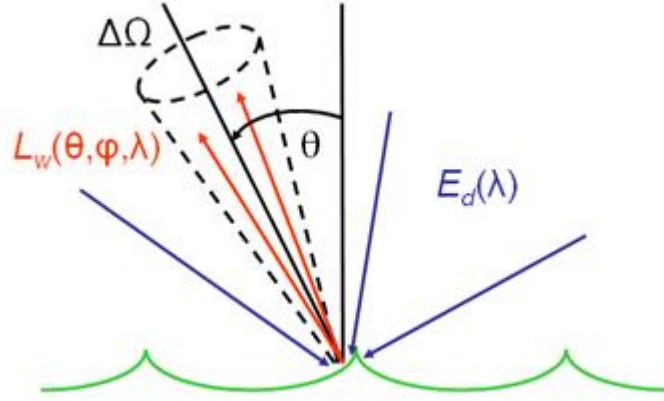


Figura 2 - Ilustração raios de luz contribuindo para a reflectância de sensoriamento remoto RSR.

A detecção da reflectância da água por sensoriamento remoto depende da detecção da radiação eletromagnética que deixa a superfície da água e atinge o sensor a bordo do satélite. A reflectância obtida pelo sensoriamento remoto (R_{SR}) está relacionada com o retro-espalhamento que redireciona os fótons em sentido contrário a incidência e que, eventualmente, deixaram a superfície da água. Assim como com a absorção da água, que converte os fótons em energia térmica ou química (transformação de compostos orgânicos, tal como a produção de clorofila). À medida que os fótons deixam a superfície da água, os mesmos interagem na interface água-ar por refração e reflexão interna. A reflectância por sensoriamento remoto (R_{SR}) pode, portanto, ser associada ao retroespalhamento e à absorção de acordo com Austin (1974); Preisendorfer (1976); Gordon et al., (1975; 1988); Lee et al., (1994) como mostrado na Equação 3.

$$R(\lambda) = \frac{f(\lambda)}{Q(\lambda)} \cdot \frac{t_{(w,a)} \cdot t_{(a,w)}}{n_w^2} \cdot \frac{b_b(\lambda)}{a(\lambda) + b_b(\lambda)} \quad (3)$$

Onde $b_b(\lambda)$ é o coeficiente de retroespalhamento total no comprimento de onda λ . $a(\lambda)$ é o coeficiente de absorção total, $t_{(w,a)}$ é a transmitância água-ar, $t_{(a,w)}$ é a transmitância do ar para água, e n_w é a parte real do índice de refração da água. A quantidade f é uma função complexa do comprimento de onda, propriedades ópticas inerentes da água (albedo de dispersão única e função de dispersão de volume), o ângulo do zênite solar (θ_o), a espessura da camada de aerosol e a rugosidade da superfície (Gordon et al., 1975; Kirk, 1994; Morel et al., 2002). A quantidade Q é a

relação entre a irradiância ascendente e a radiância ascendente, $Q(\lambda) = E_u(\lambda)/L_u(\lambda)$ (Austin, 1974). Portanto, Q é influenciado por processos ambientais e variáveis que afetam a estrutura geométrica do campo de radiação ascendente anisotrópico (i.e. propriedades ópticas inerentes e variáveis ambientais mencionadas acima, direção do fóton viajando de modo ascendente e ângulo azimutal, (Morel et al., 2002).

Os primeiros estudos sobre detecção remota de CSS foram focados principalmente na descoberta e demonstração da existência de uma relação entre a concentração de sedimentos em suspensão e a reflectância espectral e é baseado em métodos empíricos (Ritchie et al., 1976; Ritchie et al., 1988; Ritchie et al., 1990; Chen et al., 1992; Harrington et al., 1992).

O método de sensoriamento remoto para CSS baseia-se nas características da radiação refletida pela água como função da concentração de sedimento presente nele.

Em geral, a reflectância "típica" da água em função da concentração de sedimentos em suspensão CSS é dada como mostrado na Figura 3. Conforme observado, parece que uma faixa espectral útil seria entre 400 e 900 nm, uma vez que, após esse intervalo, o sinal flutua consideravelmente, dificultando a análise.

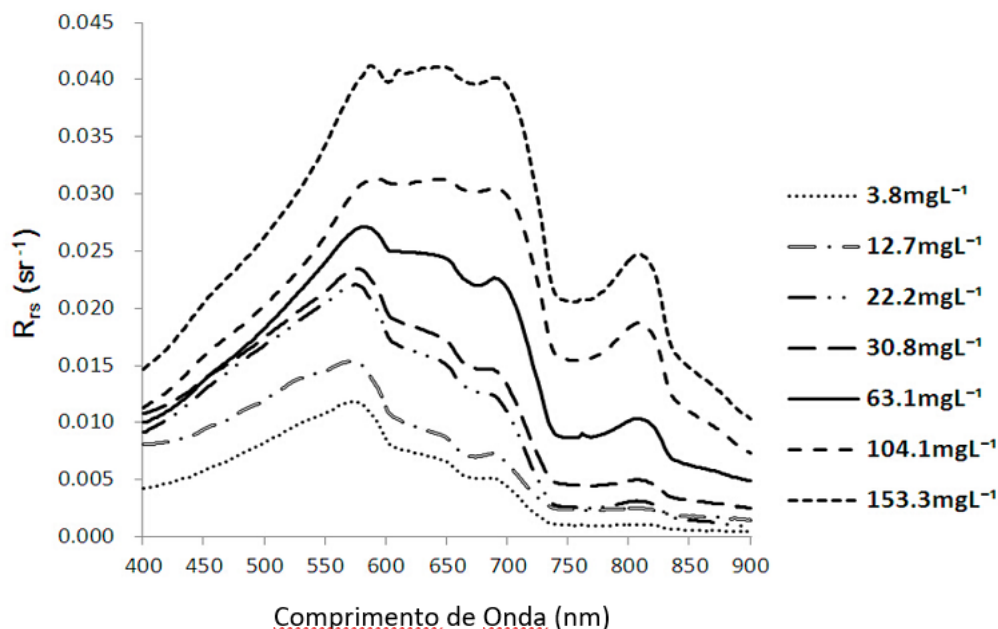


Figura 3 - Perfis de Reflectância de amostras com valores crescentes de CSS. Adaptado de Qu, (2014).

Foi utilizado o coeficiente de correlação de Pearson (r) para indicar a correlação entre os valores de CSS e a reflectância sobre a faixa de frequências. A correlação obtida é mostrada na Figura 4. Observa-se que, para os intervalos de onda entre 750nm

e 950nm, todos os valores de r estão acima de 0.7, o que parece ser uma boa opção para a estimativa de CSS. É claro, portanto, que as faixas "ótimas" para a calibração dos valores CSS estão em torno da faixa de infravermelho vermelho e próximo (Qu 2014).

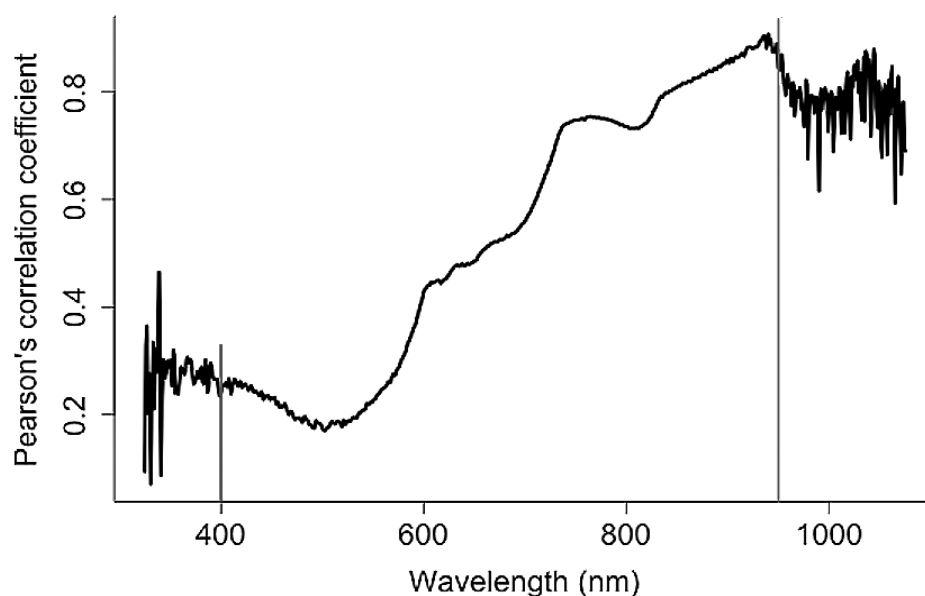


Figura 4 - Correlação típica entre CSS e reflectância. Adaptado de Qu (2014).

Os algoritmos de quantificação CSS baseados na reflectância da água podem ser grosseiramente divididos nas seguintes famílias: banda única e relação de banda. Descrições mais precisas de tais algoritmos serão dadas nos quatro artigos a seguir.

3. CONCLUSÃO

O mapeamento remoto da concentração de sedimentos em suspensão tem progredido bastante nos últimos anos. Com o lançamentos de novos produtos para o gerenciamento e processamento de milhares de imagens simultaneamente, tem-se permitido o estudo e monitoramento de grandes áreas.

No presente trabalho se explorou o potencial da plataforma Google Earth Engine em prover dados e poder de processamento, possibilitando a extração automática de dados e posterior processamento, através da linguagem de programação Java.

Assim tornou-se possível, a estimativa da concentração de sedimentos em suspensão para todo o território nacional, além cobrir, de maneira inovadora, todo o litoral brasileiro com medidas de tendência histórica dos últimos 32 anos.

Os métodos apresentados neste trabalho fornecem uma ótima ferramenta, sendo esta muito eficaz e prática para o monitoramento de grandes áreas, nas quais podem se determinar regiões nas quais o CSS aumentou ao longo dos anos, assim como levantamento de vários índices históricos. Torna-se também possível a determinação de regiões onde houve aumento ou diminuição da superfície da água.

O método pode ser usado em diferentes áreas de interesse, tais como bacias hidrográficas, países, ou até continentes inteiros.

Ainda como recomendação desse trabalho se verifica a possibilidade de se alterar os índices e assim derivar outros parâmetros de interesse, tal como a clorofila, algas, e outros constituintes de interesse presente na água, desde que os mesmos modifiquem espectralmente a reflexão da água dentro das faixas de frequência presentes nos sensores remotos embarcados em satélites de interesse.

4. REFERÊNCIAS

- Austin, R.W. 1974. The remote sensing of spectral radiance from below the ocean surface. In: Jerlov, N.G., Steemann-Nielsen, E. (Eds.), *Optical Aspects of Oceanography*. Academic Press, London, New York, pp. 317 e 344.
- Babin, M. et al. 2003. Light Scattering Properties of Marine Particles in Coastal and Open Ocean Waters as Related to the Particle Mass Concentration Light scattering properties of marine particles in coastal and open ocean waters as related to the particle mass concentration. *American Society of Limnology and Oceanography*, 48(2), pp.843–859.
- Bilotta, G. S., and R. E. Brazier. "Understanding the influence of suspended solids on water quality and aquatic biota." *Water research* 42.12 (2008): 2849-2861.
- Chen, Z., Curran, P. & Hansom, J.D., 1992. Derivative reflectance spectroscopy to estimate suspended sediment concentration., 77, pp.67–77. Available at: <http://eprints.bournemouth.ac.uk/4675/1/licence.txt>.
- Chen, J.M. et al., 2005. Distributed hydrological model for mapping evapotranspiration using remote sensing inputs. *Journal of Hydrology*, 305(1-4), pp.15–39.
- Curran, P.J.; Novo, E.M. The relationship between suspended sediment concentration and remotely sensed spectral radiance: A review. *J. Coast. Res.* 1998, 4, 351–368.

- Dean, David J., et al. "Sediment supply versus local hydraulic controls on sediment transport and storage in a river with large sediment loads." *Journal of Geophysical Research: Earth Surface* 121.1 (2016): 82-110.
- Eisma, D., 1993. *Suspended matter in the aquatic environment*. Springer-Verlag, Berlin.
- Gao, Xuelu, and Shaoyong Chen. "Petroleum pollution in surface sediments of Daya Bay, South China, revealed by chemical fingerprinting of aliphatic and alicyclic hydrocarbons." *Estuarine, Coastal and Shelf Science* 80.1 (2008): 95-102.
- Gomez, Basil, et al. "Sediment characteristics of an extreme flood: 1993 upper Mississippi River valley." *Geology* 23.11 (1995): 963-966.
- Gordon, Howard R., Otis B. Brown, and Michael M. Jacobs. "Computed relationships between the inherent and apparent optical properties of a flat homogeneous ocean." *Applied optics* 14.2 (1975): 417-427.
- Gordon, H. R., Brown O. B., Evans R. H., Brown J. W., Smith R. C., Baker K. S. & D. K. Clark. 1988. A semianalytical radiance model of ocean color. *Journal of Geophysical Research* 93: 10909-10924.
- Harrington J A Jr, Schiebe F R & Nix J F. 1992. Remote sensing of Lake Chicot, Arkansas: Monitoring suspended sediments, turbidity, and Secchi depth with Landsat MSS data. *Remote Sensing of Environment*, 39(1):15-27.
- Horowitz, Arthur J. "Monitoring suspended sediments and associated chemical constituents in urban environments: lessons from the city of Atlanta, Georgia, USA Water Quality Monitoring Program." *Journal of Soils and Sediments* 9.4 (2009): 342-363.
- Kirk, J.T.O., 1994. Light and photosynthesis in aquatic ecosystems. *Sec. Ed. Cambridge university press*, Cambridge.
- Kite G. & Pietroniro A. 1996. Remote sensing application in hydrological modeling. *Hydrological Science* 41: 563–591.
- Knighton, David. "Fluvial forms and processes: a new perspective.. ed. 2." (1998).
- Koiter, A. J., et al. "The behavioural characteristics of sediment properties and their implications for sediment fingerprinting as an approach for identifying sediment sources in river basins." *Earth-Science Reviews* 125 (2013): 24-42.
- Lee, Zhongping, et al. "Model for the interpretation of hyperspectral remote-sensing reflectance." *Applied Optics* 33.24 (1994): 5721-5732.

- Miller, Richard L., and Brent A. McKee. "Using MODIS Terra 250 m imagery to map concentrations of total suspended matter in coastal waters." *Remote sensing of Environment* 93.1-2 (2004): 259-266.
- Morel, André, David Antoine, and Bernard Gentili. "Bidirectional reflectance of oceanic waters: accounting for Raman emission and varying particle scattering phase function." *Applied Optics* 41.30 (2002): 6289-6306.
- Fahey, B. D., M. Marden, and C. J. Phillips. "Sediment yields from plantation forestry and pastoral farming, coastal Hawke's Bay, North Island, New Zealand." *Journal of Hydrology (New Zealand)* (2003): 27-38.
- Pietroniro, A. & Prowse, T.D., 2002. Applications of remote sensing in hydrology. *Hydrological Processes*, 16(8), pp.1537–1541.
- Preisendorfer, Rudolph W. Hydrologic optics. Vol. 1. 1976.
- Qu, L., 2014. Remote Sensing Suspended Sediment Concentration in the Yellow River. *Doctoral Dissertations.*, p.Paper 383.
- Ritchie J C, Schiebe F R. & McHenry J R. 1976. Remote sensing of suspended sediments in surface waters. *Journal of American Society of Photogrammetry*, 42(12):1539-1545.
- Ritchie J C., Cooper M C. & Yongqing J. 1987. Using landsat multispectral scanner data to estimate suspended sediments in Moon Lake, Mississippi. *Remote Sensing of Environment*, 23(1):65-81.
- Ritchie J C., Cooper M C. & Schiebe F R. 1990. The relationship of MSS and TM digital data with suspended sediments, chlorophyll, and temperature in Moon Lake, Mississippi. *Remote Sensing of Environment*, 33(2):137-148.
- Salomonson V. 1983. Water resources assessment. In *Manual of Remote Sensing*, Colwell J (ed.). *American Society of Photogrammetry and Remote sensing: Bethesda, Maryland*; 1497–1570.
- Schmugge, Thomas J., et al. "Remote sensing in hydrology." *Advances in water resources* 25.8-12 (2002): 1367-1385.
- Schiebe F R., Harrington J A Jr. & Ritchie J C. 1992. Remote sensing of suspended sediments: the Lake Chicot, Arkansas project. *International Journal of Remote Sensing*, 3(8):1487-1509.
- Stumpf, R. P. & Pennock J. R. 1989. Calibration of a general optical equation for remote sensing of suspended sediments in a moderately turbid estuary. *Journal of Geophysical Research* 94: 14363-14371.

Wren, D. G., et al. "Field techniques for suspended-sediment measurement." *Journal of Hydraulic Engineering* 126.2 (2000): 97-104.

ARTIGO I

State of the art on remote sensing methods for suspended sediment concentration in inland and coastal waters

A.E. Holdefer & K. Formiga
University of Goiás, Goiás, Brazil

KEY WORDS: SSC, Suspended Sediment

ABSTRACT

Interest in remote sensing of SSC is motivated by the environmental, economic and ecological importance of sediment transport in coastal and inland waters. Quantification of SSC in rivers is important in studying the hydrologic, geomorphologic and ecologic functioning of river flood plains and deltas. Applications include the optimization of dredging/dumping operations, assessing the environmental impact of construction activities, understanding geomorphologic change, evaluating fluxes of particulate organic carbon from rivers to the sea, etc.

The attractiveness of remote sensing as an information source has increased greatly over the last fifteen years as the new generation of medium resolution satellite sensors (SeaWiFS, MERIS and MODIS, SENTINEL) has become available.

This study aims to review the state of the art on remote sensing for suspended sediments concentration SSC in inland and coastal waters and to outline future perspectives.

1. INTRODUCTION

The suspended particulate matter (SPM) can be defined as all matter (organic and inorganic) that remains in a filter with pores ranging from 0.4 to 0.5 μ m (Eisma, 1993; Kirk, 1994). In practice the discrimination between suspended and dissolved material in water is determined using a Whatman glass microfiber filter GF/F with a 0.7 μ m pore size. The suspended sediment concentration (SSC) that describes the quantity of suspended material in the water-sediment mixture, usually expressed in mg/L, is a common measure to sediment transport in rivers. The terms SSC and TSS (Suspended

Sediment Concentration and Total Suspended Solids) are referred to as suspended particulate matter (SPM) (Ouillon et al., 2008) and are often interchanged in the literature. Another term commonly present in the literature for concentration of suspended sediment is turbidity, which is easily measurable *in situ* and presents a strong correlation with SSC and TSS, as exploited by some papers as Holliday et al., (2003).

The SSC data are produced by measuring the dry weight of all sediments from a known volume of water-sediment mixture. The TSS data can be produced by different methods, many of which include measuring the dry weight of sediments of a known volume of a sub-sample of the original (Gray et al., 2000). In general, when all other factors are kept the same (such as the density and composition of the particles), analytical procedures may result in different values of SSC and TSS, with the SSC being slightly larger than TSS (Gray et al., 2000b).

The problem of large temporal and spatial variations found in hydrological processes is often found by researchers in modeling hydrological cycles (Chen et al., 2005). With the Landsat-1 launch in July 1972, scientists and engineers gained a valuable new source of orbital observations to study hydrological systems and processes that are very difficult or even impossible to monitor via traditional *in situ* methods (Pietroniro & Prowse 2002). Several previous studies reviewed progress in the application of remote sensing techniques in hydrological studies and water resources management (Salomonson 1983; Kite & Pietroniro 1996; Pietroniro & Prowse 2002; Chen et al., 2005).

Due to the large space-temporal variability, the monitoring of hydrological variables requires data in relatively small time intervals. To the flow, the problem of the temporal variability is solved using the rating curve which is used to monitor the flow at a specific point. To sediment loads, turbidimeters are employed, in order to relate the turbidity values with the sediment load. However, the spatial variability of sediment loads is greater than the flow rates and yet the sediment monitoring stations are far fewer in number. So in order to fill this gap the remote sensing techniques has been used.

In remote sensing studies SPM is estimated by the optical properties of the suspended particles, assuming, directly or indirectly, a constant ratio between the mass of the particles and their dispersion or absorption. It is well known that this relationship between the mass of particles and optical properties vary depending on the size and particle composition (Babin et al., 2003), creating an important limit on the generality

and accuracy of remote sensing algorithms to estimate the SPM. In this article we chose to mention the SSC term throughout the text, because it is the term most commonly found in the literature in general to describe the transport and concentration of sediments present in water bodies and that only slightly differs from other terms listed above.

2. METHODS

The detection of the water reflectance by remote sensing relies on detecting the electromagnetic radiation that leaves the surface of the water and reaches the sensor on board the satellite, bringing about the inherent optical properties IOPs of the water. The reflectance obtained by remote sensing R_{RS} is related to backscattering which redirects the downwelling photons to travel upward and eventually leave the surface of the water. Absorption, which converts the photons into heat or chemical energy. As upward travelling photons leave the water they interact with the water-air interface by refraction and internal reflection. The reflectance R_{RS} can therefore be associated with backscattering and absorption according to Austin (1974); Preisendorfer (1976); Gordon et al., (1988); Lee et al., (1994) as shown in equation 1.

$$R(\lambda) = \frac{f(\lambda)}{Q(\lambda)} \cdot \frac{t_{(w,a)} \cdot t_{(a,w)}}{n_w^2} \cdot \frac{b_b(\lambda)}{a(\lambda) + b_b(\lambda)} \quad (1)$$

Where $b_b(\lambda)$ is the total backscattering coefficient at the wavelength λ , $a(\lambda)$ is the total absorption coefficient, $t_{(w,a)}$ is the water-air transmittance, $t_{(a,w)}$ is the transmittance from air to water, and n_w is the real part of the refractive index of the water. The quantity f is a complex function of wavelength, water IOPs (single scattering albedo and volume scattering function), the solar zenith angle (θ_o), aerosol optical thickness and surface roughness (Gordon et al., 1975; Kirk, 1984; Morel et al., 2002). The quantity Q is the ratio between the upwelling irradiance and upwelling radiance, $Q(\lambda) = E_u(\lambda)/L_u(\lambda)$ (Austin 1974). Therefore, Q is influenced by environmental processes and variables affecting the geometrical structure of the anisotropic upward radiance field (i.e. IOPs and environmental variables mentioned above, direction of the upward traveling photon and azimuth angle; Morel et al., 2002).

The first studies on remote sensing of SSC were mainly focused on the discovery and demonstration of the existence of a relationship between the concentration of suspended sediments and the spectral reflectance and it is based on empirical methods (Ritchie et al., 1987; Ritchie et al., 1998; Ritchie et al., 1990; Chen et al., 1992; Harrington et al., 1992).

The SSC remote sensing method is based on the characteristics of the radiation reflected by the water as a function of the sediment concentration present in it.

In general the "typical" reflectance of water as a function of suspended sediment concentration SSC, is given as shown in Figure 1. As noted, it appears that a useful spectral range would be between 400 and 900nm, since after this interval the signal fluctuates considerably, making it difficult to analyze.

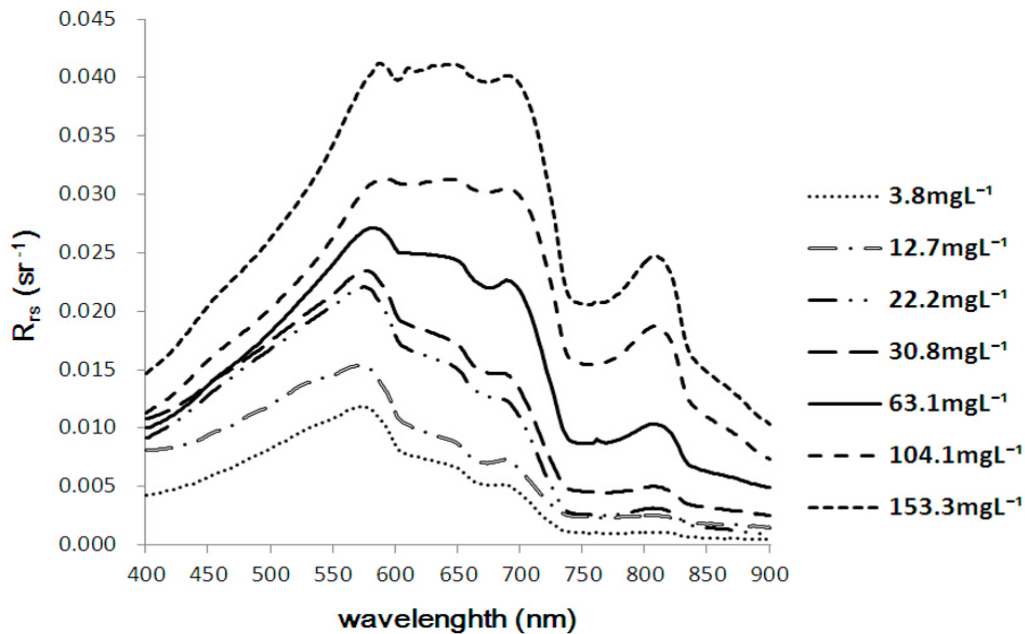


Figure 1 - Reflectance profiles of samples with increasing values of SSC. Adapted from Qu, (2014).

It was used the Pearson correlation coefficient (r) in order to indicate the correlation between the SSC values and reflectance over the frequencies range. The correlation obtained is shown in Figure 2. It is noticed that for the wavelength ranges from 750nm to 950nm, all values of r are above 0.7, which appears to be a good choice for SSC estimation. It is clear, therefore, that the tracks "great" for calibration of CSS values are around the range of red and near-infrared (Qu 2014).

SSC quantification algorithms based on the reflectance of water can coarsely be divided into the following families: single band, band ratio and spectral separation as described in the following sections.

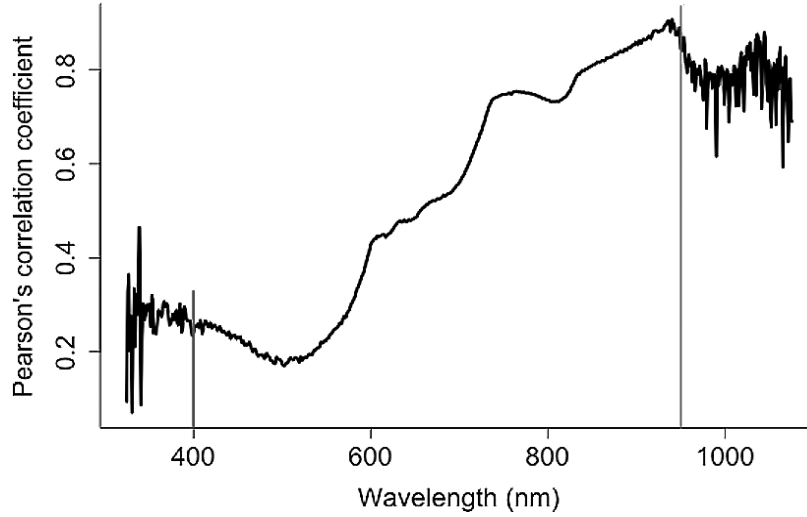


Figure 2 - Typical correlation between SSC and reflectance. Adapted from Qu (2014).

2.1. INGLE BAND ALGORITHMS

The facility of detection of SSC characteristics is due to the almost linear relationship between the SSC and the reflectance at any wavelength, at least for small and low reflectance (Althuis et al., 1995). For high reflectance values this relationship becomes nonlinear and the reflectance approaches asymptotically the maximum value of "saturation" (Bowers et al., 1998; Doxaran et al., 2002), where an increase in suspended sediment concentration, no longer affects the reflectance. Many algorithms have been developed to estimate the reflectance due the SSC on a single wavelength. For example, based on the first order reflectance model (Gordon et al., 1988) and the assumption that the scattering and absorption of the particles are proportional to the SSC here named S , and that the space-time variability (not the wavelength) can be neglected (Katlane et al., 2013; Nechad et al., 2004). It is suggested the following algorithm given by the equation 2.

$$S = A \frac{R_{rs}}{1 - \frac{R_{rs}}{c}} \quad (2)$$

Where the reflectance R_{rs} is obtained by remote sensing, defined as the radiance reflected by water divided by the irradiance, and A and C are calibration coefficients which depend on the wavelength, with C representing the reflectance saturation. A it is determined by regression analysis from measurements of R_{rs} and S , and is theoretically associated with the inherent optical properties. The relationship between S and R_{rs} defined by this family of single band algorithms is illustrated in Figure 3 for different wavelengths.

It is observed directly from the Figure 3 that for low reflectance values (<0.01) the relationship is approximately linear, becoming non-linear but still monotonous even for moderate reflectance values (0.01 to 0.03) before reaching to an asymptotic value (near 0.05).

Alternative single band algorithms have been suggested as functional forms of $S(R)$ (see Table 1 to 4 for examples), usually involving linear function for low values of reflectance and non-linear monotonic functions for high reflectance values, although various types of functions have been suggested for the latter, including logarithmic (Ouillon et al., 1997) and power functions (Ahn et al., 2001). The calibration of such algorithms can be made from simultaneous measurements of S and R (satellite or in situ) or from measurements of specific inherent optical properties (Van der Woerd et al., 2004).

The performance of such single band algorithms is actually best for low and moderate reflectance values (linear range) and their accuracy depends on the validity of assumptions, particularly as the total scattering is proportional to the SSC and that the space-time variability of absorption by a non-particle can be neglected. This latter requirement suggests that the use of the bands in the near infrared and red bands is preferred because in this case the absorption of non-particles comes essentially from pure water, reducing significantly the other absorptions. The requirement of low to moderate reflectance suggests that the optimal wavelength will depend on the suspended sediment concentration and the single-band algorithms will of course be limited to a range of concentrations. Alternatively, if more wavelengths are available, an adaptive algorithm can be developed using the basic single band algorithm given by Equation 1 but with the wavelengths being chosen according to the input reflectance spectrum.

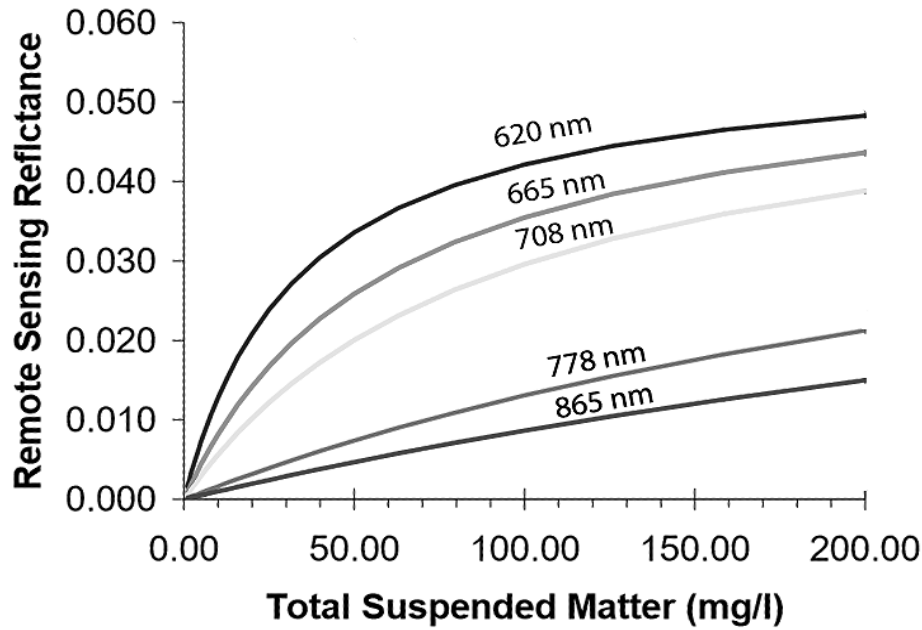


Figure 3 - Variation of the reflectance as a function of suspended sediment concentration according to Equation (2) for various wavelengths from red to near infrared.

An interesting variation of these algorithms is to use procedures based on the difference between two bands, typically red and infrared. Such algorithms have properties similar to single-band processes with the advantages of band ratio algorithms as they combine the acquisition of SSC with a full residual aerosol correction (Stumpf et al., 1989) or a residual aerosol correction after atmospheric correction (Hu et al., 2004; Sterckx et al., 2007).

2.2. BAND RATIO ALGORITHMS

As seen in the previous section, single band algorithms are highly sensitive to atmospheric scattering and, therefore, are subject to uncertainties if the scattering coefficient of air density has a high natural variability. Rather, band ratio algorithms can be developed to be less sensitive to this natural variability since the background scattering effects is largely canceled when the ratio between bands is made. The band ratio algorithms between two bands were suggested to estimate the SSC by Doxaran et al., (2002).

In addition to the individual bands, the relationship between the near-infrared reflectance and visible band (red, green and blue), and between the red and green bands, have also been proposed for estimating SSC (Topliss et al., 1990; Yuming et al., 1992; Doxaran et al., 2009). Doxaran et al., (2002) demonstrated that the use of reflectance

ratios between bands could reduce the effects of reflection from the sky, particle size, and the refractive index variations. However, Binding et al., (2005) argued that the reflectance ratios work well only for highly turbid water dispersion which compensates the strong absorption of other optically active materials in water in these wavelengths.

SSC can be estimated using remote sensors capable of detecting electromagnetic radiation, causing its reflectance to be processed (Sobrino, 2000; Zhou et al., 2017). The detection of the properties of suspended sediments in water, such as SSC, has as its principle the interaction between electromagnetic waves, water and their components (Bukata et al., 2018; Domínguez et al., 2011). Increased concentration of suspended sediment in SSC water increases visible radiation reflection, varying according to particle diameter, mainly in the blue and green bands (Chuvieco, 2008). Therefore, remote sensing uses techniques for measuring SSC through models and various algorithms, according to regional or local variations, with large-scale multitemporal and spatial potential. The costs involved in this procedure are much lower than *in situ* sampling and laboratory analysis, as the vast majority of images (Nooren et al., 2017; Ritchie et al., 1987; Topliss et al., 1990; Zhang, 2010; Long et al., 2013).

Similarly band ratio algorithms are less sensitive to lighting conditions (Doxaran et al., 2003). Band ratio algorithms can however be sensitive to natural variability of sediment absorption properties since the use of a reflectance ratio can shift the physical properties from scattering to absorbing properties (Moore et al., 1999).

2.3. SPECTRAL SEPARATION ALGORITHMS

Often aquatic environments, due to excessive nutrients, go through the eutrophication process, causing an excessive increase of algae and consequently the chlorophyll present in the environment. For such applications, which have a high organic content, it becomes necessary to use a model that extracts chlorophyll content from the SSC sample. The mathematical methods used in spectral separation algorithms are diversified. This family of algorithms are usually based on a model, as shown by Cheng et al., (2013); Xiao et al., (2006); Gilerson et al., (2007), which decomposes the sample reflectance spectrum into two parts, one for the chlorophyll spectrum and the other the SSC spectrum.

The conventional spectral separation is performed by deconvolution calculation, which is based on the curve fit method for the minimum variance. This method assumes that knowing the spectral signatures of both chlorophyll as the SSC, it is possible to

perform a spectral decomposition of them and subsequently adjusting the gain coefficients of each spectrum so that the resultant sum of two spectra results as close as possible to the original chlorophyll and SSC mixture (Zeng, 1994).

These steps may become clearer by analyzing figure 4, which shows the spectral decomposition of chlorophyll and suspended sediment in their respective Gaussian distributions (Hoepffner et al., 1991), obtained from a sample presenting the mixture of the two components.

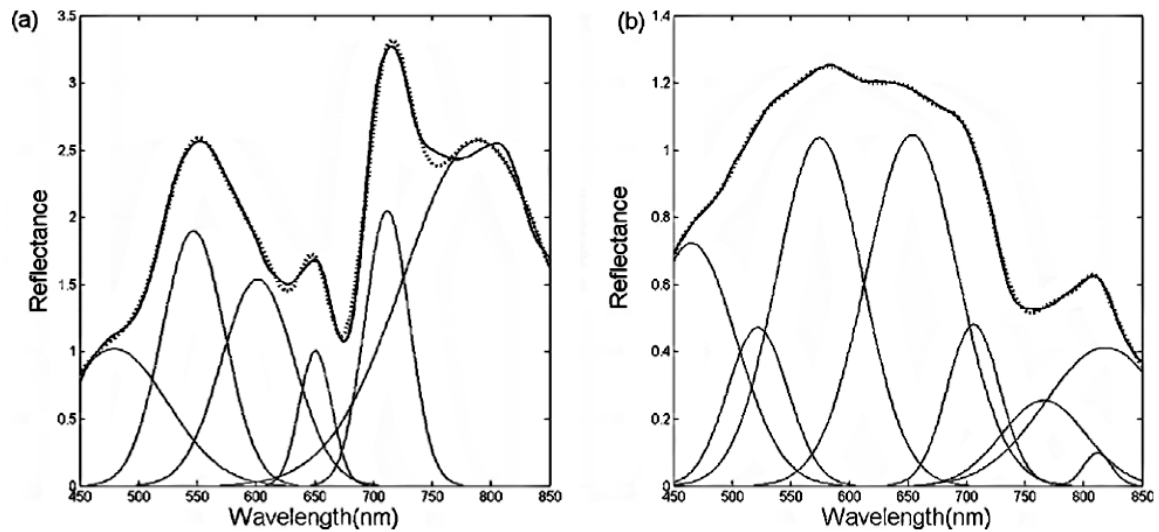


Figure 4 - Spectral decomposition in Gaussian distributions for Chlorophyll (a) and the suspended sediment concentration SSC (Cheng et al., 2013).

A great advantage of multispectral algorithms is the possibility to automatically adapt to a variable mixture of particles of algae and non-algae, thus offering greater generality.

Tables 1, 2 and 3 present a compilation of relevant articles in the area and that present models developed for the study of these locations with the respective correlation coefficients. Table 4 shows the use of different methods to the same place, checking out the best suited to the location in question.

In general we can see a better result in the band ratio algorithms, possibly due to atmospheric attenuation of the path effects.

Tabela 1 - Compilation of some models developed empirically relating the reflectance and the suspended sediment concentration SSC (Coastal Areas). Adapted from (Qu 2014).

Products / Bands	Location	Wavelengths	Empirical relationship	SSC (mg/L)	R	Samples	Reference
LANDSAT TM	Moreton Bay (Australia)	R1=520–600 R2=760–900	$TSS = 16.826 - 5.2369 * \left(\frac{R2}{R1}\right)$	~9.2	0.83	53	Gault et al., (2003)
EO-1 AL1	Pearl River Estuary(China)	R4=525–605	$TSS = -1229.5 * R4 + 53.795$	~33.2	0.91	11	Fang et al., (2010)
SPOT	Gironde Estuary (France)	R1=510–590 R2=790–890	$SPM = 27.424 * e^{0.0279 * \left(\frac{R2}{R1}\right)}$	~2500	0.89	132	Doxaran et al., (2003)
LANDSAT	Gironde Estuary (France)	R1=510–590 R2=790–890	$SPM = 29.022 * e^{0.0335 * \left(\frac{R2}{R1}\right)}$	~2500	0.88	132	Doxaran et al., (2003)
SPOT XS3 / XS1	Loire Estuary (France)	R1=510–590 R2=790–890	$SPM = 18.895 * e^{0.0322 * \left(\frac{R2}{R1}\right)}$	~2600	0.93	68	Doxaran et al., (2003)
LANDSAT	Loire Estuary (France)	R1=620–670 R2=841–876	$SPM = 26.083 * e^{0.0366 * \left(\frac{R1}{R2}\right)}$	~2600	0.93	68	Doxaran et al., (2003)
MODIS	Hangzhou Bay (China)	841–876	$\ln(SSC) = (43.233 * R) + 1.396$	2500	0.87	25	Wang et al., (2009a)

Note: The equations are written as they were published, where SPM = Suspended Particulate Matter, SSC = Suspended Sediment Concentration and TSS: Total Suspended Solids. Ri is the reflectance of water for a given wavelength.

Tabela 2 - Compilation of some models developed empirically relating the reflectance and suspended sediment concentration (Lakes and reservoirs). Adapted from (Qu 2014).

Products / Bands	Location	Wavelengths	Empirical relationship	SSC (mg/L)	R	Samples	Reference
Landsat MSS 1 and 2	Enid Reservoir(USA)	R1=500–600 R2=600–700	$\ln(SSC) = -9.21 * \left(\frac{R1}{R2}\right) + 2.71 * \left(\frac{R1}{R2}\right)^2 + 8.45$	~168	0.82	77	Ritchie & Cooper (1991)
Landsat ETM	Tailu Lake(China)	R4=760-900	$TSM = 0.221R4 + 60.293$	~37.6	0.91	11	Ma & Dai (2005)
Landsat MSS	Chicot Lake (USA)	R3=700-800	$SPM = 0.18 * (1 - e^{\left(\frac{R3}{88.8}\right)})$	~25	0.62	310	Schiebe et al., (1992)
Landsat TM	Frisian Lakes (Netherlands)	R1=520–600 R2=630–690	$TSM = 0.7581 * e^{61.683 * \left(\frac{R1+R2}{2}\right)}$	50	0.99	10	Dekker et al., (2001)
Landsat TM	Michigan Lake (USA)	R1=450–520 R2=630–690	$TSS = 0.0167 * e^{12.3 * \left(\frac{R2}{R1}\right)}$	35	-	-	Lathrop (1986); Lathrop Jr & Lillesand (1989)

Note: The equations are written as they were published, where SPM = Suspended Particulate Matter, SSC = Suspended Sediment Concentration and TSS: Total Suspended Solids. Ri is the reflectance of water for a given wavelength.

Table 3. Compilation of some models developed empirically relating the reflectance and suspended sediment concentration in rivers. Adapted from (Qu 2014).

Products / Bands	Location	Wave-lengths	Empirical relationship	SSC (mg/L)	R	Reference
MODIS	Yangtse River (China)	R1=620–670 R2=841–876	$SSC = -23.03 + 60.24 * (R1 - R2)$	74-81	0.73	Wang et al., (2010)
MODIS	Yangtse River (China)	R1=620–670 R2=841–876	$\ln(SSC) = 4.117 + 0.262 * (R1 - R2)$	45-909	0.78	Wang & Lu (2010)
Landsat	Yangtse	R3=700-800	$\ln(SSC) = 3.182 * \ln(R4) - 1.4$	22-2610	0.88	Wang et al., (2009b)

TM	River (China)					
MODIS	Ganges and Brahmaputra Rivers (Bangladesh)	R3=459-479	$SSC = 69.39 * R3 - 201$	1200	0.98	Islam et al., (2001)
MODIS	Fiorde Kangerlussuaq (Greenland)	R1=620-670	$R1 = 7.5 * \log(SSC) + 1.6$	-	0.90	Chu et al., (2009)

Note: The equations are written as they were published, where SPM = Suspended Particulate Matter, SSC = Suspended Sediment Concentration and TSS: Total Suspended Solids. Ri is the reflectance of water for a given wavelength.

Table 4. Compilation of published and empirically developed models relating the suspended sediment concentration or turbidity with the reflectance of the surface of the water. The maximum values of turbidity were converted to approximate values of SSC. In column 5 are the data obtained for the Peace-Athabasca Delta, located in northwest Alberta, Canada, these results were taken from the work of (Long & Pavelsky 2013).

Products / Bands	Wavelengths	Empirical relationship	SSC (mg/L)	R	Reference
Landsat TM 2 and 4	R1=520–600 R2=760–900	$SPM = 29.022 * e^{0.0335 * (\frac{R2}{R1})}$	~2500	0.97	Doxaran et al., (2003)
Sea WiFS	R1=545–565 R2=845–885	$SPM = 26.083 * e^{0.0366 * (\frac{R1}{R2})}$	~2500	0.96	Doxaran et al., (2003)
SPOT XS3 and XS1	R1=510–590 R2=790–890	$SPM = 18.895 * e^{0.0322 * (\frac{R2}{R1})}$	~2500	-0.96	Doxaran et al., (2003)
SPOT XS3 and XS1	R1=510–590 R2=790–890	$SPM = 27.424 * e^{0.0279 * (\frac{R2}{R1})}$	~2500	-0.96	Doxaran et al., (2003)
Landsat MSS 5 and 6	R1=600–700 R2=700–800	$\ln(SSC) = -6.2 * \frac{R1}{R2} + 1.4 * (\frac{R1}{R2})^2 + 10.8$	1000	0.96	Topliss et al., (1990)
MODIS 1 and 2	R1=620–670 R2=841–876	$SPM = 12.996 * e^{(\frac{R2}{R1})/0.189}$	~2250	0.95	Doxaran et al., (2009)
Landsat TM 1, 3, 4	R1=450–520 R2=630–690 R3=760–900	$Turbidity = 11.31 * \frac{R3}{R1} - 2.03 * R2 - 16.42$	~12	0.87	Song et al., (2011)
Landsat TM 4	790–900	$Turbidity = 16.1 * R - 12.7$	~5	0.76	Fraser (1998)
MODIS 2	841–876	$\ln(SSC) = (43.233 * R) + 1.396$	2500	0.75	Wang et al., (2008)
Espectrômetro de Campo	782	$Turbidity = 1181 * R^2 + 4062 * R$	~2.5	0.72	Holyer (1978)
Espectrômetro de Campo	R1=652 R2=782	$Turbidity = 233.7 * R1^2 - 1384 * R2^2 + 1120 * R1 + 4853 * R2 - 5.08$	50	0.67	Holyer (1978)
CASI Channel 11	755.5–780.8	$SSC = 529 * R$	2000	0.65	Wass et al., (1997)
AHS Advanced Hyperspectral Sensor	R1=819–847 R2=989–1019	$\ln(TSM) = 34.18 * (R1 - R2) + 3.16$	336	0.60	Sterckx et al., (2007)
Sea WiFS	R1=660–680 R2=545–565	$SPM = 17.783 * (\frac{R1}{R2})^{1.11}$	~20	0.47	Miller et al., (2007)
IKONOS red	632–698	$Turbidity = 0.078 * R - 8.7$	~1	0.44	Hellweger et al., (2007)
Landsat TM 3	630–690	$Turbidity = 10.0 * R - 24.8$	~5	0.43	Fraser (1998)
Landsat TM 1	450–520	$Turbidity = 19.0 * R - 97.9$	~5	0.43	Fraser (1998)
Field Spectrometer	652	$Turbidity = 33.96 * R^2 + 5352 * R - 4.38$	~2.5	0.43	Holyer (1978)
MODIS 1	620–670	$Turbidity = 12.039 * R^{1.087}$	~1	0.43	Chen et al., (2007)
Landsat TM 2	520–600	$Turbidity = 6.4 * R - 28.0$	~5	0.39	Fraser (1998)

CMODIS	R1=540–560 R2=660–680	$\text{Log}_{10}S = 0.892 + 6.2244 * (\frac{R1 + R2}{R1/R2})$	~1000	0.36	Han et al., (2006)
Landsat TM 3	630–690	$SSC = 69.39 * R - 201$	1150	0.36	Islam et al., (2001)
Landsat MSS 1 and 2	R1=500–600 R2=600–700	$\ln(SSC) = -9.21 * (\frac{R1}{R2}) + 2.71 * (\frac{R1}{R2})^2 + 8.45$	~150	0.34	Ritchie & Cooper (1991)
MOS/MESSR	R1=510–590 R2=610–690	$\ln(SSC) = -4.8 * (\frac{R1}{R2}) + 0.9 * (\frac{R1}{R2})^2 + 10.4$	1000	0.33	Topliss et al., (1990)
Landsat TM 3	630–690	$\text{Log}_{10}S = 0.334 + 0.098 * R$	30	0.32	Keiner et al., (1998)
Landsat MSS 5	600–700	$R = 0.16 + 0.03 * \ln(S)$	30	0.32	Aranuvachapun & Walling (1988)
MODIS 1	620–670	$\ln(SSC) = 50.171 * R - 1.523$	~2500	0.31	Wang et al., (2008)
MODIS 1	620–670	$TSM = -1.91 + 1140.25 * R$	60	0.31	Miller & McKee., (2004)
MODIS 1	620–670	$R = 7.5 * \log(SSC) + 1.6$	500	0.31	Chu et al., (2009)
Landsat TM 2 and 3	R1=520–600 R2=630–690	$TSM = 0.7581 * e^{61.683 * (\frac{R1+R2}{2})}$	50	0.30	Dekker et al., (2001)
Landsat TM 1 and 3	R1=450–520 R2=630–690	$TSS = 0.0167 * e^{12.3 * (\frac{R2}{R1})}$	35	-0.05	Lathrop et al., (1991)

Note: The equations are written as they were published, where SPM = Suspended Particulate Matter, SSC = Suspended Sediment Concentration, SS = Suspended Solids and TSS: Total Suspended Solids. Ri is the reflectance of water for a given wavelength. To equations measuring turbidity, the maximum values shown in column 4 were converted to values SSC in order to facilitate comparison.

3. DISCUSSION

SSC mapping using remote sensing is currently well established and routine, and the existing algorithms, although very different, show robust and consistent values. The generation of products has matured from the "basic" level of snapshots to now contemplate the time series for fixed locations and composite multispectral images now contemplate the time series for fixed locations and composite multispectral images.

Based on section 2 tables we see that basically there are no methods or algorithms for sensing suspended sediment concentration that are more suitable for use in continental waters than in coastal waters (both can use single band or band ratio algorithms). The main factors for the choice of methods or algorithms depend on the concentration of sediments in the sample as well as the most suitable satellite, regarding mainly the temporal and spatial resolution than necessarily whether the waters are inland or coastal.

3.1. LIMITATIONS

Among the limiting factors of remote sensing use for SSC stand out:

- The frequent cloud cover can be a serious obstacle to the acquisition of data in many regions.

- Only information of the SSC close to the surface of water can be provided via remote sensing techniques.

- The absolute accuracy of the SSC estimation may be poor if the characteristics of the particles, particularly backscatter, are significantly different from the data set used for algorithm calibration.

- Atmospheric correction errors can have an impact on the SSC estimation, particularly in coastal areas and inland waters, with strong adjacency effects.

- The temporal coverage of polar orbiting satellite sensors, such as AVHRR, MODIS and MERIS, may be insufficient in coastal regions with tide dynamics.

4. CONCLUSION

In conclusion, the sediment concentration mapping greatly progressed in recent years, as witnessed by the appearance of new products as well as the maturation of products and applications. A few years ago the investigation was focused primarily on the development of algorithms and creating some instant maps of SSC. SSC data is a currently standard output of products from some ocean sensors and often have quality and confidence indicators. The development progressed to the use of top-level products (e.g, multi-temporal composite) and / or time series analysis. Search Challenges remain, but new and exciting prospects have been identified, in particular the use of geostationary sensors (Neukermans et al., 2008) and the the exploitation of geostatistical correlations in space and time (Sirjacobs et al., 2008).

5. REFERENCES

- Ahn, Y.-H., J.-E. Moon & Gallegos S. 2001. Development of suspended particulate matter algorithms for ocean color remote sensing. *Korean Journal of Remote Sensing* 17: 285-295.
- Althuis I. & Shimwell S. 1995. Modelling of remote sensing reflectance spectra for suspended matter concentration detection in coastal waters. *EARSEL Advances in*

- Remote Sensing*. Available at: http://www.earsel.org/Advances/4-1-1995/4-1_08_Althuis.pdf.
- Austin, R.W. 1974. The remote sensing of spectral radiance from below the ocean surface. In: Jerlov, N.G., Steemann-Nielsen, E. (Eds.), *Optical Aspects of Oceanography*. Academic Press, London, New York, pp. 317 e 344.
- Babin, M. et al. 2003. Light Scattering Properties of Marine Particles in Coastal and Open Ocean Waters as Related to the Particle Mass Concentration Light scattering properties of marine particles in coastal and open ocean waters as related to the particle mass concentration. *American Society of Limnology and Oceanography*, 48(2), pp.843–859.
- Binding C E., Bowers D G. & Mitchelson-Jacob E G. Estimating suspended sediment concentrations from ocean colour measurements in moderately turbid waters; The impact of variable particle scattering properties. *Remote Sensing of Environment*, 94(3):373-383, 2005.
- Bowers, D.G., Boudjelas, S. & Harker, G.E.L., 1998. The distribution of fine suspended sediments in the surface waters of the Irish Sea and its relation to tidal stirring. *International Journal of Remote Sensing*, 19(14), pp.2789–2805.
- Bukata, Robert P., et al. Optical properties and remote sensing of inland and coastal waters. CRC press, 2018.
- Chen, J.M. et al., 2005. Distributed hydrological model for mapping evapotranspiration using remote sensing inputs. *Journal of Hydrology*, 305(1-4), pp.15–39.
- Chen, Z., Curran, P. & Hansom, J.D., 1992. Derivative reflectance spectroscopy to estimate suspended sediment concentration., 77, pp.67–77. Available at: <http://eprints.bournemouth.ac.uk/4675/1/licence.txt>.
- Cheng, C. et al., 2013. Remote sensing estimation of Chlorophyll a and suspended sediment concentration in turbid water based on spectral separation. *Optik*, 124(24), pp.6815–6819. Available at: <http://dx.doi.org/10.1016/j.ijleo.2013.05.078>.
- Chuvieco, Emilio. Earth observation of global change: The role of satellite remote sensing in monitoring the global environment. Springer, 2008.
- Dominguez., et al. "Integrated assessment of mangrove sediments in the Camamu Bay (Bahia, Brazil)." *Ecotoxicology and environmental safety* 74.3 (2011): 403-415.
- Doxaran, D. et al., 2002. Spectral signature of highly turbid waters: Application with SPOT data to quantify suspended particulate matter concentrations. *Remote Sensing of Environment*, 81(1), pp.149–161.

- Doxaran, D., Froidefond J.-M & Castaing P. 2003. Remote-sensing reflectance of turbid sediment-dominated waters. Reduction of sediment type variations and changing illumination conditions effects by use of reflectance ratios. *Applied Optics* 42: 2623-2634.
- Doxaran, D., Froidefond J.-M., Lavender S. & Castaing P. 2002. Spectral signatures of highly turbid waters. Application with SPOT data to quantify suspended particulate matter concentrations. *Remote Sensing of the Environment* 81: 149-161.
- Doxaran, David, et al. "Spectral variations of light scattering by marine particles in coastal waters, from the visible to the near infrared." *Limnology and oceanography* 54.4 (2009): 1257-1271.
- Eisma, D., 1993. *Suspended matter in the aquatic environment*. Springer-Verlag, Berlin.
- Gault, A. G., et al. "Preliminary EXAFS studies of solid phase speciation of As in a West Bengali sediment." *Mineralogical Magazine* 67.6 (2003): 1183-1191.
- Gilerson, A., et al. "Fluorescence component in the reflectance spectra from coastal waters. Dependence on water composition." *Optics Express* 15.24 (2007): 15702-15721.
- Gordon, Howard R., Otis B. Brown, and Michael M. Jacobs. "Computed relationships between the inherent and apparent optical properties of a flat homogeneous ocean." *Applied optics* 14.2 (1975): 417-427.
- Gordon, H. R., Brown O. B., Evans R. H., Brown J. W., Smith R. C., Baker K. S. & D. K. Clark. 1988. A semianalytical radiance model of ocean color. *Journal of Geophysical Research* 93: 10909-10924.
- Gray, J.R. et al., 2000. Comparability of Suspended-Sediment Concentration and Total Suspended Solids Data. *Water-Resources Investigations Report* 00-4191, (August), p.20 pp.
- Gray J R., Glysson G D. & Turcios L M. 2000. Comparability and reliability of total suspended solids and suspended-sediment concentration data. *USGS Water-Resources Investigations Rep.* No. 00-4191.
- Han, Z., Y-Q. Jin, and C-X. Yun. "Suspended sediment concentrations in the Yangtze River estuary retrieved from the CMODIS data." *International Journal of Remote Sensing* 27.19 (2006): 4329-4336.
- Harrington J A Jr, Schiebe F R & Nix J F. 1992. Remote sensing of Lake Chicot, Arkansas: Monitoring suspended sediments, turbidity, and Secchi depth with Landsat MSS data. *Remote Sensing of Environment*, 39(1):15-27.

- Holliday, C.P., Rasmussen, T.C. & Miller, W.P., 2003. Establishing the Relationship Between Turbidity and Total Suspended Sediment Concentration. *Proceedings of the 2003 Georgia Water Resources Conference*, pp.23–24 April.
- Holyer, Ronald J. "Toward universal multispectral suspended sediment algorithms." *Remote Sensing of Environment* 7.4 (1978): 323-338.
- Hoepffner, N., & Sathyendranath S. 1991. Effect of pigment composition on absorption properties of phytoplankton, *Mar. Ecol. Prog. Ser.*, 73, 11–23.
- Hu, C., Chen Z., Clayton T. D., Swarzenski P., Brock J. C. & Muller-Karger F. E. 2004. Assessment of estuarine water-quality indicators using MODIS medium-resolution bands: initial results from Tampa Bay, FL. *Remote Sensing of the Environment* 93: 423-441.
- International Standards Organisation (ISO), 1989. Water quality - terminology.
- International Standards Organisation (ISO), 1997. Water quality - determination of suspended solids by filtration through glass-fibre filters.
- Islam, Mohammad Rezwanaul, Yasushi Yamaguchi, and Katsuro Ogawa. "Suspended sediment in the Ganges and Brahmaputra Rivers in Bangladesh: observation from TM and AVHRR data." *Hydrological Processes* 15.3 (2001): 493-509.
- Katlane, R., Nechad, B. & Ruddick, K., 2013. *Optical remote sensing of turbidity and total suspended matter in the Gulf of Gabes.* , pp.1527–1535.
- Keiner, Louis E., and Xiao-Hai Yan. "A neural network model for estimating sea surface chlorophyll and sediments from thematic mapper imagery." *Remote sensing of environment* 66.2 (1998): 153-165.
- Kirk, J.T.O., 1994. Light and photosynthesis in aquatic ecosystems. *Sec. Ed. Cambridge university press*, Cambridge.
- Kite G. & Pietroniro A. 1996. Remote sensing application in hydrological modeling. *Hydrological Science* 41: 563–591.
- Lathrop, Richard G., Thomas M. Lillesand, and Brian S. Yandell. "Testing the utility of simple multi-date Thematic Mapper calibration algorithms for monitoring turbid inland waters." *Remote Sensing* 12.10 (1991): 2045-2063.
- Lee, Zhongping, et al. "Model for the interpretation of hyperspectral remote-sensing reflectance." *Applied Optics* 33.24 (1994): 5721-5732.
- Long, C.M. & Pavelsky, T.M., 2013. Remote sensing of suspended sediment concentration and hydrologic connectivity in a complex wetland environment.

- Remote Sensing of Environment*, 129, pp.197–209. Available at: <http://dx.doi.org/10.1016/j.rse.2012.10.019>.
- Miller, Richard L., Brent A. McKee, and Eurico J. D'sa. "Monitoring bottom sediment resuspension and suspended sediments in shallow coastal waters." *Remote sensing of coastal aquatic environments*. Springer, Dordrecht, 2007. 259-276.
- Moore, G. F., Aiken J. & Lavender S. J. 1999. The atmospheric correction of water colour and the quantitative retrieval of suspended particulate matter in Case II waters: application to MERIS. *International Journal of Remote Sensing* 20: 1713-1734.
- Morel, André, David Antoine, and Bernard Gentili. "Bidirectional reflectance of oceanic waters: accounting for Raman emission and varying particle scattering phase function." *Applied Optics* 41.30 (2002): 6289-6306.
- Nechad, B., V. De Cauwer, Y. Park, and K. Ruddick. 2003. Suspended Particulate Matter (SPM) mapping from MERIS imagery. Calibration of a regional algorithm for the Belgian coastal waters. MERIS user workshop, 10-13th November 2003. European Space Agency.
- Nechad, B. et al., 2004. Suspended Particulate Matter (SPM) mapping from MERIS imagery. Calibration of a regional algorithm for the Belgian coastal waters. European Space Agency, (Special Publication) ESA SP, (549), pp.43–48.
- Nechad, B., Ruddick K. G., Park Y., & Van Mol B. 2008 (in preparation). Total Suspended Matter (TSM) mapping from MERIS, MODIS and SeaWiFS imagery. Calibration of a regional algorithm for the Belgian coastal waters.
- Neukermans, G., Nechad B. & Ruddick K. 2008. Optical remote sensing of coastal waters from geostationary platforms: a feasibility study. *Ocean Optics 2008 CDROM*.
- Nooren, K., Hoek, W. Z., Winkels, T. G., Huizinga, A., van der Plicht, J., Van-Dam, R., Van-Heteren, S., Van-Bergen, M., Prins, M. A., Reimann, T., Wallinga, J., Cohen, K., Minderhoud, P., Middelkoop, H. (2017): The Usumacinta-Grijalva beach-ridge plain in southern Mexico: A high-resolution archive of river discharge and precipitation. – *Earth Surface Dynamics* 5(3): 529-556.
- Ouillon, S., Forget P., Froidefond J. M. & Naudin J. J. 1997. Estimating suspended matter concentrations from SPOT data and from field measurements in the Rhone River plume. *Marine Technology Society* 31: 15-20.

- Ouillon, Sylvain, et al. "Optical algorithms at satellite wavelengths for total suspended matter in tropical coastal waters." *Sensors* 8.7 (2008): 4165-4185.
- Pietroniro, A. & Prowse, T.D., 2002. Applications of remote sensing in hydrology. *Hydrological Processes*, 16(8), pp.1537–1541.
- Preisendorfer, Rudolph W. Hydrologic optics. Vol. 1. 1976.
- Qu, L., 2014. Remote Sensing Suspended Sediment Concentration in the Yellow River. *Doctoral Dissertations.*, p.Paper 383.
- Salomonson V. 1983. Water resources assessment. In *Manual of Remote Sensing*, Colwell J (ed.). *American Society of Photogrammetry and Remote sensing: Bethesda, Maryland*; 1497–1570.
- Ritchie J C, Schiebe F R. & McHenry J R. 1976. Remote sensing of suspended sediments in surface waters. *Journal of American Society of Photogrammetry*, 42(12):1539-1545.
- Ritchie J C., Cooper M C. & Yongqing J. 1987. Using landsat multispectral scanner data to estimate suspended sediments in Moon Lake, Mississippi. *Remote Sensing of Environment*, 23(1):65-81.
- Ritchie J C., Cooper M C. & Schiebe F R. 1990. The relationship of MSS and TM digital data with suspended sediments, chlorophyll, and temperature in Moon Lake, Mississippi. *Remote Sensing of Environment*, 33(2):137-148.
- Ritchie J C. & Cooper M C. 1991. Algorithm for estimating surface suspended sediment concentrations with Landsat MSS digital data. *Water Resources Bulletin*, 27(3):373-379.
- Ritchie J C. & Cooper C M. 1998. Comparison of measured suspended sediment concentrations with suspended sediment concentrations estimated from Landsat MSS data. *International Journal of Remote Sensing*, 9(3):379-387.
- Schiebe F R., Harrington J A Jr. & Ritchie J C. 1992. Remote sensing of suspended sediments: the Lake Chicot, Arkansas project. *International Journal of Remote Sensing*, 3(8):1487-1509.
- Sirjacobs, D., Alvera-Azcárate A., Barth A., Lacroix G., Nechad B., Park Y., Ruddick K. & Beckers J.-M. 2008. Reconstruction of Missing Satellite Total Suspended Matter Data over the Southern North Sea and English Channel using Empirical Orthogonal Function Decomposition of Satellite Imagery and Hydrodynamical Modelling. *Ocean Optics 2008 CDRM*.

- Sobrino, J. A., and N. Raissouni. "Toward remote sensing methods for land cover dynamic monitoring: Application to Morocco." *International journal of remote sensing* 21.2 (2000): 353-366.
- Sterckx, Sindy, et al. "Retrieval of suspended sediment from advanced hyperspectral sensor data in the Scheldt estuary at different stages in the tidal cycle." *Marine Geodesy* 30.1-2 (2007): 97-108.
- Stumpf, R. P. & Pennock J. R. 1989. Calibration of a general optical equation for remote sensing of suspended sediments in a moderately turbid estuary. *Journal of Geophysical Research* 94: 14363-14371.
- Tilstone, G. & Moore G. 2002. REVAMP Regional Validation of MERIS Chlorophyll products in North Sea coastal waters: *Protocols document*.
- Topliss B J., Almos C L. & Hill P R.. Algorithms for remote sensing of high concentration, inorganic suspended sediment. *International Journal of Remote Sensing*, 11(6):947-966, 1990.
- Van der Woerd, H. & Pasterkamp, R., 2004. Mapping of the North Sea turbid coastal waters using SeaWiFS data. *Can. J. Remote Sensing* 30(1), pp. 44-53.
- Vos, R.J., Ten Brummelhuis, P.G.J. & Gerritsen, H., 2000. Integrated data-modelling approach for suspended sediment transport on a regional scale. *Coastal Engineering*, 41(1-3), pp.177–200.
- Xiao Q., Wen J G., Liu Q H. & Zhou Y. 2006. Study on spectral unmixing model and it's application in extracting chlorophyll concentration of water body, *J. Remote Sens.* 10 559–567.
- Yuming Y. & Min H. 1992. Remote sensing analysis of the suspended sedimenttransport in Lingdingyang. *China Ocean Engineering*, 6(3):331-349.
- Zhang, Minwei, et al. "Retrieval of total suspended matter concentration in the Yellow and East China Seas from MODIS imagery." *Remote Sensing of Environment* 114.2 (2010): 392-403.
- Zeng, Q.Y. 1994. *Weak Signal Detection*, 2nd ed. ed.; Zhejiang University Press: Hangzhou, China; pp. 256–261.
- Zhou, Z., Bian, C., Wang, C., Jiang, W., Bi, R. (2017): Quantitative assessment on multiple timescale features and dynamics of sea surface suspended sediment concentration using remote sensing data. – *Journal of Geophysical Research: Oceans* 122: 8739-8752.

Wass, P. D., et al. "Monitoring and preliminary interpretation of in-river turbidity and remote sensed imagery for suspended sediment transport studies in the Humber catchment." *Science of the Total Environment* 194 (1997): 263-283.

ARTIGO II

Study on remote sensing methods for suspended sediment concentration SSC in large rivers with mobile sandbanks. The case of the Araguaia river - Brazil

A. Holdefer, K. Formiga, M. Bayer & N. Ferreira
University of Goiás, Goiás, Brazil

KEY WORDS: SSC, Sentinel-2, Landsat, Araguaia River, Suspended Sediment

ABSTRACT

The present study proposes a new methodology for the remote sensing of suspended sediment concentrations (SSC) in large rivers with mobile sandbanks. This is obtained by determining the areas with greater depths along the water body in order to have an extraction of SSC values without contamination of the bottom reflection in such rivers. This study particularly used the present method for quantitative analyzes for the concentration of suspended sediments along the Araguaia River – Brazil. In particular, the Araguaia River plays an important role in the Brazilian environment as one of the main rivers, with a length of approximately 2,627 km and being well known for its mobile sandbanks.

Our results revealed an expressive variation in SSC due to the tropical wet-dry climate, and an important variation along the Araguaia River, during the rainy season, caused by geologic characteristics of Bananal Island. The approach here presented in this work can be adapted to monitor SSC values in large bodies of water across the world and can be expanded to obtain other important indices for the morphological and biological characterization of water bodies with mobile sandbanks such as chlorophyll, turbidity, nitrates, among others.

Keywords: SSC, Sentinel-2, Landsat, Araguaia River, Suspended Sediments.

1. INTRODUCTION

SSC has important implications in the geomorphological and ecological dynamics of several aquatic systems, such as rivers and seas (Zhou et al., 2017), also being an important natural part of river system and playing an essential role in structuring the landscape, creating ecological habitats and transporting nutrients. It is also a common management problem where changes in the quantity and quality of sediments has a negative impact on ecological communities, increasing the risk of flooding and shorten the life of the infrastructure (Vercruysse et al., 2018).

The quantification of SSC in large rivers, such as Araguaia River, is vital for the study of hydrological, geomorphological and ecological functioning of alluvial plains and deltas. The main applications include the optimization of dredging operations, evaluation of the environmental impact of construction activities, understanding of geomorphological changes, evaluation of river nutrient fluxes to the sea among others.

Therefore, valid observations of the values as well spatial variations of suspended sediment concentrations (SSC) should be obtained to improve the understanding of the dynamics of hydrological systems and to allow the development of effective monitoring methods (Volpe et al., 2011).

In situ measurements using the gravimetric analysis technique produce fairly accurate SSC values. The values obtained from filtered sediments are usually considered the correct concentration that should be used for the calibration of the values measured by other methods (Guillén et al., 2000). Despite the accuracy of the local measurement method, the cost and time required to acquire these samples are high and the logistics required are usually quite complex, resulting in samples with limited spatial and temporal distribution (Montanher et al., 2014).

In situ measurements and remote sensing techniques via satellite are standard methods of obtaining estimates of SSC values.

Remote sensing has been shown to have the ability to retrieve suspended sediment concentration SSC from bodies of water. The concentration of suspended sediments SSC is an constituent of water that has optical characteristics thus allowing measurement via remote sensing. However, the direct and accurate extraction of SSC values for large bodies of water presents some challenges.

The advent of remote sensing by satellites allowed over the years the increase in availability of data from different satellites and created new opportunities to monitor

large rivers from space, providing an enormous opportunity for geomorphologists to study the temporal and spatial dynamics of large rivers.

Remote sensing has an immense potential to contribute to the identification of variants occurring in large hydrological systems. The optical quality indicators of water obtained through remote sensing have the ability to enable water managers to monitor large bodies of water in a promising and economical way.

Several spectral indices were developed over the years to estimate turbidity, suspended particulate matter, suspended sediment concentration in water, among others (Zhao et al., 2018). The methods of optical remote sensing are generally divided into passive and active. Passive methods typically use sensor spectrometers embedded in the satellite to measure the radiance entering through the sensor aperture. SSC values can be obtained through passive remote sensing, through calibration using sufficient auxiliary measurements available at the site studied. An extensive literature has validated the use of remote sensing data from satellites to estimate SSC values (Montaner et al., 2014; Curran et al., 1998; Giardino et al., 2015). The estimation of SSC values through passive remote sensing is developed, generally for use in coastal waters; since the low spatial resolution satellite sensors are generally unsuitable for applications in continental rivers and lagoons and are usually suitable for open sea (Volpe et al., 2011).

Over the years, the unavailability of satellite sensors that offered high spatial and radiometric resolutions and reasonable time to revisit prevented the use of this technology in monitoring the water quality of the rivers.

The latest generation of medium to high resolution multispectral space sensors present in the Sentinel2 satellites allows an acceptable spatial and temporal resolution in the acquisition of the spectral bands necessary for the estimation of SSC present in the bodies of water under analysis.

The effectiveness of remote sensing as an information source for the quantitative analysis of the SSC in Araguaia River has been studied using Sentinel2 images collections. In the present article, it is shown that the latest generation of sentinel2 data enables the efficient monitoring of the Araguaia River by estimating the suspended sediment concentration (CSC) along the river. Thus, a complete image-based method for quantitative analysis is presented.

To perform the present work and obtain reliable values of SSC along the river, sediment data available from the hidroweb system, which has historical data of the Brazilian hydrometric network under the management of the Brazilian water agency

(ANA, 2017) were used, to cross-reference these data with the derived index values obtained from Sentinel2 images and to perform the correct calibration of SSC values.

The sediment estimation methods of remote sensing must be used together with river bathymetry estimation. These methods are required in cases such as inaccessible rivers or large-scale depth mapping. Rivers such as Araguaia and others are well known for having many mobile sandbanks, which move along the seasons and years, commonly turning deep areas shallow and vice versa (Figure 1). In this way a satellite image-based algorithm for estimating river bathymetry for each image was developed to determine the deeper areas of the river, so as not to allow the pollution of the SSC measurement values due to the reflectance of the sediments of the river bottom.

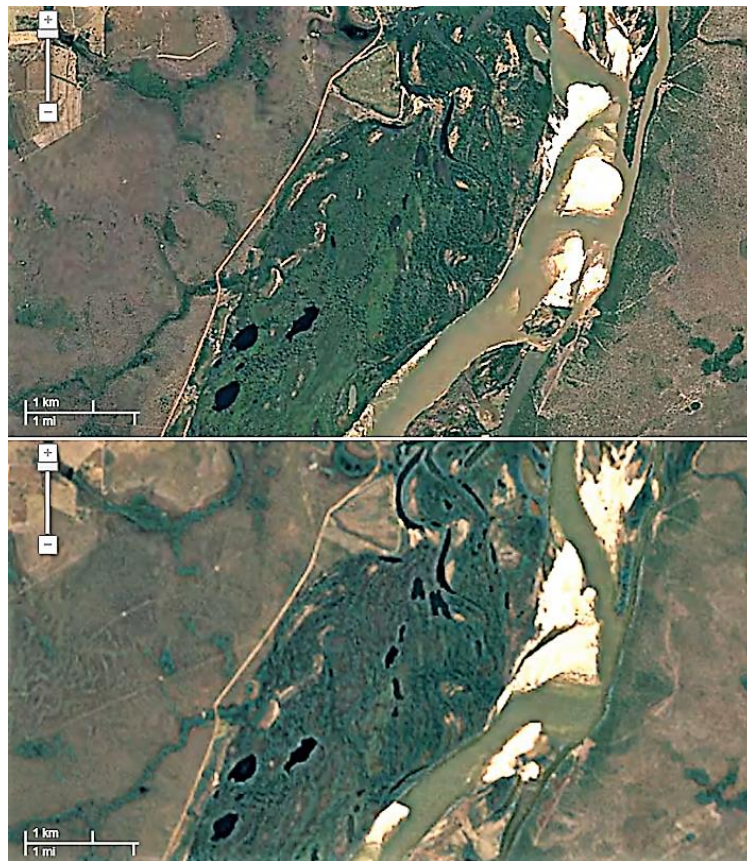


Figure 1: Mobile Sandbanks on the Araguaia River for the city of Sao Felix do Araguaia in the years 2009 (below) and 2016 (above). Location: (Lat: -11.640674, Long: -50.663634).

The method presented here can be expanded to other indexes of great relevance for the study of the geomorphological and biological aspects of large rivers with mobile sandbanks, such indexes of major importance are chlorophyll, nitrates, turbidity, among others.

In the present article, it was hypothesized that the method presented was practical when used in the Araguaia River and could raise interesting characteristics of

the geology along the river as well as monitoring temporal changes in its margins, such as deforestation, agriculture or cattle breeding that could increase the deposition of sediments along the river, consequently increasing SSC values.

2. AREA OF STUDY

The study area is in the Araguaia - Tocantins depression, in the states of Mato Grosso, Tocantins, Pará and Goiás, Brazil. The total length of Araguaia river is approximately 2,627 km, and is located as shown in Figure 2, which also shows the location of the sediment monitoring stations along the river, which will be used later in section 4.3 for the calibration of the values collected through the use of the index analyzed in section 3.1 and derived from satellite images, Figure 2 also shows basin altimetry for a better understanding of the region under study.

The Araguaia river basin has an area of approximately 377,000 km², and its annual average flow is 6,420 m³/s (Latrubesse et al., 2002).

The rainfall regime in the Araguaia river basin is determined by two well-defined seasons, the dry season and the rainy season (Aquino et al., 2008). During the rainy season the speed of flooding is rapid, connecting the adjacent lakes for short periods of time. The Araguaia basin has two of the main Brazilian biomes, the Amazon biome at north and the Cerrado biome at south (Aquino et al., 2005).

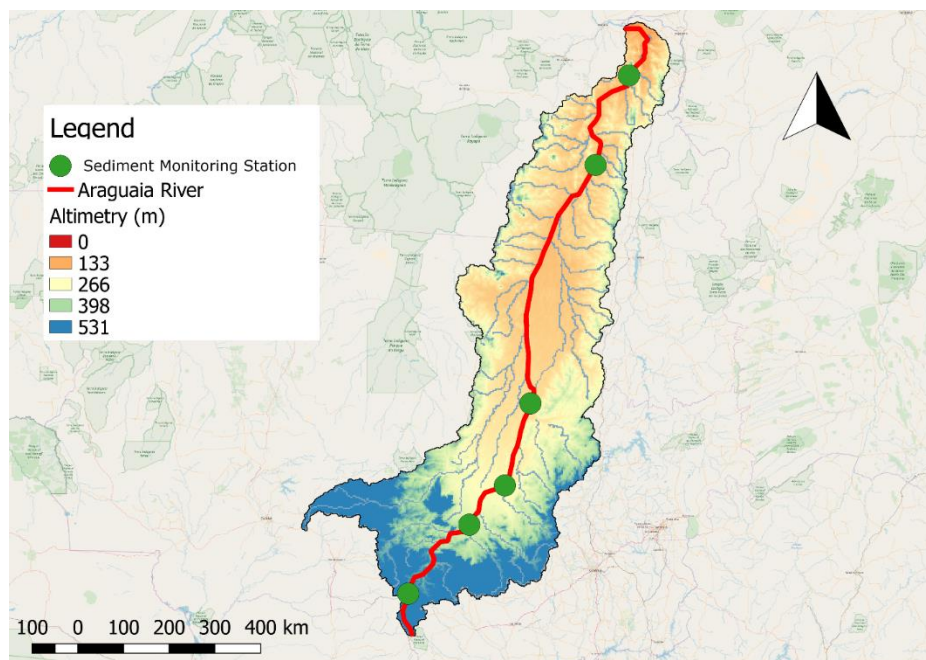


Figure 2: Map of the Araguaia River watershed with the sediment monitoring stations.

The dry season period in the Araguaia river basin occurs from May to September and the rainy season from October to April, corresponding to the flood season. The annual precipitation in the region ranges from 1,300 to 2,000 mm, with about 95% of the annual precipitation between October and April (Aguas, 2012). The flood of the river occurs a little after the beginning of the rainy season, usually occurring from November to May (Latrubesse et al., 2002). The biome that prevails in most of the Araguaia river basin is classified as Cerrado, known as the Brazilian savannah, although a small portion of the northern part of the basin is characterized as an Amazonian biome.

The Cerrado is known for its high biodiversity (Myers et al., 2000) and includes pastures, forests and flooded vegetation (Sano et al., 2010). However, in recent decades the Araguaia River basin has been dramatically affected by changes in land use for pasture and agriculture, particularly in the Cerrado biome (Sano et al., 2010). Several parts along the Araguaia River are preserved by national parks and forest reserves, such as the well-known Emas National Park and Araguaia National Park.

3. METHODS

The first studies on the use of remote sensing to obtain SSC values were mainly focused on the discovery of the relationship between the concentration of suspended sediments in water and the corresponding spectral reflectance values, such deduction being based on empirical methods (Ritchie et al., 1990, Chen et al., 1992, Harrington et al., 1992, Ritchie et al., 1987). The method of obtaining SSC values through the use of remote sensing is obtained by crossing the characteristics of the radiation reflected by the water with the values of the sediment concentration present in water. In general, the typical reflectance values of water as a function of the SSC values present therein are as shown by the graph of Figure 3. As noted, it would appear that a useful spectral range would be between 400 and 900 nm. SSC quantification algorithms based on water reflectance can be roughly divided into the following families: single band and band ratio.

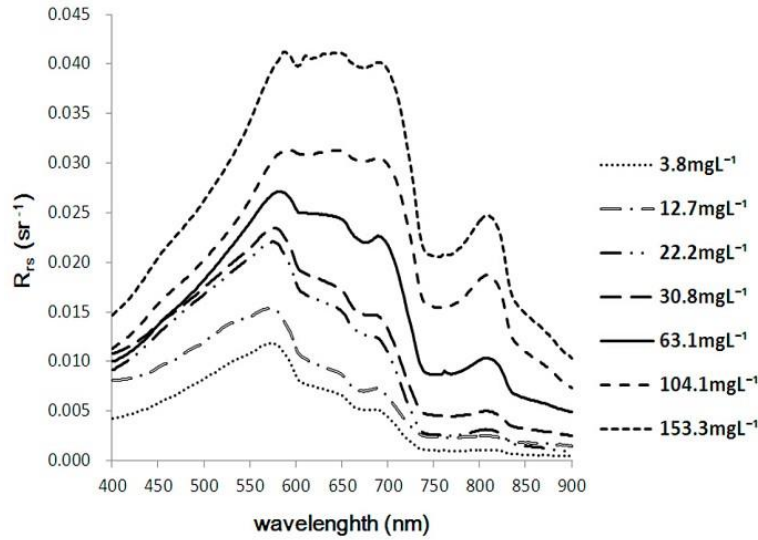


Figure 3: Reflectance values for different SSC values in water samples. Adapted (Qu, 2014)

The band ratio algorithms are less sensitive to atmospheric scattering and, therefore, are not subject to uncertainties if the scattering coefficient of air density has a high natural variability.

Rather, band ratio algorithms can be developed to be less sensitive to this natural variability since the background scattering effects is largely cancelled when the ratio between bands is made. The band ratio algorithms between two bands were suggested to estimate the SSC by (Qu, 2014).

Therefore, the band ratio algorithm is preferred in the present work, because the collection of images of the Sentinel2 satellites currently available are of top atmosphere reflectance (TOA), thus not having an atmospheric correction.

In addition to the use of individual bands, the relationship between red and green bands has also been used to estimate SSC values (Topliss et al., 1990; Yuming et al., 1992; Doxaran et al., 2009). It has also been demonstrated that the use of reflectance ratios between bands makes the measurement more robust to reduce the variational effects, such as the atmospheric reflection, the particle size present in the water column, as well as the variations of the index of refraction in water. Another advantage of using the red and green bands as proposed above is that they have a spatial resolution of 10m for the sentinel2, this is significant since the width of the Araguaia River varies along its path and it's very known for having sandbanks all over its path, being an small spatial resolution necessary to skip areas that can contaminate the measurements not related with SSC.

Comparing the images of Sentinel2 with Landsat8 in Figure 4, it is clear to observe the significant differences in the sizes of the pixels, evidencing the preference for the choice of Sentinel2 images. In Figure 4 the larger square represents one pixel of the Landsat8 image and the smaller square one pixel of the Sentinel2 image. From this image, it is clear that by using Sentinel2 images it is easier to avoid areas of sandbanks that can contaminate measurements and are not related to SSC values.



Figure 4 – Image pixel size comparison between Sentinel2 (smaller square) and Landsat8 (bigger square), showing that Sentinel2 images are more suitable for the required application.

Three different indices will be analyzed in this article to verify the most convenient for using in SSC estimates.

3.1 NSMI INDEX

The index derived from the ratio between bands suggested to be used in this article is the NSMI (Equation 1) presented in (Montalvo, 2010; Fiuza et al., 2011). This index was developed based on the fact that the clean water has a peak of reflectance in the blue band (ρ_{blue}), while the concentration of suspended sediments SSC promotes an increase of the reflectance in all visible bands, especially in the green band and red ($\rho_{\text{green}} + \rho_{\text{red}}$) where clean water tends to absorb radiation rather than reflect (Fiuza et al., 2011). The equation is derived by summing the spectral response of the red and green

bands and subtracting the blue band, and then dividing the result by the sum of the red, green and blue bands, in order to normalize the result. The equation gives values between -1 and +1. Lower values correspond to cleaner water, while higher values correspond to water with more presence of suspended sediments.

$$NSMI = \left(\frac{\rho_{red} + \rho_{green} - \rho_{blue}}{\rho_{red} + \rho_{green} + \rho_{blue}} \right) \quad (1)$$

3.2 NDSSI INDEX

The NDSSI index has been used by many authors (Hossain, 2010) to derive models of suspended sediment cocentration in diverse water bodies. The index is obtained by subtracting the near infrared band (ρ_{nir}) from the blue band (ρ_{blue}) and the divining the by the sum of both bands (Equation 2). NDSSI ranges from -1 to +1, where higher values indicate the presence of clearer water and lower values indicate more presence of sediments in suspension (Hossain, 2010).

$$NDSSI = \left(\frac{\rho_{nir} - \rho_{blue}}{\rho_{nir} + \rho_{blue}} \right) \quad (2)$$

3.3 BAND RATIO GREEN/BLUE

For this index, the green band is used because the suspended sediment concentration in the water (SSC) increases the reflectance in the green spectrum (ρ_{green}), while clearer water present the peak reflectance in the blue spectrum (ρ_{blue}). The index ranges from 0 to infinity. Where higher values indicates the presence of more suspended sediments and lower values indicate clearer water (Aber, 2011).

$$GREEN/BLUE = \left(\frac{\rho_{green}}{\rho_{blue}} \right) \quad (3)$$

3.4 SPECTRALLY-BASED DEPTH RETRIEVAL

The Araguaia river has several sandbanks that usually appear between May and October every year. They are most common during the dry season and may also occur during the rainy season. As these banks are constantly moving, many deep areas of the river become shallow and vice versa. The use of remote sensing for the estimation of the concentration of suspended sediment (SSC) in shallow water should therefore consider the influence of background reflection, as it has a great influence on the estimated values of SSC.

Remote sensing techniques have been used to perform river bathymetry. Non-contact methods for depth estimation in rivers are required in several cases, such as: large-scale mapping and inaccessible regions. Firstly, these techniques were developed for marine environments and later adapted to rivers and other continental water bodies. The techniques of remote bathymetry can be divided into two types: active and passive. The active method, using radar and passive, using multispectral satellites with the use of radiometric models, for example. The passive technique consists in finding a logarithmic relationship between the depth of the river and the values of the spectral bands of the satellite image. This can be achieved using more recent multispectral satellites with good spatial and temporal resolution, such as Landsat8 or Sentinel2, seems to be the most widely used technique.

To avoid sandbanks and shallow water areas, a method was suggested to choose the deeper areas along the river. This method is derived in the following way: according to the Beer's Law, light is attenuated exponentially in relation to the water depth. See Equation 4.

$$L(z) = L(0)e^{-Kz} \quad (4)$$

However, this relationship is exponential and can produce many uncertainties. The availability of several spectral bands allows us to estimate the depth in a qualitative way, allowing to deduce the deeper areas of different aquatic bodies. It has been shown that for certain combinations of wavelengths, the value derived from the image

$$\ln\left(\frac{R(\lambda_1)}{R(\lambda_2)}\right) \quad (5)$$

is linearly related to depth (Legleiter et al., 2009). Thus, equation 5 is used to identify (estimate) deep waters to ignore shallow waters to avoid reflectance values from the river bottom that could profoundly affect the SSC measurements along the body of water.

3.5 ACQUISITION POINTS

Eighty points were chosen along the river for remote measurement as shown in Figure 5. The points were selected to avoid clouds and shallow spots along the river, to ensure a good reliability in the obtained data. These points are covering most of the river, over 2000 km, except at the beginning of the river, which is very narrow and shallow and does not allow a reliable reading of the data, having contamination by bottom reflectance and riparian vegetation. All images along the river in the dry and rainy season for the years 2016, 2017 and 2018 were respectively taken on the same day, taking advantage of the fact that the sentinel2 path covers exactly the river path, as shown in Figure 3. This increases the confidence level in the estimated data, since we can produce a mosaic of same-day images for the SSC estimation, avoiding a mosaic that can be produced by images that, in some cases, have a separation interval of one month, since the revisit time for Sentinel2 for this area is on average one month.

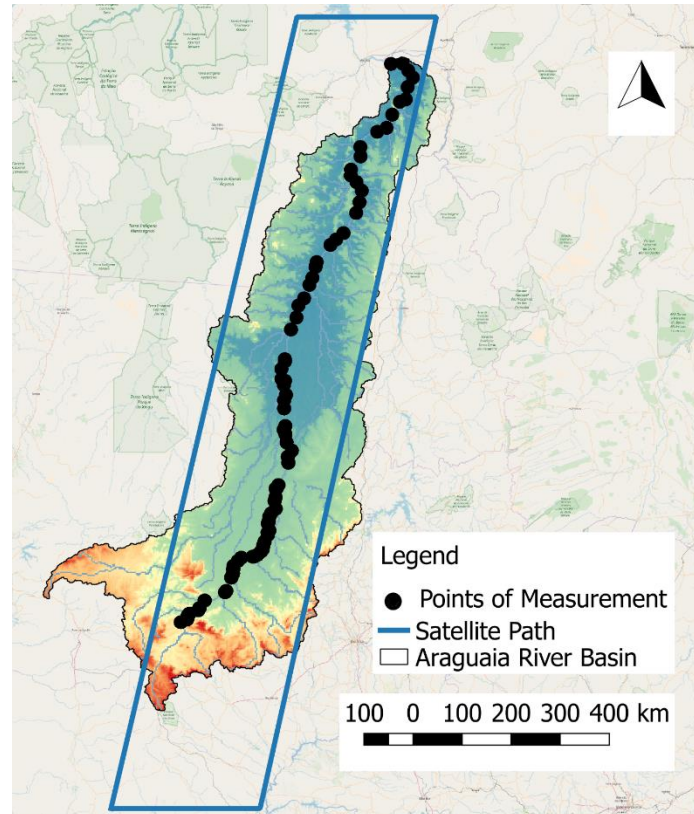


Figure 5: Points of measurement and Sentinel2 path over the Araguaia River Basin.

4. RESULTS

4.1 COMPARISON OF INDEXES

To verify the most adequate index to be used in the present study, among equations 1, 2 and 3, all three indices were plotted on the same graph. The indices were derived for the points shown in Figure 5, for March 17, 2016. The result is shown in Figure 6. As we can see, by analyzing Figure 6, all three indices have the same qualitative behavior, so we can obtain similar results by calibrating these indices with values obtained *in situ*. So, in that case, choosing an index to use is a matter of convenience. Thus, in this work, the chosen index to be used is the NSMI.

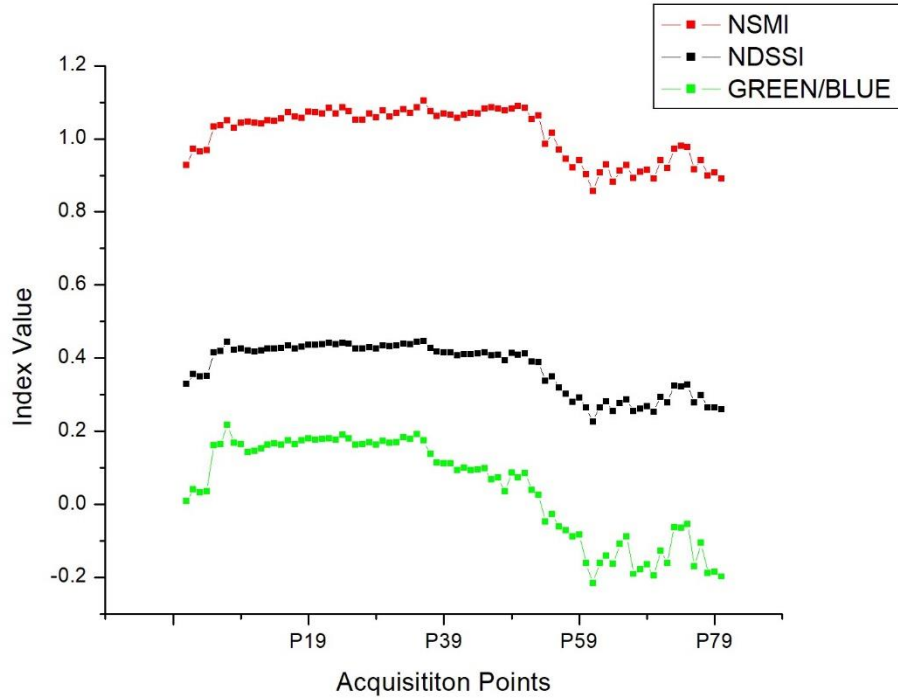


Figure 6: SSC indexes applied for the points shown in Figure 5.

4.2 WATER DEPTH RETRIEVAL

As a result of the application of Equation 5, Figure 7 shows the estimation of the depth of the river, in a section of the Araguaia River. For this, the green and red bands of the Sentinel2 image were used. In Figure 7 the reddest areas correspond to shallower areas and bluer areas correspond to deeper areas. The black spot corresponding to the deepest location in this section of the river, which was used to estimate the SSC value, so as to have little or no influence of the river bottom reflection. This method was validated by visual inspection of some images, verifying the location of the bluest areas at the deepest points.

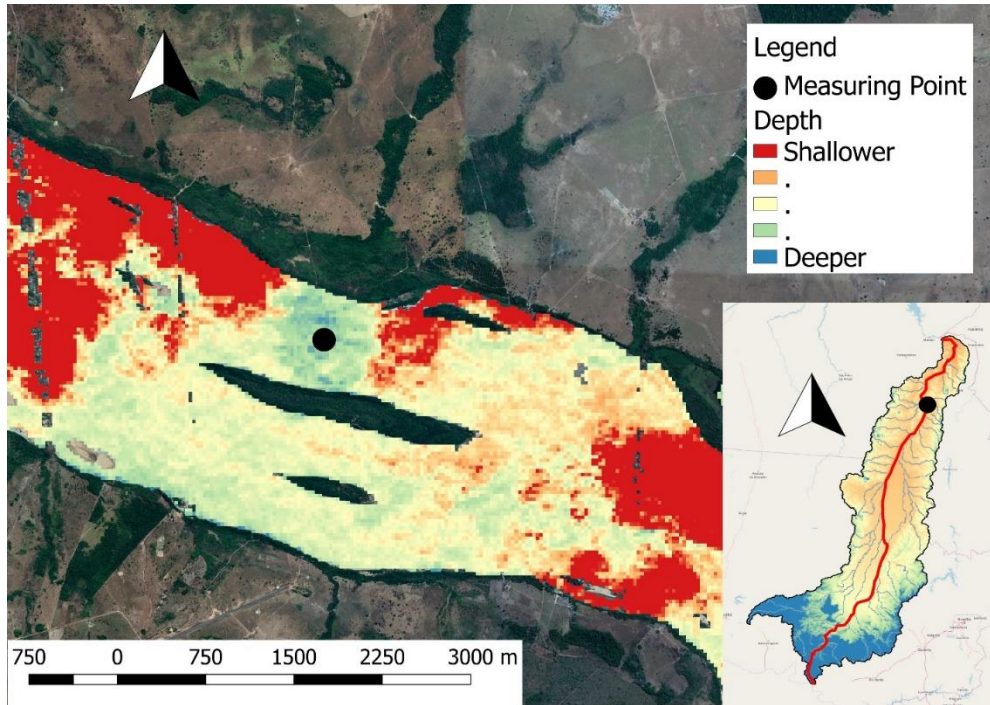


Figure 7: Depth retrieval. Color scalebar from shallow areas to deeper areas. The black dot shows where the measurement takes place.

4.3 CALIBRATION

To perform the calibration, suspended sediments data, available in the Brazilian hydrometric network under the management of the Brazilian water agency (ANA, 2017) were used. However, sediment data are scarce, and often do not match satellite passage day, while flow information is available for most days and for most sediment monitoring stations. For such a way, sediment key curves were used to relate solid discharge to flow for the determination of SSC values, as shown in (Veiga et al., 2015), obtaining enough data to carry out the calibration. Landsat images were used for calibration, the reason being that Landsat images have been available since 1984, while Sentinel2 images have only been available since 2015, so this is necessary for better and more consistent calibration of the data.

To have a consistent estimate of SSC for the Araguaia River, it was decided to use the data of sediment monitoring stations along the river, since available, as shown in Figure 2, with the locations tabulated in the table 1.

Thus, the estimated SSC values obtained through the flows (Veiga et al., 2015) were crossed with the respective NSMI index values for respective days. It was decided to acquire data in 30 different days, to better visualize the trend of the data. The

acquired results are plotted in Figure 8, as well as the best fit curve with the respective equation.

Table 1: Location of sediment monitoring stations, with average flow and drainage area information.

Station	River	Lat-Long	Drainage Area (km ²)	Average Annual Flow (m ³ /s)
Cachoeira	Araguaia	-53.1386, -17.1611	4504	88
Araguaiana	Araguaia	-51.8278, -15.7363	50930	871
Aruanã	Araguaia	-51.0866, -14.9204	76964	1185
Luiz Alves	Araguaia	-50.5850, -13.2142	117580	1720
Conceição	Araguaia	-49.2517, -8.2625	320290	5306
Xambioá	Araguaia	-48.54876, -6.4064	364500	5585

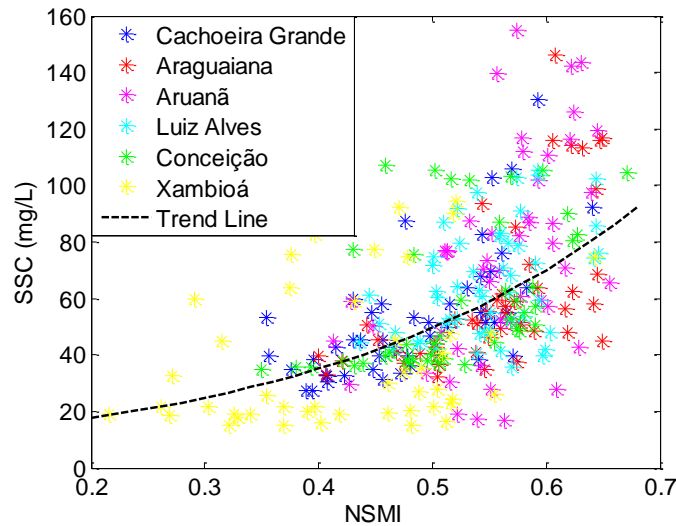


Figure 8: NSMI index versus SSC for different sediment monitoring stations.

The best fit curve that relates the SSC and the NDSSI index was derived, as shown in (Equation 6) with the respective Coefficient of Determination (R^2).

$$CSS = 147 * NSMI^{1.451} \quad (6)$$

with a $R^2 = 0.3407$.
p-value = 0.2637

4.4 SSC MEASUREMENTS

The image of the dry season was taken on July 5, 2016 and the image of the rainy season was performed on March 17, 2016. Equation 6 was applied to dry and rain season images for a section of the river generating an image as shown in Figure 9, where reddest areas should indicate a higher value of SSC. However, this is a false

estimate, because these areas are also shallow areas, which can be proved by comparison with the image of the dry season, having a great influence of the bottom reflectance in the SSC estimation. The Figure 9 confirms the great necessity of the use of an algorithm for the estimation of the depth in the point of measurement, as detailed in item 3.4

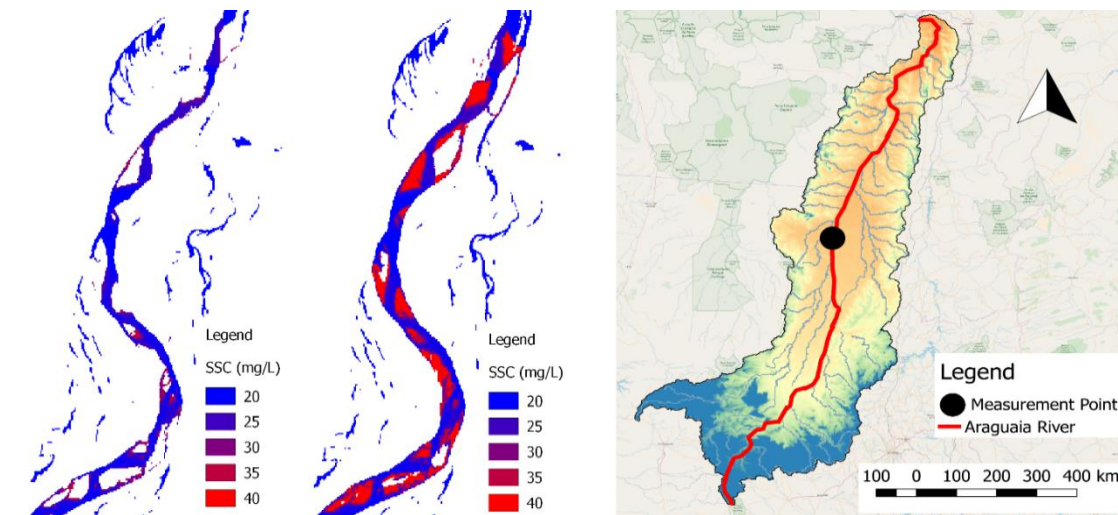


Figure 9: Dry (left) and Rain (right) season SSC for the year 2016 in a section of the river using the NSMI index – Position (-50.64835, -11.10935).

All points used to measure the SSC along the Araguaia River used the depth recovery algorithm to avoid shallow water.

The graphics were obtained from the year 2016, not before, because the date of availability of images of Sentinel2 began on June 23, 2015, and in the first months the images were scarcer due to the commissioning of the satellite images recently placed in terrestrial orbit.

Three consecutive years of data were selected to make it evident that the timeless characteristics of the sediment variation along the river were highlighted, thus masking possible temporal variations such as floods carrying sediment to the river as well as flood waves flowing along the river, among others. In this way, it was evident that the changes in the sediment variation along the river, as shown in Figure 10, are due to geological factors of the river structure, thus being timeless. Care was also taken to carefully observe the less cloudy days, to have a complete coverage of the entire river, making it difficult to obtain many images in the course of a year, due to the presence of many clouds during the rainy season. In that way they have chosen to obtain only one image for the dry season and only one image for the rainy season for each

year. The graphs for the rainy season were obtained for the end of the rainy season, around the months of May and April, where the incidence of clouds is less frequent, facilitating the data collection. The resulting three graphs, one for each year of 2016, 2017 and 2018, are shown in Figure 10.

From those graphs we can conclude the following:

The Rainy season has a higher value of SSC;

During the rainy season SSC suddenly drops after the point P49.

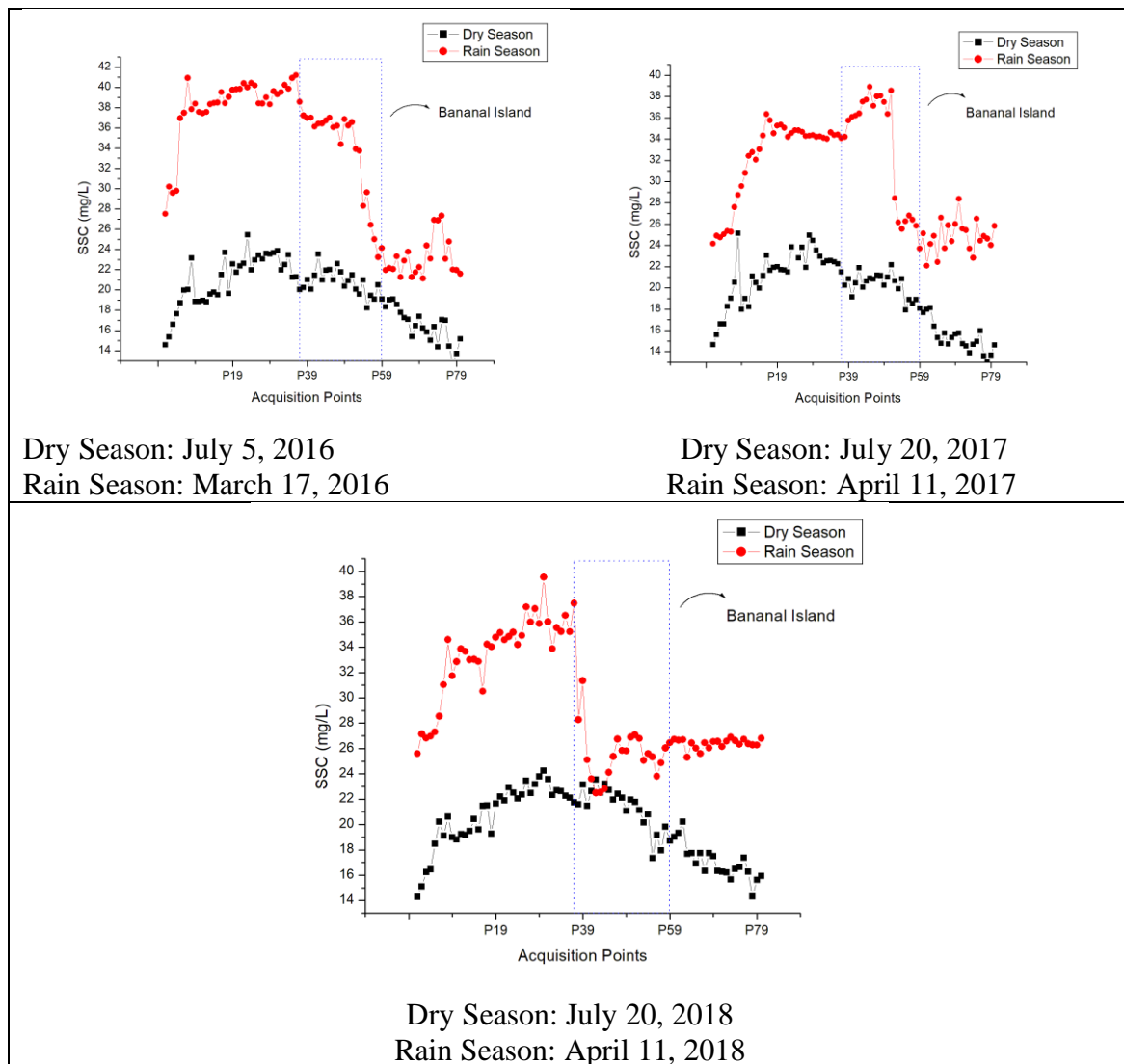


Figure 10: The SSC in the rain and dry season for three consecutive years (2016,2017,2018) showing where the Bananal Island begins and ends.

After a brief verification, it was observed that such an alteration occurs over an area known as Bananal Island (Figure 11). In order to confirm it, a section was drawn over each graph to show where exactly the Bananal Island begins and ends. This is shown in the Figure 10.

5. A GEOLOGICAL EXPLANATION

To explain the changes in the concentration of suspended SSC sediments along the river, a study of the river's geology was carried out in order to search for logical responses, as shown below.

Bananal Island is a river island, located on the Araguaia River, with an area of approximately twenty thousand square kilometers. The Island of Bananal is formed from the bisection of the river Araguaia, in the southwest of the state of Tocantins, Brazil. The island is formed by a fork in a very flat section of the river Araguaia. The size of Bananal Island is 350 kilometers long and 55 kilometers wide, being considered by some to be the largest river island in the world (Latrubesse et al., 2002). All regions in the middle course of the Araguaia River have a tendency to sedimentation, based on studies of gravimetry and seismic anomalies (Hales, 1981), which also interpreted as the deepest part of the island of Bananal the region between the city of Luiz Alves and the southern part of Bananal Island.

So, basically the large depth of sediments associated with the constant seismic anomalies shaped the Bananal Island to be very flat and low, as showed in Figure 11, where it is evident through the map of hypsometry of the Araguaia river basin, that in this region of banana island is low-altitude floodplain. Thus, putting in simple words we can assume that the sediments flowing through the Araguaia River suffer a slowdown in speed as they reach Bananal Island and after some kilometers they precipitate in the bottom of the River, decreasing the value of SSC in this region.

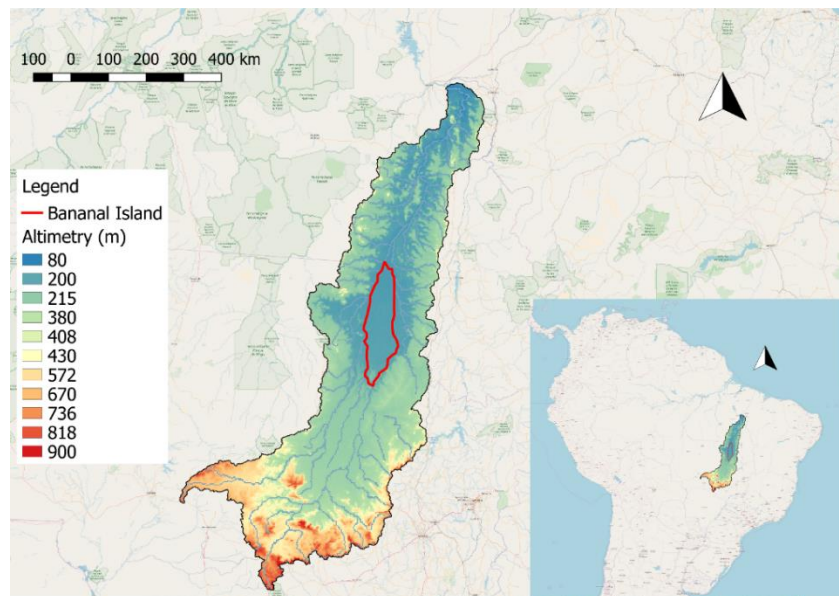


Figure 11: Hypsometry map of the Bananal Island.

6. DISCUSSION

This study demonstrates that the remote sensing multi-band technique can be a useful tool to monitor the distributions of suspended sediment concentration in large rivers. In this study, the NSMI index proved to be the most adequate for monitoring the concentration of suspended sediments. Correlation analysis between remotely detected data and suspended sediment concentrations SSC measured In-situ indicated the possibility of accurately mapping suspended sediment concentration along large scale rivers with mobile sandbanks.

The developed method also employs depth estimation techniques in order to collect suspended sediment information only in deep river regions, due to the high variability of the sandbanks' position over the seasons and years, allowing a high reliability of that the information acquired about the concentration of suspended sediments SSC was not polluted due to the reflectance of the bottom of the body of water.

The use of sentinel2 satellite imagery instead of using Landsat8 images also allowed greater data accuracy and reliability by restricting the collection of information from the body of water to a 10x10m area as opposed to using Landsat8 images that would be restricted to an area 9 times larger in a 30x30m square, allowing the diversion of obstacles that could pollute the measurement, such as sandbanks and vegetation along the river bank..

The method developed in the present article was applied to a large brazilian river known for its movable sandbanks - the Araguaia River. And after applying the method in 3 consecutive years, as much during the rain season as during the dry season, there was a clear variation of the concentration of suspended sediments SSC along the river, with an expressive reduction in the concentration of suspended sediments SSC along of an area called Bananal Island, this area is characterized by a floodplain geology, being fairly flat and uniform, acting as a sediment trap as the sediment flow traveled over its area, thus significantly reducing the concentration of suspended sediment concentration SSC that precipitate in the bottom of the river.

A strong relationship between the variation of SSC concentration along the Bananal Island and its geology was obtained and could satisfactorily answer the questions raised. The achievement of these values throughout almost the entire river

course was only possible due to the availability of the new series of Sentinel2 satellites with spatial resolution of 10m and with data collected for the entire river at the same day for both the dry and rain seasons for the years 2016, 2017 and 2018.

Therefore, the efficacy of the method in obtaining important information about the body of water based on SSC information has been proven.

7. CONCLUSION

The proposal of the present study of presenting a new and complete method of measuring the variations of the suspended sediment concentration of SSC along large rivers with characteristics of having mobile sandbanks has been fully met.

The choice of the new generation of Sentinel2 satellites, launched in 2015, proved to be correct, due to its greater spatial resolution, allowing a higher accuracy of the values retrieved in such bodies of water, which are known for the high variability of their sandbanks, producing several shallow areas that can mask the correct measurement.

In addition, a great improvement suggested in the present work was the use of an estimation of the depth at the measurement points using the same satellite images used to retrieve the SSC information. This allowed to have greater certainty about the depth at the measurement point, avoiding shallow areas that could influence in the correct measurement.

The proposed method used data measured in-situ by the Brazilian National Water Agency (ANA) to calibrate the suspended sediment concentration measurements SSC in order to have more confidence in the data derived from remote measurements by satellite images. Such step is of great importance for a greater reliability in the use of the proposed method.

The proposed method is also suitable to obtain several other indexes and its methodology can be extended, being necessary only to use other indices derived from the spectral bands of the satellites for such. Thus, important information could also be obtained from other indexes, such as chlorophyll, nitrate, turbidity and others.

In conclusion, the sediment concentration mapping over the Araguaia River using the new series of satellites Sentinel2 show to be a great tool for mapping almost the entire river, retrieving fundamental information like SSC. This tool was able to produce results that led to further conclusions related with the geology of the River.

This methodology can be further used for deriving another important indexes such chlorophyll, turbidity, and so on for different rivers and water bodies with mobile sandbanks, thus extending even more the understanding the complexity of both the biological and geological functioning of different bodies of water.

REFERENCES

- Aber, James S. 2011. Landsat Image Processing.
http://academic.emporia.edu/aberjame/remot e/landsat/landsat_proc.htm
- Aguas, A. N. das, Relatório de conjuntura dos recursos hídricos no brasil– informe 2012.
- Aquino, Sâmia, José Cândido Stevaux, and Edgardo Manuel Latrubesse. "Regime hidrológico e aspectos do comportamento morfohidráulico do rio Araguaia." *Revista brasileira de geomorfologia* 6.2 (2005).
- Aquino, Sâmia, Edgardo Manuel Latrubesse, and Edvard Elias de Souza Filho. "Relações entre o regime hidrológico e os ecossistemas aquáticos da planície aluvial do rio Araguaia." (2008).
- Chen, Zhimin, Paul J. Curran, and Jim D. Hansom. "Derivative reflectance spectroscopy to estimate suspended sediment concentration." *Remote Sensing of Environment* 40.1 (1992): 67-77.
- Curran, P.J.; Novo, E.M. The relationship between suspended sediment concentration and remotely sensed spectral radiance: A review. *J. Coast. Res.* 1998, 4, 351–368.
- Doxaran, David, et al. "Dynamics of the turbidity maximum zone in a macrotidal estuary (the Gironde, France): Observations from field and MODIS satellite data." *Estuarine, Coastal and Shelf Science* 81.3 (2009): 321-332.
- FIUZA, B. et al. Detection of suspended sediments in Grande River and Ondas River-Bahia. Brazil, Federal University of Bahia Institute of Environment Sciences and Sustainable Developments, Brazil, 2011.Montalvo, I.,2010. Spectral analysis of suspended material in coastal waters: A comparison between band math equations. gers.uprm.edu/geol6225/pdfs/l_montalvo.pdf.
- Giardino, C.; Bresciani, M.; Valentini, E.; Gasperini, L.; Bolpagni, R.; Brando, V.E. Airborne hyperspectral data to assess suspended particulate matter and aquatic vegetation in a shallow and turbid lake. *Remote Sens. Environ.* 2015, 157, 48–57.

- Guillén, J.; Palanques, A.; Puig, P. Field calibration of optical sensors for measuring suspended sediment concentration in the western Mediterranean. *Sci. Mar.* 2000, 64, 427–435.
- Hales, F. W. "Anomalias magnéticas de origem profunda na Fossa do Araguaia e no Pantanal: suas implicações geológicas." *Mineração e Metalurgia* 44.425 (1981): 24-30. ised August 2017.
- Harrington, John A., Frank R. Schiebe, and Joe F. Nix. "Remote sensing of Lake Chicot, Arkansas: Monitoring suspended sediments, turbidity, and Secchi depth with Landsat MSS data." *Remote Sensing of Environment* 39.1 (1992): 15-27.
- Hossain, A. K. M. A., Y. Jia, and X. Chao. "Development of remote sensing based index for estimating/mapping suspended sediment concentration in river and lake environments." *Proceedings of 8th international symposium on ECOHYDRAULICS (ISE 2010)*. 2010.
- Latrubesse, E. M., and J. C. Stevaux. "Geomorphology and environmental aspects of the Araguaia fluvial basin, Brazil." *Zeitschrift fur Geomorphologie Supplementband* (2002): 109-127.
- Legleiter, Carl J., Dar A. Roberts, and Rick L. Lawrence. "Spectrally based remote sensing of river bathymetry." *Earth Surface Processes and Landforms* 34.8 (2009): 1039-1059.
- Montalvo, I. "Spectral analysis of suspended material in coastal waters: A comparison between band math equations." (2010).
- Montanher, O.C.; Novo, E.M.; Barbosa, C.C. Empirical models for estimating the suspended sediment concentration in Amazonian white water rivers using Landsat 5/TM. *Int. J.Appl. EarthObs. Geoinf.* 2014, 29, 67–77.
- Myers, Norman, et al. "Biodiversity hotspots for conservation priorities." *Nature* 403.6772 (2000): 853.
- Qu, Liqin. "Remote sensing suspended sediment concentration in the Yellow River." (2014).
- Ritchie, Jerry C., Charles M. Cooper, and Jiang Yongqing. "Using Landsat multispectral scanner data to estimate suspended sediments in Moon Lake, Mississippi." *Remote Sensing of Environment* 23.1 (1987): 65-81.
- Ritchie, Jerry C., Charles M. Cooper, and Frank R. Schiebe. "The relationship of MSS and TM digital data with suspended sediments, chlorophyll, and temperature in Moon Lake, Mississippi." *Remote Sensing of environment* 33.2 (1990): 137-148.

- Sano, Edson E., et al. "Land cover mapping of the tropical savanna region in Brazil." *Environmental monitoring and assessment* 166.1 (2010): 113-124.
- Topliss, B. J., C. L. Almos, and P. R. Hill. "Algorithms for remote sensing of high concentration, inorganic suspended sediment." *International Journal of Remote Sensing* 11.6 (1990): 947-966.
- Veiga, Aldrei Marucci, et al. "Determinação da produção de sedimento através da curva-chave sedimentométrica na Bacia Hidrográfica do Rio Araguaia-GO." (2015).
- Vercruysse, K., Grabowski, R. and Rickson, R. (2018). Suspended sediment transport dynamics in rivers: Multi-scale drivers of temporal variation.
- Volpe, V.; Silvestri, S.; Marani, M. Remote sensing retrieval of suspended sediment concentration in shallow waters. *Remote Sens. Environ.* 2011, 115, 44–54.
- Yuming, You, and Hou Min. "Remote sensing analysis of the suspended sediment transport in Lingdingyang." *China Ocean Engineering* 6 (1992): 331-331.
- Zhao, Xinglei, et al. "Remote Sensing of Suspended Sediment Concentrations Based on the Waveform Decomposition of Airborne LiDAR Bathymetry." *Remote Sensing*, vol. 10, no. 2, June 2018, p. 247., doi:10.3390/rs10020247.
- Zhou, Xiaochi, et al. "Hyperspectral and Multispectral Retrieval of Suspended Sediment in Shallow Coastal Waters Using Semi-Analytical and Empirical Methods." *Remote Sensing*, vol. 9, no. 4, 2017, p. 393., doi:10.3390/rs9040393.

ARTIGO III

Temporal Analysis of Suspended Concentration for Over 30 Years in the Main Brazilian Watersheds

A.E. Holdefer & K. Formiga
University of Goiás, Goiás, Brazil

KEY WORDS: Landsat images, Google Earth Engine, Suspended Sediment Concentration; Brazilian Watersheds, Temporal Analysis, Water Reflectance, Water Pixels

ABSTRACT

This study presents a method of temporal analysis for suspended sediments in the main Brazilian watersheds for over 30 years using remote sensing. The interest in the use of remote sensing for the estimation of the sediment suspension concentration SSC is motivated by the wide spatial coverage that such tool presents, besides the relatively high temporal resolution. The SSC study is motivated by the environmental, economic and ecological importance of sediment transport in coastal and inland waters. The quantification of SSC in rivers is important for the study of the geomorphological and ecological functioning of river flood plains and deltas. The efficacy of remote sensing as an information source for the quantitative analysis of SSC was studied using Landsat images on the Google Earth Engine, which is a planetary scale platform. Our results revealed an expressive variation in SSC over the decades. The approach proposed in this work can be adapted to SSC monitoring another large areas of the world. However, in the present study the method is used for the entire Brazilian territory, showing historical changes in sediment concentration in the water, as well as changes (increase or decrease) in the water surface area over the decades.

1. INTRODUCTION

The objective of this study is, among others, to examine the variation and spatial distribution of SSC and water surface area along the main Brazilian basins for more than three decades, while verifying the validity and usefulness of the proposed method.

Quantification of SSC (Suspended Sediment Concentration) in large basins and rivers is important in studying the hydrologic, geomorphologic and ecologic functioning of river flood plains and deltas. From the applications that may require the evaluation of suspended sediment quantities, we can highlight: dredging operations, environmental impact assessments in construction activities, geomorphological changes, estimation of particulate organic carbon flows from rivers to the sea, among others.

The results presented in this study provide an overview of how the SSC and the water surface varied for more than three decades throughout the country's territorial extension, as well as giving us a good understanding of how the SSC is distributed over the whole territory.

Global data sets documenting surface water location and seasonality have been produced from inventories and national descriptions (Lehner et al., 2004), statistical extrapolation of regional data (Downing et al., 2006) and satellite imagery (Verpoorter et al., 2014; Feng et al., 2015; Yamazaki et al., 2015; Prigent et al., 2012), measuring long-term changes at high resolution (Pekel et al., 2016). But measuring long-term changes in SSC along with water surface area remains a challenge.

In this work, using more than 100,000 Landsat images (Wulder et al., 2016), we quantified changes in SSC and water surface in the last 32 years at a resolution of 30 meters for the entire Brazilian territory. To do so, use has been made of the Google Earth Engine platform to provide a tool for accessing Landsat images for the past 32 years, as well as high processing power, creating a basis for SSC monitoring in large areas over the last three decades.

Brazil is endowed with a vast and dense hydrographic network, and many of its rivers are remarkable for their great flow and depth, making them ideal for the construction of hydroelectric plants, being this the main energetic source of the Brazilian electrical matrix.

The use of hydroelectric plants is shown in this work as the main reason for the reduction of suspended sediment concentration SSC in the Brazilian basins, and its use is justified by the economic development in a renewable basis, avoiding carbon

emission. Unfortunately, the impact studies normally take into consideration only the vicinity of the dams, ignoring the impacts in a larger environmental scale (Latrubesse et al., 2017).

The main result obtained in the present article shows the tendency of a decrease in the concentration of suspended sediments SSC in the main Brazilian basins, demonstrating that sediments are likely to be captured by the construction of the many hydroelectric dams and reservoirs along the courses of large rivers that flow towards the sea during the last three decades of analysis.

The method presented here can be used in any area of interest, however, in the present study, the method will be used for the entire Brazilian territory.

Brazil is recognized for having an extensive hydrographical network, many of its rivers being known for their large dimensions and high flows. Due to the nature of the relief that prevails in the plateau, the rivers that flow in its bed follow ruptures and deep valleys among other characteristics that confer great potential for generation of electric energy, apropos the sustainability of hydropower stations are endangered by reservoir sedimentation, causing loss of power generation capability by sedimentation, reducing its lifetime and increasing risk of flood (Okumura, 2012).

The navigability of rivers is not suitable for large vessels due to their passage through uneven terrain. Among the great national rivers, only the Amazon and Paraguay are predominant and widely used for navigation.

In a general way, the rivers do not have their origins in areas of very high elevation, except the Amazon and some of its tributaries that originate in the Andean mountain range

As shown in the map in Figure 1, we can divide the Brazilian hydrographic net into seven main basins: Amazon River Basin; Tocantins-Araguaia River Basin; South Atlantic Basin - region north and northeast; San Francisco River Basin; South Atlantic Basin - region east; Platina Basin, composed of the sub-basins of the rivers Paraná and Uruguay; and Atlantic South Basin - regions southeast and south.

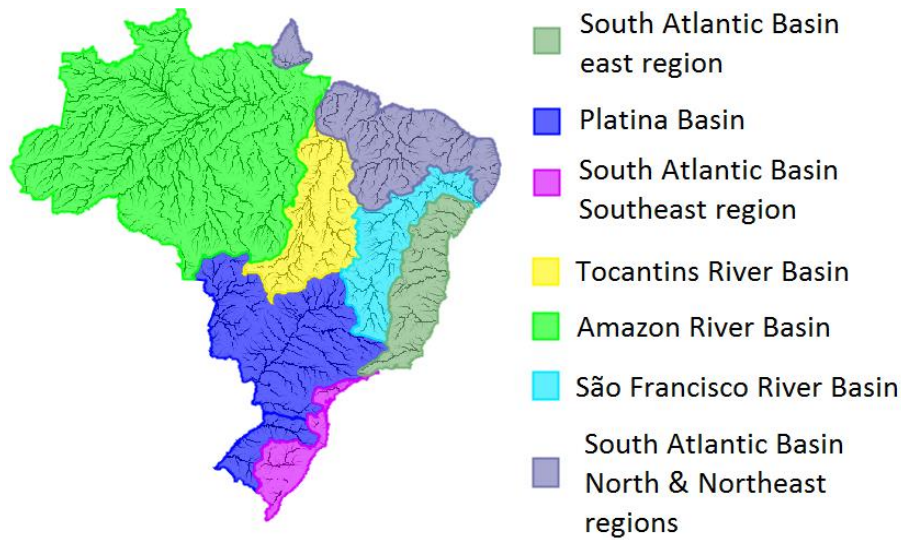


Figure 1 - The main Brazilian Watersheds.

2. MATERIALS AND METHODS

In the present article, all calculations were made using the Google earth engine platform (Gorelick et al., 2017), due mainly to its practicality in processing thousands of images of satellites at the same time and in a reasonable time.

The first step was to select the satellites suitable for such the analysis. Landsat 8 was not used because of substantial differences in bandwidth when compared to other satellites of the Landsat family, which could lead to significant variations in the indices studied. Such variations in bandwidth are shown in Figure 2 and summarised in Table 1.

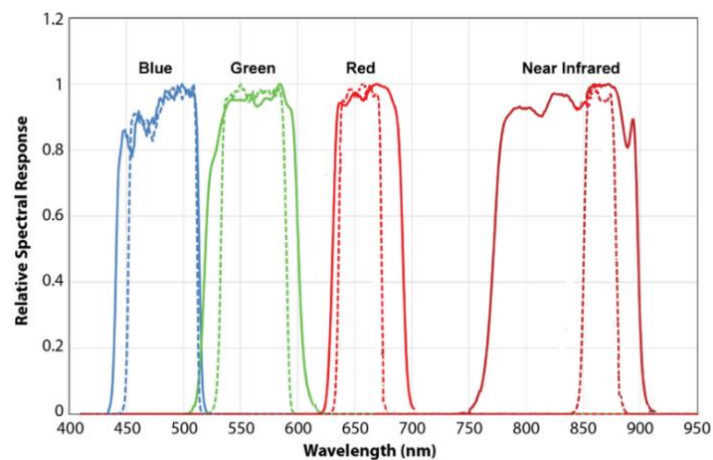


Figure 2 - Band average relative spectral response of Landsat 7 ETM+ (solid line), Landsat 8 OLI (dash line). Adapted from (Ke et al., 2015).

Thus, to cover the 32 years of images, the following selection of satellites covering their respective data ranges is shown in Table 2. The images used are part of the Surface Reflection Collections (terminate with SR) that are atmospherically corrected, providing greater reliability in the water indexes derived.

Table 1. Spectral Band range comparison for Landsat 5, 7 and 8.

Bands	Landsat 5	Landsat 7	Landsat 8	Resolution (m)
Blue	0.441- 0.514	0.441 - 0.515	0.452- 0.512	30
Green	0.519 - 0.601	0.519 - 0.602	0.533 - 0.590	30
Red	0.631 - 0.692	0.631 - 0.693	0.636 - 0.673	30
Nir	0.772 - 0.898	0.772 - 0.899	0.851 - 0.879	30

Table 2. Satellite selection and Data range.

Satellite	Date Range
LANDSAT/LT5_SR	1984 to 1998
LANDSAT/LE7_SR	1999 to 2003
LANDSAT/LT5_SR	2004 to 2011
LANDSAT/LE7_SR	2012 to 2015

2.1. SSC INDEXES

The first studies on remote sensing of the SSC were mainly focused on the discovery and demonstration of the existence of a relation between the suspended sediment concentration and the spectral reflectance and is based on empirical methods (Ritchie et al., 1988; Ritchie et al., 1990; Chen et al., 1992; Harrington et al., 1992; Ritchie et al., 1987).

The remote sensing method for SSC is based on the characteristics of the radiation reflected by the water as a function of the sediment concentration present in it.

In general, the "typical" reflectance of water as a function of the SSC is given as shown in Figure 3. As noted, it appears that a useful spectral range would be between 400 and 900 nm.

SSC quantification algorithms based on the reflectance of water can coarsely be divided into the following families: single band, band ratio and spectral separation.

The band ratio algorithms are less sensitive to atmospheric scattering and, therefore, are not subject to uncertainties if the scattering coefficient of air density has high natural variability. Rather, band ratio algorithms can be developed to be less

sensitive to this natural variability since the background scattering effects are largely cancelled when the ratio between bands is made.

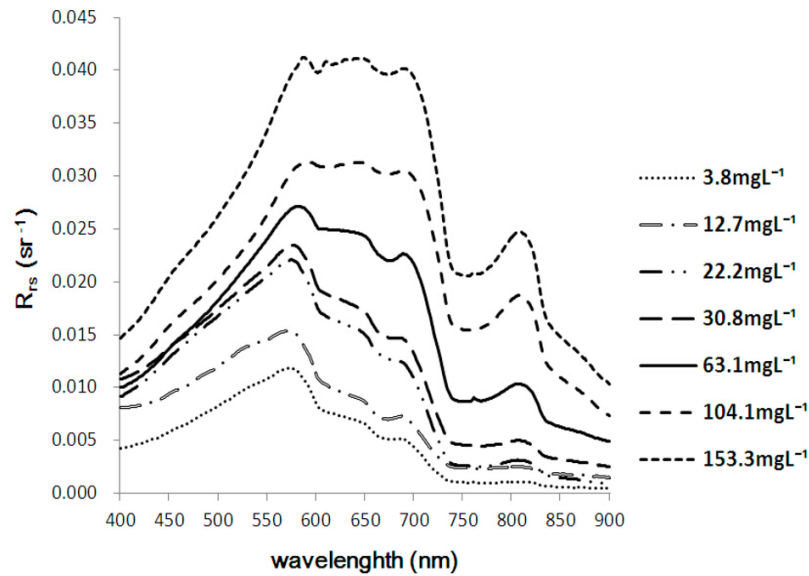


Figure 3 - Reflectance profiles of samples with increasing values of SSC. Adapted from (Qu, 2014).

The band ratio algorithms between two bands were suggested to estimate the SSC (Doxaran et al., 2002).

In addition to the individual bands, the relationship between the red and green bands, have also been proposed for estimating SSC (Topliss et al., 1990; Yuming et al., 1992; Doxaran et al., 2009). It was demonstrated in (Doxaran et al., 2002) that the use of reflection ratios between bands have the ability to reduce the influence of sky reflection, particle size and variation in the refractive index. However, (Binding et al., 2005) argued that reflection indices work well only for highly turbid water dispersion, which compensates for the strong absorption of other optically active materials in water at these wavelengths.

Three different indices will be analysed in this article to verify the most convenient for use in SSC estimates.

2.1.1. NSMI

The index NSMI (Equation 1) is presented in (Montalvo, 2010; Fiuza et al., 2011) and is deducted considering that clean water has a peak reflectance in the blue band (ρ_{blue}), while the presence of SSC produces an increase of reflectance in the whole visible bands, especially in the range of green and red ($\rho_{\text{red}} + \rho_{\text{green}}$) (Fiuza et al., 2011).

The equation is derived by adding the Red and Green bands and subtracting the Blue band, then dividing the result by the sum of the Red, Green and Blue bands to normalize the result. The equation produces values ranging from -1 to +1. Lower values represents clearer water, while greater values correspond to water with presence of sediments in suspension. Note that, when the blue band has a higher value than the sum of the red and green band, the equation produces a negative value, indicating the presence of clear water.

$$NSMI = \left(\frac{\rho_{red} + \rho_{green} - \rho_{blue}}{\rho_{red} + \rho_{green} + \rho_{blue}} \right) \quad (1)$$

2.1.2. NDSSI

The NDSSI index has been used to develop models of suspended sediment in rivers, lakes, estuaries and many other water bodies (Hossain, 2006). It was observed that Landsat ETM imagery is more sensitive to water transparency on the blue (ρ_{blue}) and near-infrared (ρ_{nir}) bands (Hossain, 2006). The index is derived by subtracting the near infrared band from the blue band and the dividing the result by the sum of both bands (Equation 2). The NDSSI index also ranges from -1 to +1 where higher values indicate clearer water and lower values indicate the presence of sediment in suspension (SSC) (Hossain, 2006).

$$NDSSI = \left(\frac{\rho_{nir} - \rho_{blue}}{\rho_{nir} + \rho_{blue}} \right) \quad (2)$$

2.1.3. BAND RATIO GREEN/BLUE

The quotient between bands are usefull to achieve many purposes in remote sensing. For Landsat ETM+ imagery one of the quotient between bands to retrieve suspended sediment concentration (SSC) in water is the green band divided by the blue band (Equation 3) (Aber, 2011). This equation is deducted due the fact that the suspended sediment concentration in water increases the reflectance in the green band while clearer water has the peak reflectance in the blue band. The quotient produces

values that range from 0 to infinite. In this case the highest value indicates the presence of more suspended sediment concentration (Aber, 2011).

$$NSMI = \left(\frac{\rho_{\text{green}}}{\rho_{\text{blue}}} \right) \quad (3)$$

2.2. METHODOLOGY

The following steps were used to make the trend analysis over the 32 years of imagery:

1. An image collection from 1984 to 2016 is produced selecting the satellites as shown in table 2;
2. In each image of the image collection obtained in 1 a mask is applied to the water pixels using the cfmask algorithm (Foga et al., 2017) to select only the pixels classified as water;
3. In each pixel classified as water, a SSC index is derivate utilizing the indexes shown in equation (1), (2) and (3).
4. A mean annual image for each pixel is derived for each year of the image collection in 3. This step is accomplished taking a mean value of the SSC indexes for all the pixels classified as water and located at the same position, as shown in Figure 4. This step is important considering that is very likely that water pixels will be covered by clouds in some scenes throughout a year. Considering that we have about 20 Landsat images per year (an average of one scene every 16 days), it will be very unlikely for the same area to have water pixels covered by clouds in all scenes.

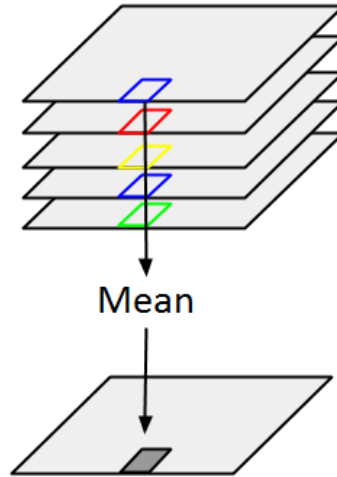


Figure 4 - Illustration of a mean operation applied for the pixels of the same position in an Image Collection, adapted from (Gorelick et al., 2017).

5. A mean value is obtained from each annual image in 4, taking a mean operation over the entire area of the basin in consideration, to derive qualitative indexes for each annual image. In this step is derived the amount of pixels of water counted over the image. Such operation is illustrated in Figure 5;

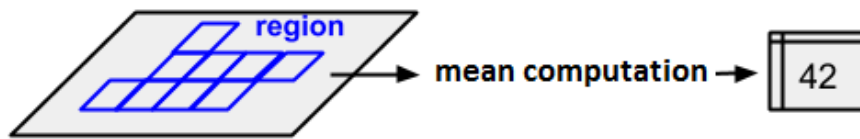


Figure 5 - Illustration of a mean operation applied in an Image Region adapted from (Gorelick et al., 2017).

6. A linear regression which computes the least squares estimate of a linear function of one variable with a constant term is applied in the collection of 32 images obtained in 4), each of them representing one year. This linear regression is taken over the pixels located at the same position such operation is illustrated in Figure 6;

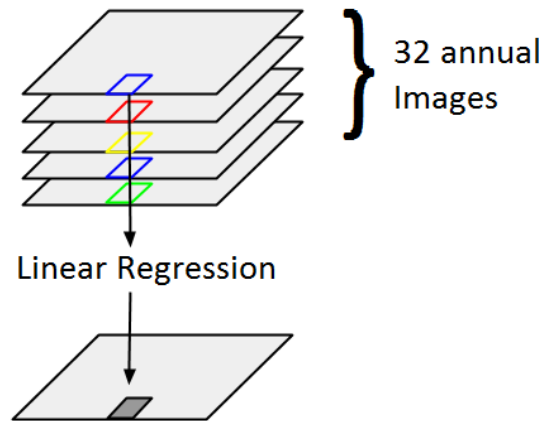


Figure 6 - Illustration of Linear Regression applied to an Image Collection, adapted from (Gorelick et al., 2017).

To map SSC distribution and other parameters throughout the Brazilian territory, 30,000 randomly generated points of 30 km in diameter were used to cover the entire area and to collect information on the mean value of SSC as well as the amount of water present at each point.

The information on the amount of water is important to visualize the dynamics of the changes from flooded areas to dry areas and vice versa that occurred during the years.

For the creation of the maps, it was decided to use the initial five years (1984-1989) and the last five years (2011-2016) to visualize the changes that occurred between the initial and final years and give an overview of the changes that occurred in the period in relation to the SSC values and the amount of water present in the Brazilian basins during the 3 decades.

Then an interpolation map is produced to visualize the amount of water and the lowest and highest SSC values along the Brazilian territory. The acquisition points used are shown in Figure 7. It can be seen that they completely cover the Brazilian territory.



Basins	Área (km ²)	Points
Amazon	3843.402	13515
Tocantins - Araguaia	967.059	3400
South atlantic - North and Northeast Regions	875.561	3079
Sao Francisco	636.92	2240
Platina Basin	1417.719	4986
South Atlantic - East Region	604.649	2126
South Atlantic	185.856	653

Figure 7 - Acquisition points.

3. RESULTS

To verify which is the most suitable index to be used in the present study, among those shown in equations 1, 2 and 3, all three indices were plotted in the same graph, with different scales, for better visualization, as shown in Figure 8, for the Tocantins Basin. As we can see by analyzing the figure, all three indices present the same behaviour. So, in qualitative terms, choosing one index is a matter of convenience. Thus, in this work, the index to be used was decided to be the NSMI.

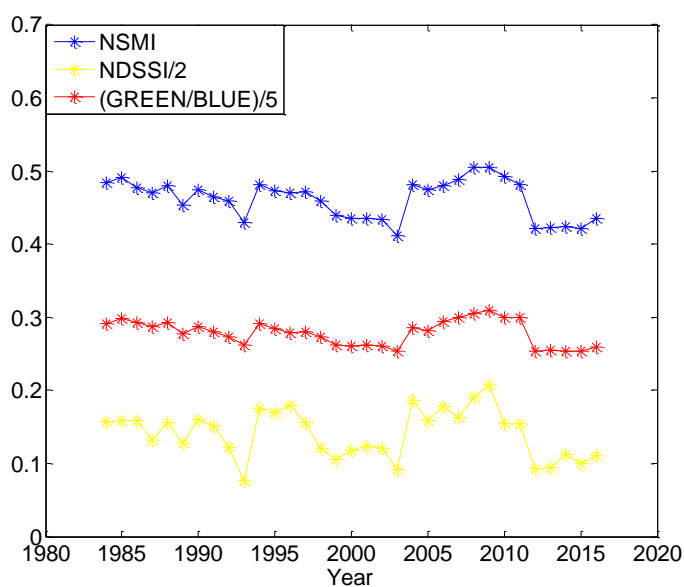


Figure 8 - SSC indexes applied for the Tocantins basin.

3.1. CALIBRATION

The Hidroweb system (Hidroweb, 2017), which has the historical data of the Brazilian hydrometric network under the management of the Brazilian water agency (ANA, 2017), was used to perform this work.

Since sediment data from Hidroweb are scarce, while flow information is available for most days and most sediment monitoring stations, the flow information provided is used to derive the SSC values for days on which Landsat images are available, we considered the Flow x Sediment relation obtained by the best fit curve (least square method).

To have a consistent estimate of SSC throughout the Brazilian territory, it was decided to add the data of sediment monitoring stations in the major rivers of the main Brazilian basins, being one station per basin, as shown in table 3. Thus, the estimated SSC values obtained through the flows were crossed with the respective NSMI index values, obtained from Landsat images, for the respective days. It was decided to acquire data in 30 different days, to better visualize the trend of the data. The acquired results are plotted in Figure 9, as well as the best fit curve.

Table 3. Location of sediment monitoring stations.

Station	Basin	River	Lat	Long
Guaraí	Platina	Paraná	-24.069	-54.248
Xambioá	Tocantins	Araguaia	-6.4097	-48.5422
Traipu	São Francisco	São Francisco	-9.9714	-37.0028
Óbidos	Amazonas	Amazonas	-1.9192	-55.5131
Indaial	South Atlantic – Southeast Region	Itajaí	-26.891	-49.235
Antas	South Atlantic – East Region	Paraíba do Sul	-22.035	-42.9908
Teresina	South Atlantic – North and Northeast Region	Parnaíba	-5.1350	-42.8111

The best fit curve that relates the SSC and the NDSSI index was derived, as shown in (Equation 4).

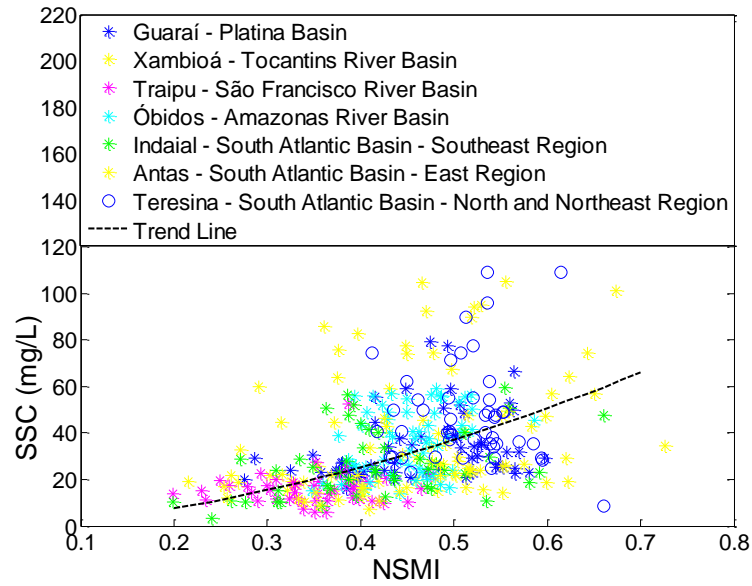


Figure 9 - NSMI index versus SSC for different sediment monitoring stations.

$$CSS = 121.8 * NSMI^{1.717} \quad (4)$$

with a $R^2 = 0.3666$.
p-value = 0.223

3.2. SSC TREND ANALYSIS

Some areas were chosen to study the SSC trend over the 32 years of imagery. The results are presented in Figure 10. The red colour in the figure means increasing in SSC along the years, and the blue color means decreasing SSC along the years. The areas are described as follow:

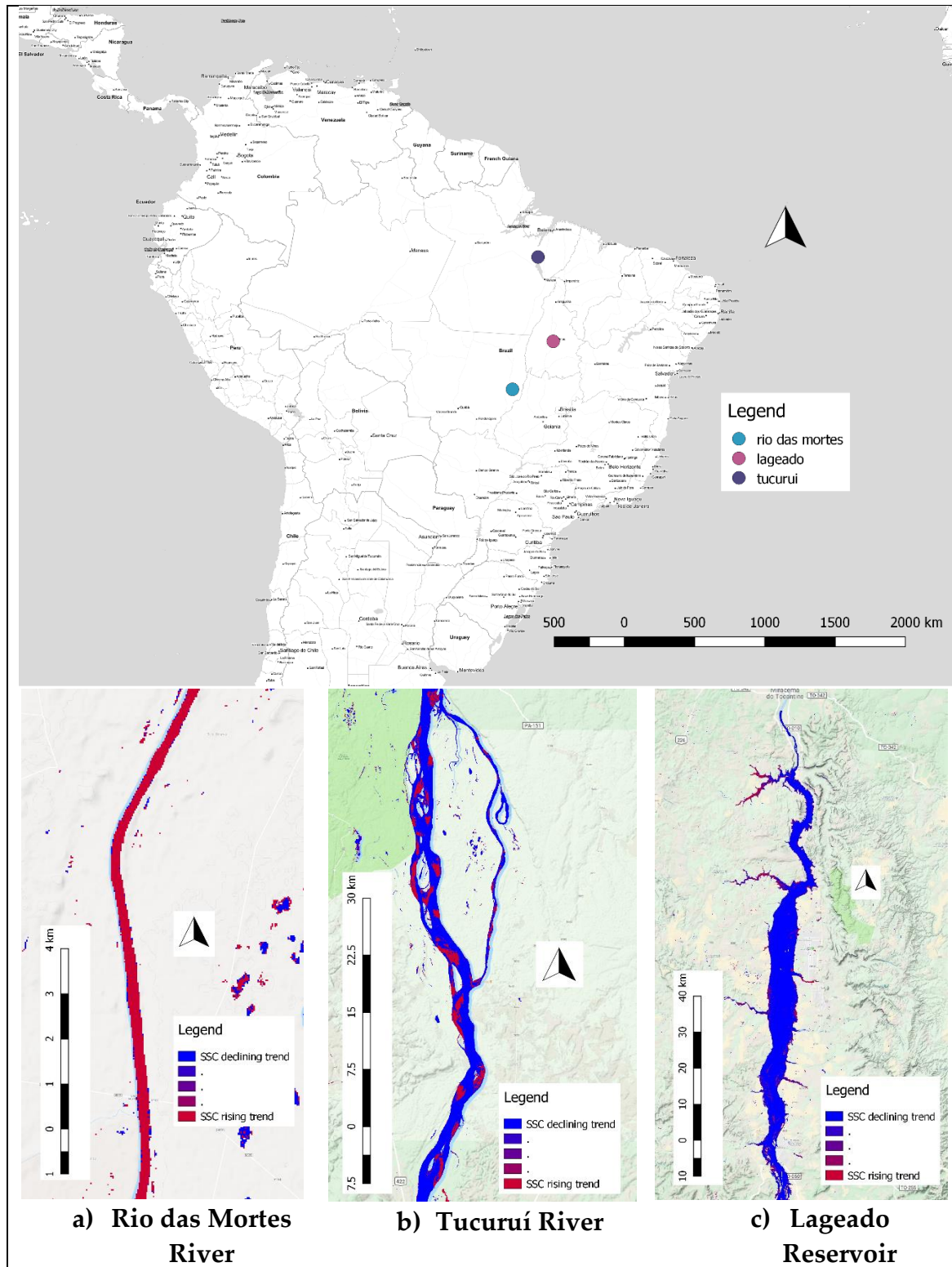


Figure 10 - SSC trend analysis.

1. Das Mortes River: Lat: -14.0693, Lon: -51.6981, The das Mortes River, is a water course that bathes the state of Mato Grosso, Brazil. It is located in the Amazon Basin, with a total extension of 1,200 kilometers. It flows into the Araguaia River, 20 kilometers from São Félix do Araguaia city. It is one of the great attractions for

ecotourism in the region. The increase along the years of the SSC value agrees with the fact that this area is suffering an intensive and indiscriminate deforestation of the original dominant savannah (83%) in the landscape in the last 40 years (Oliveira et al., 2005);

2. Tucuquí River: Lat: -3.2583, Lon: -49.6082, is a river downstream a major reservoir (Tucurui Reservoir) and presents a decreasing trend for SSC, this agrees with the fact that the reservoir upstream is acting as a sediment “trap” avoiding the sediments to flow through the river downstream.

3. Lageado Reservoir: Lat: -10.3578, Lon: -48.4016, is a 630 km² reservoir opened in 2002 and presents a decreasing trend in SSC, this agrees with the fact that reservoirs work as sediment “traps” and depositing the sediments at the bottom of the reservoir along the time.

We should take into consideration during our analysis that during the last three decades an large number of large and small hydraulic power plants were constructed in Brazil, contributing with the changing in the dynamics of sediments during the past years.

3.3. CHARTS

To get an overview of the basins, two charts were plotted, one showing the mean annual value of SSC for each basin, and the other showing the normalized amount of pixels classified as water per year, as shown respectively in Figure 11 and Figure 12.

In Figure 11, it is important to note that the SSC trend is decreasing for all the basins, as can be seen by the Trend Line. This is an interesting result because, due to deforestation and the advance of agriculture in larger areas in Brazil, an increase in SSC was expected and not a decrease. The downward trend in SSC could be explained by the construction of many large and small reservoirs over these three decades; which contribute to the reduction of the mean value of the SSC, this can be verified by the water amount normalized index in Figure 12, showing an increasing trend in all the basins.

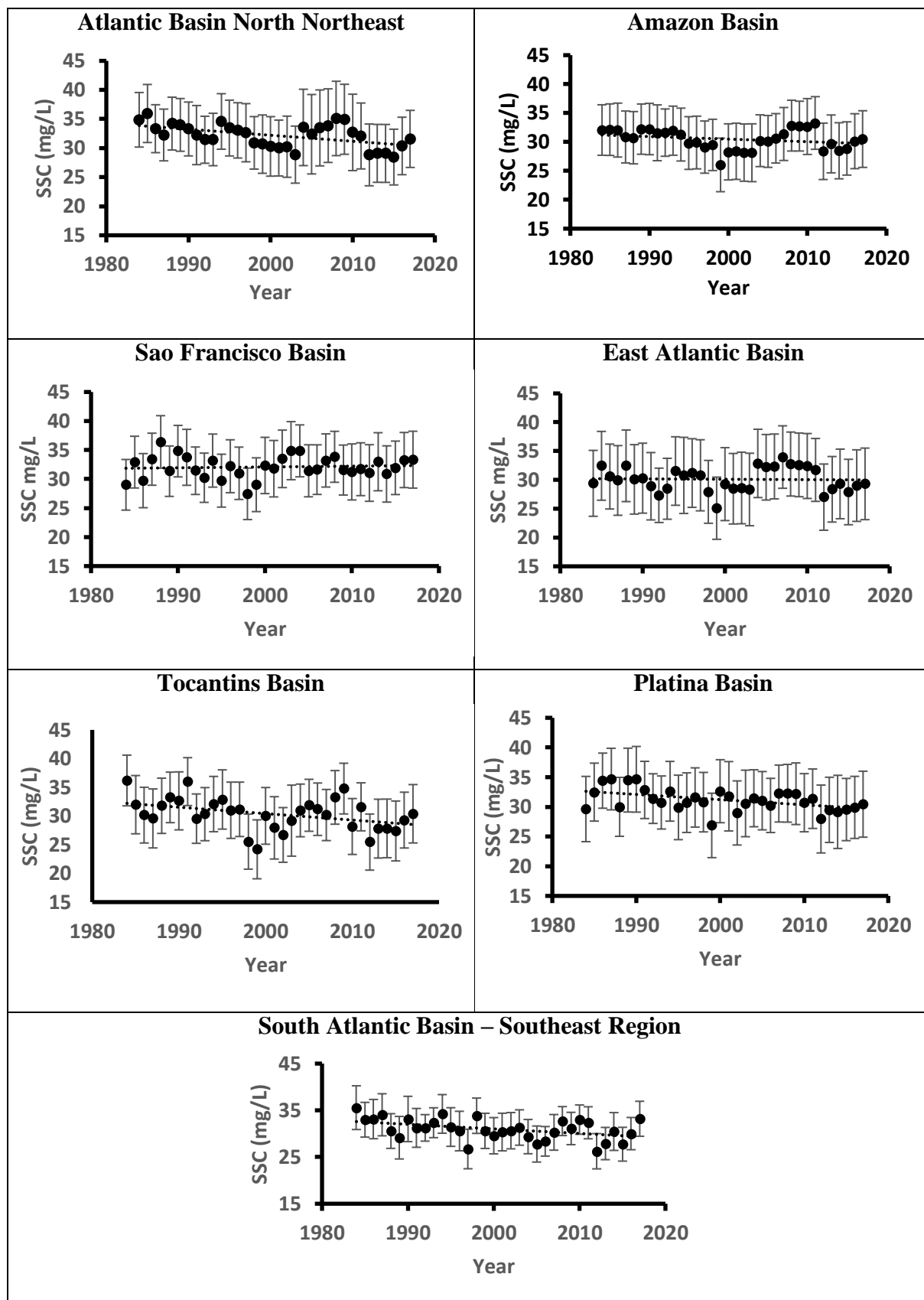


Figure 11 - Mean annual estimated SSC trend analysis for all basins.

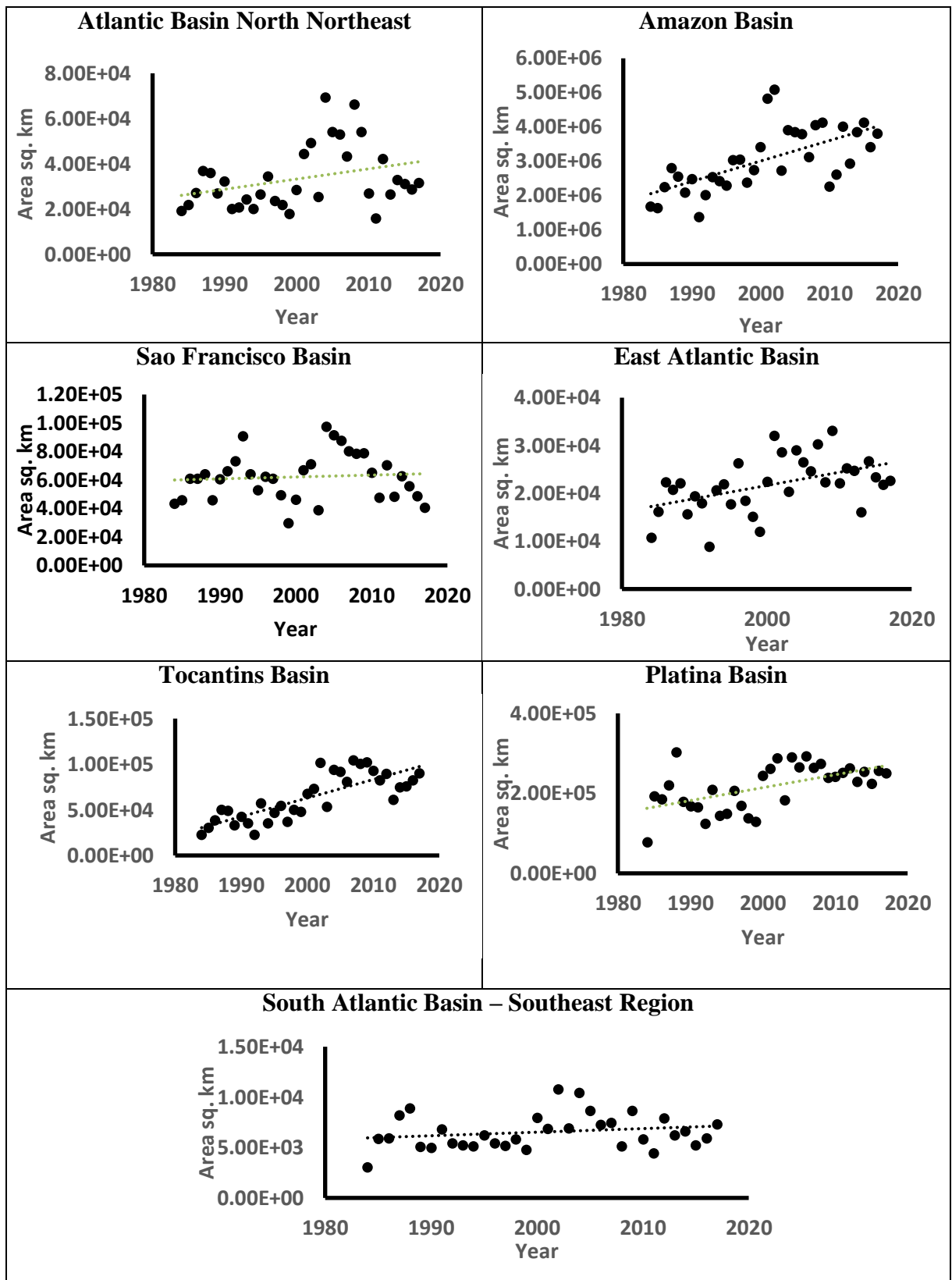


Figure 12 - Water area count for all basins.

3.4. MAPS

For a more complete and spatially detailed view of the data, to verify the changes occurred over the course of the 32 years in the Brazilian territory as a wholesome maps were generated. Thus to first verify the long-term change, SSC estimation maps were generated for the first five years, the last five years and the difference between the five final and initial years, as shown respectively in Figures 12, 13 and 14.

In Figure 15 we have a clear view of the areas that have increased the SSC value as well as those that have decreased. We verified that there was a significant increase in the SSC value in the central regions of the country, usually related to the advance of agricultural production and deforestation allowing erosion and run-off to carry soil into local creeks and rivers.

Another map was generated showing the variations of the water surface area, showing the regions that lost and gained water area (Figure 15).

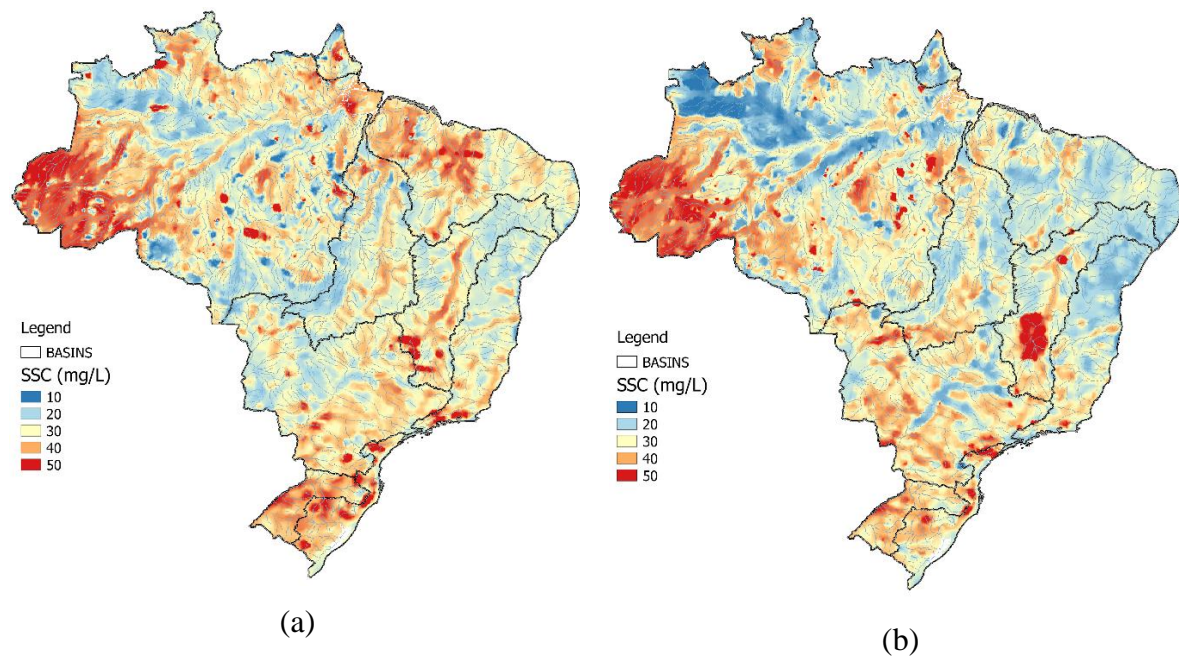


Figure 13 - Estimation of mean SSC: (a) 1984-1989; (b) (2012-2017).

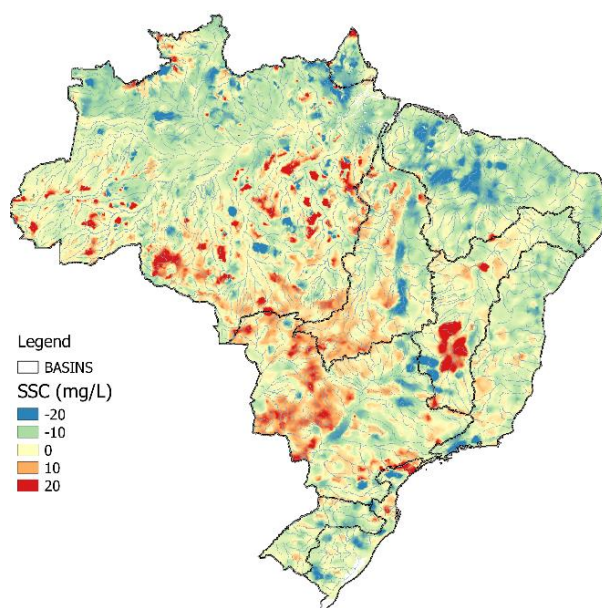


Figure 14 - Estimation of mean SSC difference between the five final years (2012-2017) and the five initial years (1984-1989).

Most of the areas that have increased their water surface are related to regions where hydroelectric dams were built, while some regions of great importance such as the Pantanal and some areas of the Araguaia and Amazon basin lost water area.

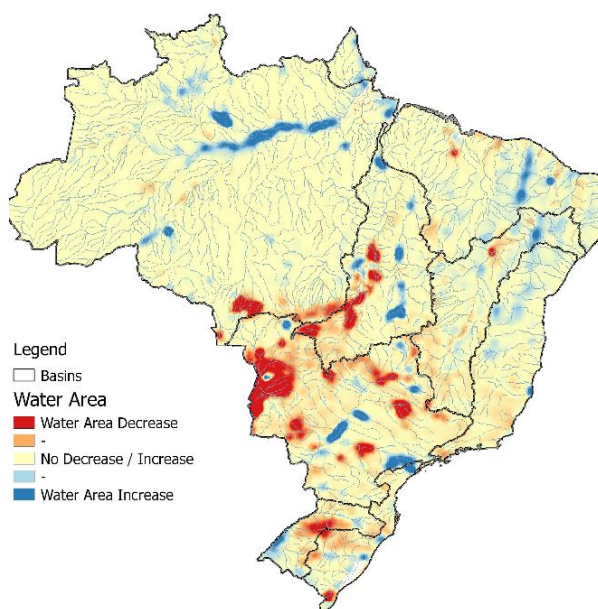


Figure 15 - Estimation of water area difference between the five final years (2012-2017) and the five initial years (1984-1989).

4. CONCLUSION

The sediment concentration mapping greatly progressed in recent years, as witnessed by the appearance of new products as well as the maturation of products and applications. A few years ago, the investigation was focused primarily on the development of algorithms and creating some instant maps of SSC.

In this paper, we explored the potentiality of the Google earth engine platform in providing data and processing power, achieving an innovative framework for SSC estimation for great areas and along the decades since 1984.

As conclusion, we can affirm that the method developed in the present work allowed the deduction of factors pertinent to the concentration of sediment in suspension throughout the Brazilian territorial extent, as well as to the variation in the water surface area. Important factors, such as the tendency to decrease of the SSC values for practically all regions, were observed, together with the increase in the water surface area. It is possible to conclude that such behavior is due to the constant construction of hydroelectric plants and water reservoirs along the great Brazilian rivers. This conclusion is based on the analysis of the trend of the sediment concentration SSC at three points of interest (Section 3.2). Finally, we can state that the technique developed here can be applied to other large water bodies or areas, and it is also possible to use other relevant indices, such as chlorophyll, suspended organic matter, etc. depending on the application of interest

The method presented in this article proved to be a great tool being very effective and practical for the determination of areas in which SSC varies over the years, as well as the determination of areas where there was increase or decrease of water surface. The method can be used in different areas of interest or countries in order to verify the dynamics of SSC and water surface over the years.

5. REFERENCES

Aber, James S. 2011. Landsat Image Processing.http://academic.emporia.edu/aberjame/remote/landsat/landsat_proc.htm

- Chen, Zhimin, Paul J. Curran, and Jim D. Hansom. "Derivative reflectance spectroscopy to estimate suspended sediment concentration." *Remote Sensing of Environment* 40.1 (1992): 67-77.
- Downing, J. A. et al. The global abundance and size distribution of lakes, ponds, and impoundments. *Limnol. Oceanogr.* 51, 2388–2397 (2006).
- Doxaran, D., J-M. Froidefond, and P. Castaing. "A reflectance band ratio used to estimate suspended matter concentrations in sediment-dominated coastal waters." *International Journal of Remote Sensing* 23.23 (2002): 5079-5085.
- Doxaran, David, et al. "Dynamics of the turbidity maximum zone in a macrotidal estuary (the Gironde, France): Observations from field and MODIS satellite data." *Estuarine, Coastal and Shelf Science* 81.3 (2009): 321-332.
- Feng, M., Sexton, J. O., Channan, S. & Townshend, J. R. A global, high-resolution (30-m) inland water body dataset for 2000: first results of a topographic– spectral classification algorithm. *Int. J. Digit. Earth* 9, 113–133 (2015).
- FIUZA, B. et al. Detection of suspended sediments in Grande River and Ondas River-Bahia. Brazil, Federal University of Bahia Institute of Environment Sciences and Sustainable Developments, Brazil, 2011. Montalvo, I., 2010. Spectral analysis of suspended material in coastal waters: A comparison between band math equations. gers.uprm.edu/geol6225/pdfs/I_montalvo.pdf.
- Foga, Steve, et al. "Cloud detection algorithm comparison and validation for operational Landsat data products." *Remote Sensing of Environment* 194 (2017): 379-390.
- Gorelick, N., Hancher, M., Dixon, M., Ilyushchenko, S., Thau, D., & Moore, R., 2017. Google Earth Engine: Planetary-scale geospatial analysis for everyone. *Remote Sensing of Environment*.
- Harrington, John A., Frank R. Schiebe, and Joe F. Nix. "Remote sensing of Lake Chicot, Arkansas: Monitoring suspended sediments, turbidity, and Secchi depth with Landsat MSS data." *Remote Sensing of Environment* 39.1 (1992): 15-27.
- Hossain, A.K.M; Chao, Xiaobo; Jia, Yafei. 2006. Development of Remote Sensing based Index for estimating/mapping Suspended Sediment Concentration in River and Lake Environments, The University of Mississippi.
- Latrubesse, Edgardo M., et al. "Damming the rivers of the Amazon basin." *Nature* 546.7658 (2017): 363.
- Lehner, B. & Döll, P. Development and validation of a global database of lakes, reservoirs and wetlands. *J. Hydrol.* 296, 1–22 (2004).

- Montalvo, I. "Spectral analysis of suspended material in coastal waters: A comparison between band math equations." (2010).
- Okumura, Hirofumi, and Tetsuya Sumi. "Reservoir Sedimentation Management in Hydropower Plant Regarding Flood Risk and Loss of Power Generation." International Symposium on Dams For A Changing World ICOLD 2012, Kyoto, Japan. 2012.
- OLIVEIRA, Victoria Christina Vilela, and Selma Simões de CASTRO. "Susceptibility and risks to water erosion in the upper of Araguaia river basin (Go/Mt), Brazil." *Sociedade & Natureza* 1.1 (2005): 697-708.
- Prigent, C. et al. Changes in land surface water dynamics since the 1990s and relation to population pressure. *Geophys. Res. Lett.* 39, L08403 (2012).
- Pekel, Jean-François, et al. "High-resolution mapping of global surface water and its long-term changes." *Nature* (2016).
- Qu, Liqin. "Remote sensing suspended sediment concentration in the Yellow River." (2014).
- Ritchie, Jerry C., Charles M. Cooper, and Jiang Yongqing. "Using Landsat multispectral scanner data to estimate suspended sediments in Moon Lake, Mississippi." *Remote Sensing of Environment* 23.1 (1987): 65-81.
- Ritchie, Jerry C., and Charles M. Cooper. "Comparison of measured suspended sediment concentrations with suspended sediment concentrations estimated from Landsat MSS data." *Title REMOTE SENSING* 9.3 (1988): 379-387.
- Ritchie, Jerry C., Charles M. Cooper, and Frank R. Schiebe. "The relationship of MSS and TM digital data with suspended sediments, chlorophyll, and temperature in Moon Lake, Mississippi." *Remote Sensing of environment* 33.2 (1990): 137-148.
- Topliss, B. J., C. L. Almos, and P. R. Hill. "Algorithms for remote sensing of high concentration, inorganic suspended sediment." *International Journal of Remote Sensing* 11.6 (1990): 947-966.
- Verpoorter, C., Kutser, T., Seekell, D. A. & Tranvik, L. J. A global inventory of lakes based on high-resolution satellite imagery. *Geophys. Res. Lett.* 41, 6396–6402 (2014).
- Wulder, M. A. et al. The global Landsat archive: status, consolidation, and direction. *Remote Sens. Environ.* 185, 271–283 (2016).

- Yamazaki, D., Trigg, M. A. & Ikeshima, D. Development of a global ~ 90m water body map using multi-temporal Landsat images. *Remote Sens. Environ.* 171, 337–351 (2015).
- Yuming, You, and Hou Min. "Remote sensing analysis of the suspended sediment transport in Lingdingyang." *China Ocean Engineering* 6 (1992): 331-331.

ARTIGO IV

Temporal Analysis of Suspended Concentration for Over 30 Years in the Brazilian Coastline

A.E. Holdefer & K. Formiga
University of Goiás, Goiás, Brazil

KEY WORDS: Landsat images, Google Earth Engine, Suspended Sediment Concentration; Brazilian Coastline, Temporal Analysis, Water Reflectance, Water Pixels

ABSTRACT

The study here developed presents the temporal analysis of the sediment concentration in suspension for the entire Brazilian coast for over three decades. The SSC in coastal areas is essential in the study of the hydrological, geomorphological and ecological functioning of the river deltas. The efficacy of remote sensing as a source of information for the qualitative analysis of SSC along the Brazilian coastline was studied using Landsat images on the Google Earth Engine planetary scale platform. Our results revealed a significant decrease in SSC over the three decades.

This decrease is believed to be a consequence of the large number of hydroelectric power plants and reservoirs along the great rivers that flow into the sea.

The approach proposed in this work can be adapted for monitoring SCC in large areas of the world, however, in the present study, the method is used only for the entire Brazilian coastline, to show historical changes in sediment suspension concentration in water.

1. INTRODUCTION

The main purpose of this study is to examine the variation and spatial distribution of the SSC along the Brazilian coastline for over three decades, while it has been verified the validity of the used method.

Quantification of SSC (Suspended Sediment Concentration) offshore is vital in studying the hydrologic, geomorphologic and ecologic functioning of river deltas as well as for ecological studies of marine life. Applications among others include understanding geomorphologic changes, evaluating fluxes of particulate organic carbon from rivers to the sea, etc.

Monitoring offshore water quality with satellites has been limited by the lack of sensors offering high spatial and radiometric resolutions besides a reasonable revisit time. MODIS-Aqua seems to be the right choice, but it was only launched in 2002, so do not cover time variations for over three decades, does not have a good spatial resolution for coastlines (250 – 1000m), and it is designed to cover only sea waters and not coastal regions. Therefore, in this article, we propose to take advantage of the 32 years of Landsat satellite images; which despite being a satellite designed only for the acquisition of continental images, has images which borders capture marine waters at distances of up to 50km offshore of the coastline, being very useful in quantifying variations in the SSC in the entire Brazilian coastline with good spatial resolution (30m) and good temporal revisit time (around 18 days) during over three decades. To accomplish the goal we took advantage of the Google earth engine platform (Gorelick et al., 2017) for doing large calculations with thousands of images in a reasonable time.

The work here presented gives a global picture of how the SSC have changed during the three decades in the entire Brazilian Coastline, as well gives a good understanding of how SSC is distributed along the entire Coast.

Here, using over 100 thousand Landsat images (Wulder et al., 2016), we quantify changes in SSC for over the past 32 years at 30-meter resolution for the entire Brazilian Coastline up to 50km offshore. For that purpose use was made of the google earth engine platform to provide a Landsat access tool for the last 32 years as well as processing power, creating a basis for SSC monitoring in large areas over the past three decades.

The main result shows the decrease of suspended sediment concentration SSC in the coastal areas. This result demonstrated that the suspended sediments are most likely to be trapped by the construction of many hydroelectric and reservoir plants along the courses of large rivers that flow into the sea during the three decades of analysis (Latrubesse et al; 2017). The use of hydroelectricity is normally justified by the economic development in a renewable way, avoiding carbon emission. Unfortunately,

the impact studies normally take into consideration only the vicinity of the dams, ignoring the impacts in a larger environmental scale (Latrubesse et al; 2017).

The use of hydroelectric plants as main source of electric power in Brazil is due to the fact that Brazil is endowed with a vast and dense hydrographic network, and many of its rivers are remarkable for their great width and depth. Due to the nature of the relief that prevails in the plateau, the rivers that flow in its bed follow ruptures and deep valleys among other characteristics that confer great potential for generation of electric energy (Okumura, 2012).

The method presented here can be used in any body of water of interest, being a general methodology that can be used in different bodies of water.

2. MATERIALS AND METHODS

In the present article, all calculations were made using the Google earth engine platform (Gorelick et al., 2017), due mainly to its practicality in processing thousands of images of satellites at the same time and in a reasonable time.

The first step was to select the family of satellites suitable for such the analysis.

The choice here was made comparing two families of satellites - MODIS-Aqua and the Landsat family. MODIS-Aqua, at first, seems to be the right choice, since it monitors the seas of the world. However, it has some limitations for the present study, among which we can mention: 1) It was only released in 2002, so it does not cover variations for more than three decades, 2) It does not have a good spatial resolution for the coastal areas (250 - 1000m). 3) It is designed to cover open seas and not coastal regions. Therefore, in this article, we propose to take advantage of the 32 years of Landsat satellite imagery; which despite being a satellite designed for the acquisition of continental images, has images that capture coastal areas at distances up to 50km from the coastline, being very useful in quantifying variations in SSC along the Brazilian coastline with good spatial resolution (30m) and good temporal resolution (18 days) for over three decades.

Among the Landsat family the Landsat 8 was not used here because of substantial differences in bandwidth when compared to other satellites of the Landsat family, which could lead to significant variations of the indices analyzed. Such variations in bandwidth are shown in Figure 1 and summarised in Table I.

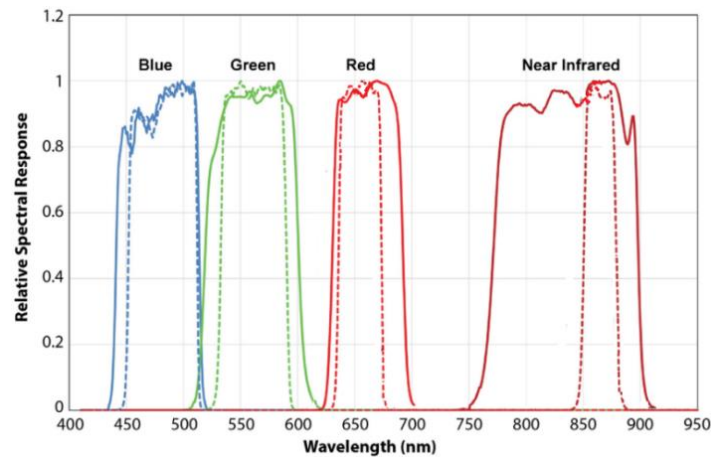


Figure 1 - Band average relative spectral response of Landsat 7 ETM+ (solid line), Landsat 8 OLI (dash line). Adapted from (Ke et al., 2015).

Thus, to cover the 32 years of images, the following selection of satellites and their respective data ranges is shown in Table 2. The images used are part of the Surface Reflection Collections (terminate with SR) that are atmospherically corrected, providing greater reliability in the water indexes derived.

Table 1. Spectral Band range comparison for Landsat 5, 7 and 8

Bands	Landsat 5	Landsat 7	Landsat 8	Resolution (m)
Blue	0.441- 0.514	0.441 - 0.515	0.452- 0.512	30
Green	0.519 - 0.601	0.519 - 0.602	0.533 - 0.590	30
Red	0.631 - 0.692	0.631 - 0.693	0.636 - 0.673	30
Nir	0.772 - 0.898	0.772 - 0.899	0.851 - 0.879	30

Table 2. Satellite selection and Data range

Satellite	Date Range
LANDSAT/LT5_SR	1984 to 1998
LANDSAT/LE7_SR	1999 to 2003
LANDSAT/LT5_SR	2004 to 2011
LANDSAT/LE7_SR	2012 to 2017

2.1. SSC INDEXES

The first studies on remote sensing of the SSC were mainly focused on the discovery and demonstration of the existence of a relation between the suspended sediment concentration and the spectral reflectance and is based on empirical methods (Ritchie et al., 1988; Ritchie et al., 1990; Chen et al., 1992; Harrington et al., 1992; Ritchie et al., 1987).

The remote sensing method for SSC is based on the characteristics of the radiation reflected by the water as a function of the sediment concentration present in it.

In general, the "typical" reflectance of water as a function of the SSC is given as shown in Figure 2. As noted, it appears that a useful spectral range would be between 400 and 900 nm.

SSC quantification algorithms based on the reflectance of water can coarsely be divided into the following families: single band, band ratio and spectral separation.

The band ratio algorithms are less sensitive to atmospheric scattering and, therefore, are not subject to uncertainties if the scattering coefficient of air density has high natural variability. Rather, band ratio algorithms can be developed to be less sensitive to this natural variability since the background scattering effects are largely cancelled when the ratio between bands is made.

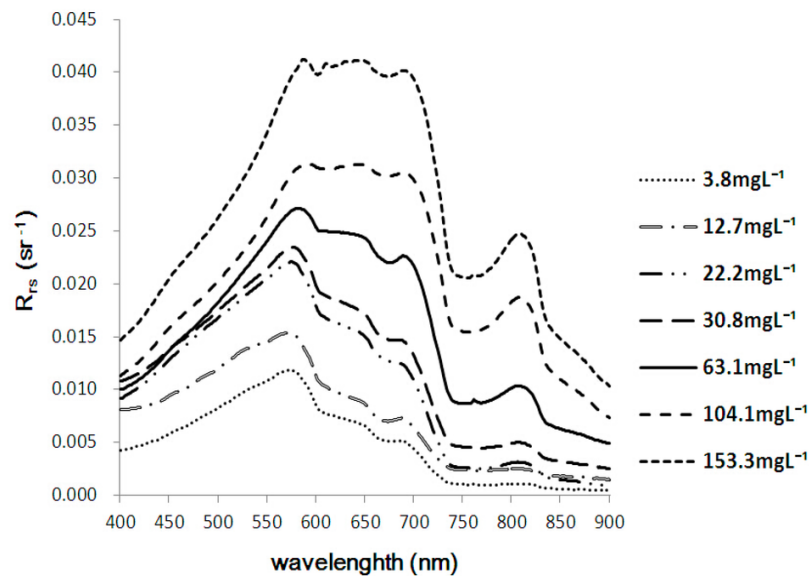


Figure 2 - Reflectance profiles of samples with increasing values of SSC. Adapted from (Qu, 2014).

The band ratio algorithms between two bands were suggested to estimate the SSC (Doxaran et al., 2002).

In addition to the individual bands, the relationship between the red and green bands, have also been proposed for estimating SSC (Topliss et al., 1990; Yuming et al., 1992; Doxaran et al., 2009). It was demonstrated in (Doxaran et al., 2002) that the use of reflection ratios between bands have the ability to reduce the influence of sky reflection, particle size and variation in the refractive index. However, (Binding et al., 2005) argued that reflection indices work well only for highly turbid water dispersion,

which compensates for the strong absorption of other optically active materials in water at these wavelengths.

Three different indices will be analysed in this article to verify the most convenient for use in SSC estimates.

2.1.1. NSMI

The index NSMI (Equation 1) is presented in (Montalvo, 2010; Fiuza et al., 2011) and is deducted considering that clean water has a peak reflectance in the blue band (ρ_{blue}), while the presence of SSC produces an increase of reflectance in the whole visible bands, especially in the range of green and red ($\rho_{\text{red}} + \rho_{\text{green}}$) (Fiuza et al., 2011). The equation is derived by adding the Red and Green bands and subtracting the Blue band, then dividing the result by the sum of the Red, Green and Blue bands to normalize the result. The equation produces values ranging from -1 to +1. Lower values represents clearer water, while greater values correspond to water with presence of sediments in suspension. Note that, when the blue band has a higher value than the sum of the red and green band, the equation produces a negative value, indicating the presence of clear water.

$$\text{NSMI} = \left(\frac{\rho_{\text{red}} + \rho_{\text{green}} - \rho_{\text{blue}}}{\rho_{\text{red}} + \rho_{\text{green}} + \rho_{\text{blue}}} \right) \quad (1)$$

2.1.2. NDSSI

The NDSSI index has been used to develop models of suspended sediment in rivers, lakes, estuaries and many other water bodies (Hossain, 2006). It was observed that Landsat ETM imagery is more sensitive to water transparency on the blue (ρ_{blue}) and near-infrared (ρ_{nir}) bands (Hossain, 2006). The index is derived by subtracting the near infrared band from the blue band and the dividing the result by the sum of both bands (Equation 2). The NDSSI index also ranges from -1 to +1 where higher values indicate clearer water and lower values indicate the presence of sediment in suspension (SSC) (Hossain, 2006).

$$NDSSI = \left(\frac{\rho_{nir} - \rho_{blue}}{\rho_{nir} + \rho_{blue}} \right) \quad (2)$$

2.1.3. BAND RATIO GREEN/BLUE

The quotient between bands are usefull to achieve many purposes in remote sensing. For Landsat ETM+ imagery one of the quotient between bands to retrieve suspended sediment concentration (SSC) in water is the green band divided by the blue band (Equation 3) (Aber, 2011). This equation is deducted due the fact that the suspended sediment concentration in water increases the reflectance in the green band while clearer water has the peak reflectance in the blue band. The quotient produces values that range from 0 to infinite. In this case the highest value indicates the presence of more suspended sediment concentration (Aber, 2011).

$$NSMI = \left(\frac{\rho_{green}}{\rho_{blue}} \right) \quad (3)$$

2.2. METHODOLOGY

The following steps were used to make the trend analysis over the 32 years of imagery:

1. An image collection from 1984 to 2016 is produced selecting the satellites as shown in table 2;
2. In each image of the image collection obtained in 1 a mask is applied to the water pixels using the cfmask algorithm (Foga et al., 2017) to select only the pixels classified as water;
3. In each pixel classified as water, a SSC index is derivate utilizing the indexes shown in equation (1), (2) and (3).
4. A mean annual image for each pixel is derived for each year of the image collection in 3. This step is accomplished taking a mean value of the SSC indexes for all the pixels classified as water and located at the same position, as shown in Figure 3. This step is important considering that is very likely that water pixels will be covered by clouds in some scenes throughout a year. Considering that we have about 20 Landsat

images per year (an average of one scene every 16 days), it will be very unlikely for the same area to have water pixels covered by clouds in all scenes.

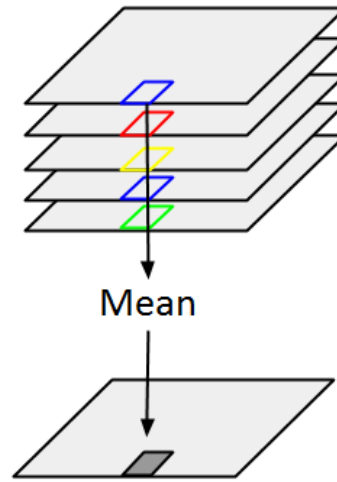


Figure 3 - Illustration of a mean operation applied for the pixels of the same position in an Image Collection, adapted from (Gorelick et al., 2017).

5. A mean value is obtained from each annual image in 4, taking a mean operation over the entire area of the basin in consideration, to derive quantitative indexes for each annual image. Such operation is illustrated in Figure 4;



Figure 4 - Illustration of a mean operation applied in an Image Region adapted from (Gorelick et al., 2017).

To map the SSC value and distribution throughout the Brazilian coastline, 30,000 randomly generated points of 2 km in diameter were used to cover the entire area and to collect information on the mean value of SSC present at each point.

For the creation of the maps, it was decided to use the initial five years (1984-1989) and the last five years (2012-2017) to visualize the changes that occurred between the initial and final years and give an overview of the changes that occurred in the period in relation to the SSC values for over the three decades.

The acquisition are used are shown in Figure 5. It can be seen that this area completely cover the entire Brazilian coastline.



Figure 5 - Area of Acquisition.

3. RESULTS

To verify which is the most suitable index to be used in the present study, among those shown in equations 1, 2 and 3, all three indices were plotted in the same graph, as shown in Figure 6, for the southwest coast. As we can see by analyzing the figure, all three indices present the same behavior. So, in qualitative terms, choosing one index is a matter of convenience. Thus, in this work, the index to be used was decided to be the NSMI.

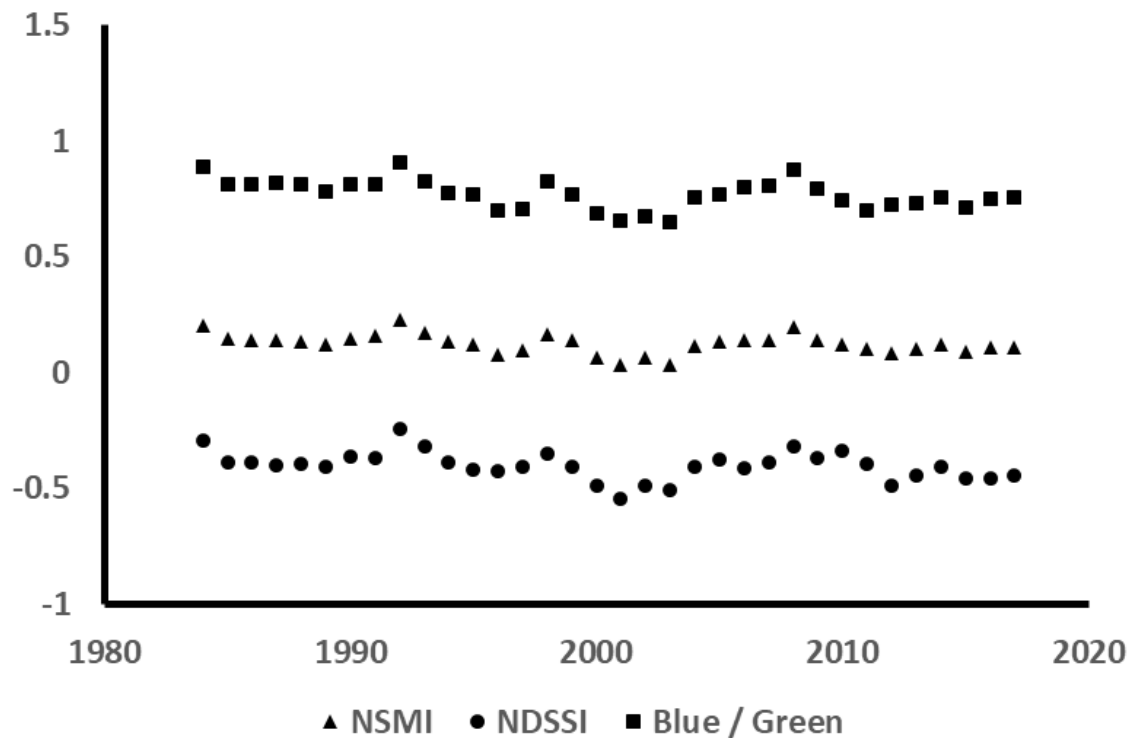


Figure 6 - SSC indexes applied for the southwest coast.

3.1. CALIBRATION

Due to the shortage of sedimentological stations present in the Brazilian coast, and also due to the fact that in the coastal areas the great part of the sediments found there are brought by the rivers that flow in the sea, it was chosen to make the calibration of the suspended sediment concentration data (SSC) using data from Brazilian rivers.

The Hidroweb system (Hidroweb, 2017), which has the historical data of the Brazilian hydrometric network under the management of the Brazilian water agency (ANA, 2017), was used to perform this work.

Since sediment data from Hidroweb are scarce, while flow information is available for most days and most sediment monitoring stations, the flow information provided is used to derive the SSC values for days on which Landsat images are available, we considered the Flow x Sediment relation obtained by the best fit curve (least square method).

To have a consistent estimate of SSC throughout the Brazilian territory, it was decided to add the data of sediment monitoring stations in the major rivers of the main Brazilian basins, being one station per basin, as shown in table 3. Thus, the estimated SSC values obtained through the flows were crossed with the respective NSMI index values, obtained from Landsat images, for the respective days. It was decided to acquire

data in 30 different days, to better visualize the trend of the data. The acquired results are plotted in Figure 7, as well as the best fit curve.

Table 3. Location of sediment monitoring stations

Station	Basin	River	Lat	Long
Guaraí	Platina	Paraná	-24.069	-54.248
Xambioá	Tocantins	Araguaia	-6.4097	-48.5422
Traipu	São Francisco	São Francisco	-9.9714	-37.0028
Óbidos	Amazonas	Amazonas	-1.9192	-55.5131
Indaial	South Atlantic – Southeast Region	Itajaí	-26.891	-49.235
Antas	South Atlantic – East Region	Paraíba do Sul	-22.035	-42.9908
Teresina	South Atlantic – North and Northeast Region	Parnaíba	-5.1350	-42.8111

The best fit curve that relates the SSC and the NDSSI index was derived, as shown in (Equation 4).

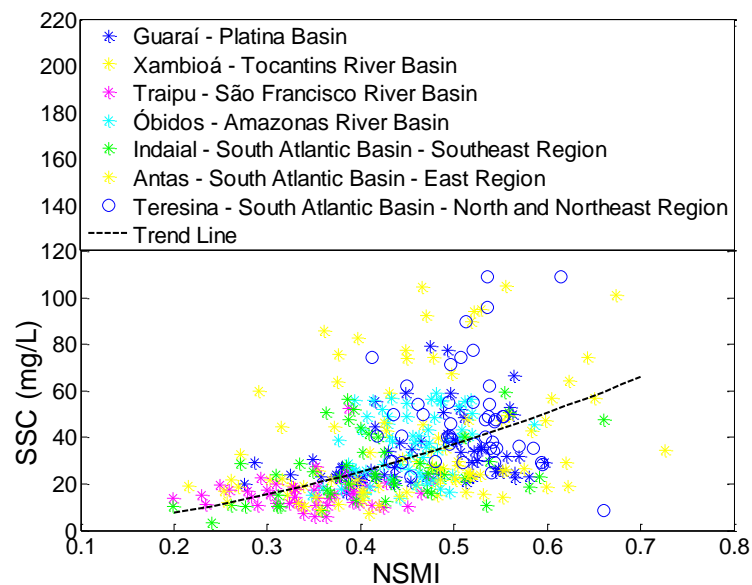


Figure 7 - NSMI index versus SSC for different sediment monitoring stations.

$$CSS = 121.8 * NSMI^{1.717} \quad (4)$$

with a $R^2 = 0.3666$.
p-value = 0.223

3.2. MAPS

For a more complete and spatially detailed view of the data, in order to verify the changes that occurred during the 32 years in the Brazilian coast, a map with a general vision with the SSC values for the first five years was generated: 1984-1989, and for the last five years: 2012-2017. Such a map is shown in figure 8.

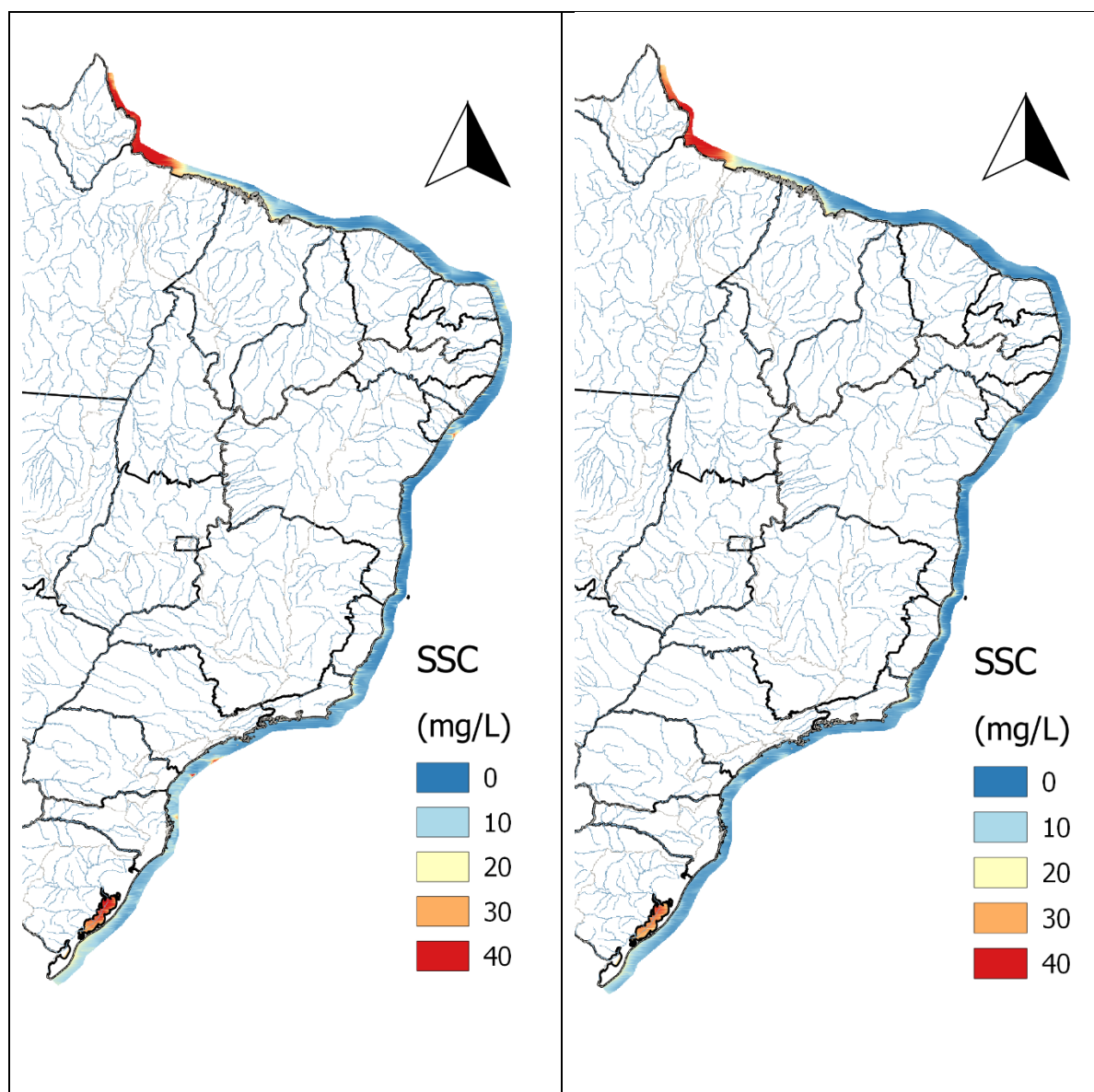


Figure 8 - Estimation of mean SSC map: year 1984 to 1989 (Left), year 2012 to 2017 (Right).

Figure 9 shows the difference between the final 5 years: 2012-2017 and the initial 5 years: 1984-1989, in order to allow with more clarity the variations between the initial and final values.

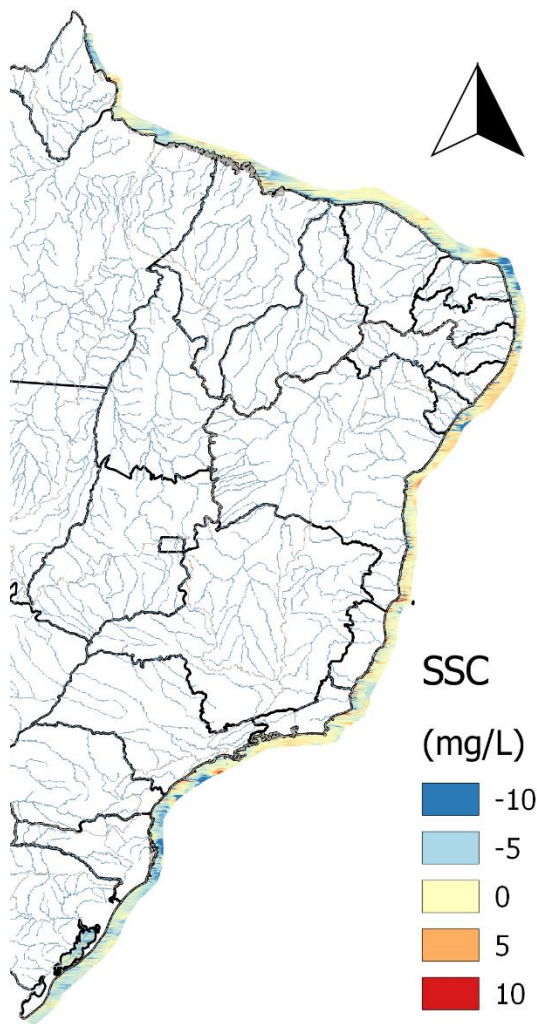


Figure 9 - Estimation of mean SSC difference between the five final years (2011-2016) and (2012-2017).

Although the map shown in Figure 9 is a good map, it is still difficult to see if the mean value of SSC has increased or decreased for a given latitude value. For this, the graph in figure 10 was generated, which was obtained by calculating the mean value of the SSC for a specific latitude value along the entire Brazilian coast. Through this graph, it becomes clear that the average value of the SSC decreases when comparing the final years: 2012-2017 with the initial years: 1984-198

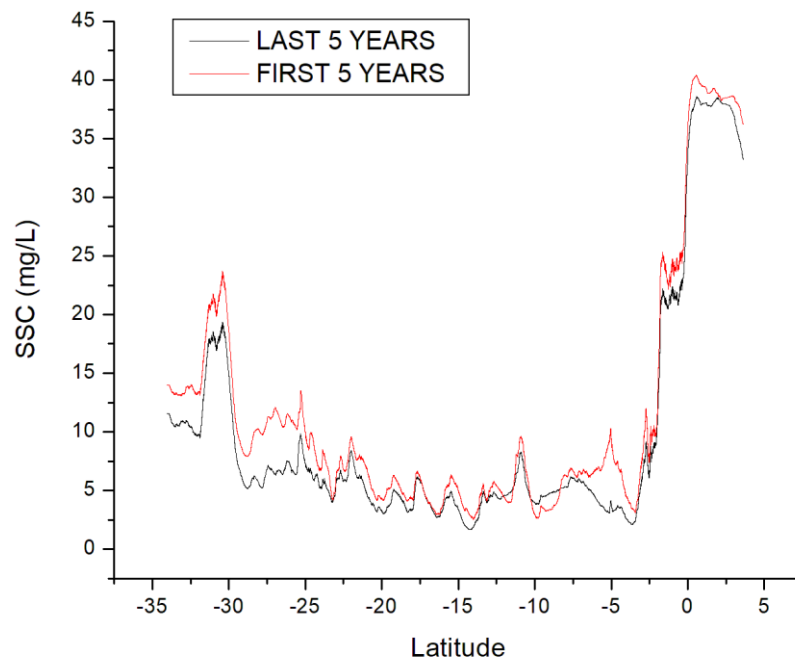
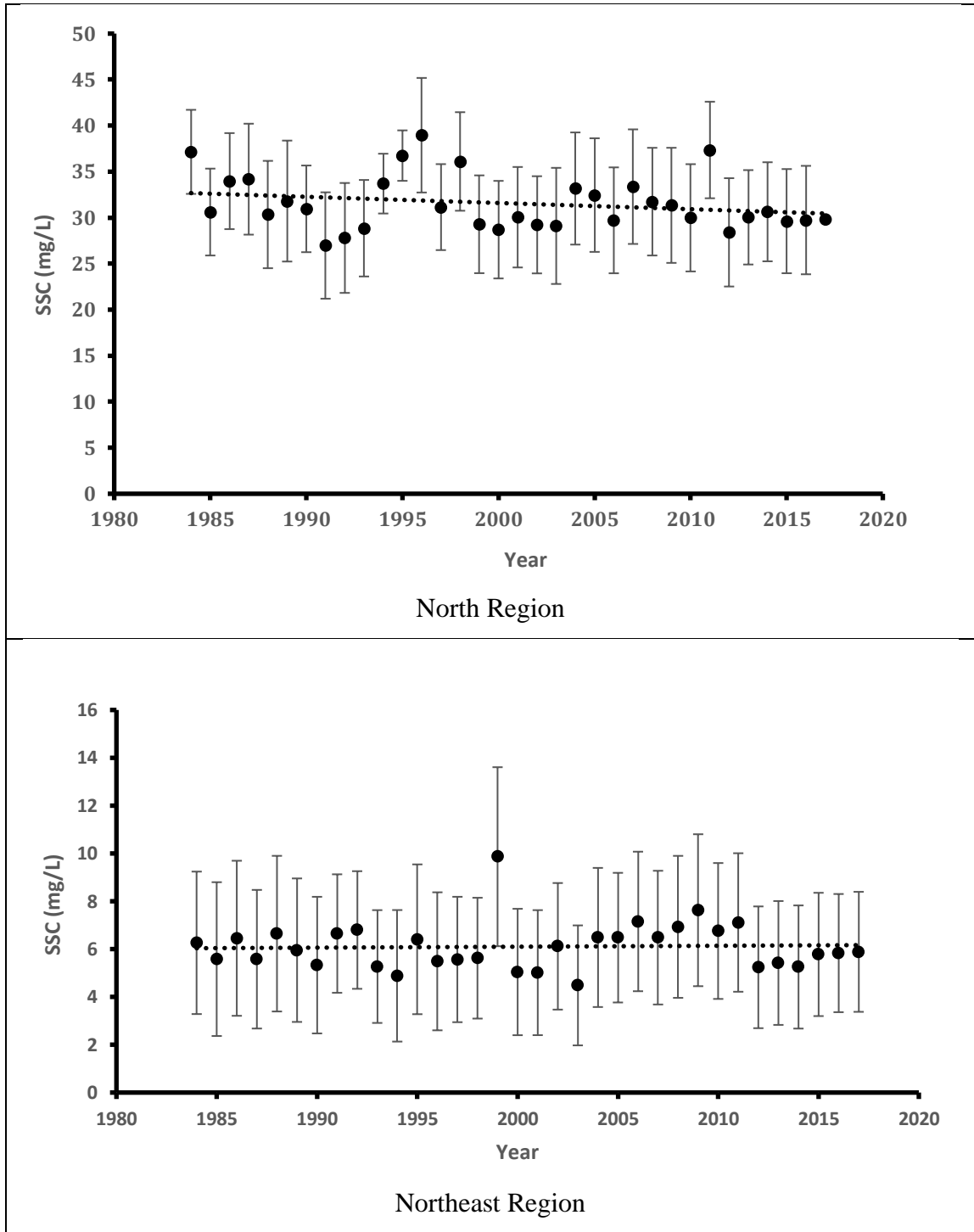


Figure 10 - Estimation of the mean SSC value per latitude degree for five final years (2012-2017) and the five initial years (1984-1989).

In addition, graphs were elaborated with mean values of sediment concentration in SSC suspension for all years from 1984 to 2017, selecting different regions of the Brazilian coast. The respective values of standard deviation std were added as well as trendlines to check whether the values of SSC are increasing or decreasing along the years. These values are shown in Figure 11 below.



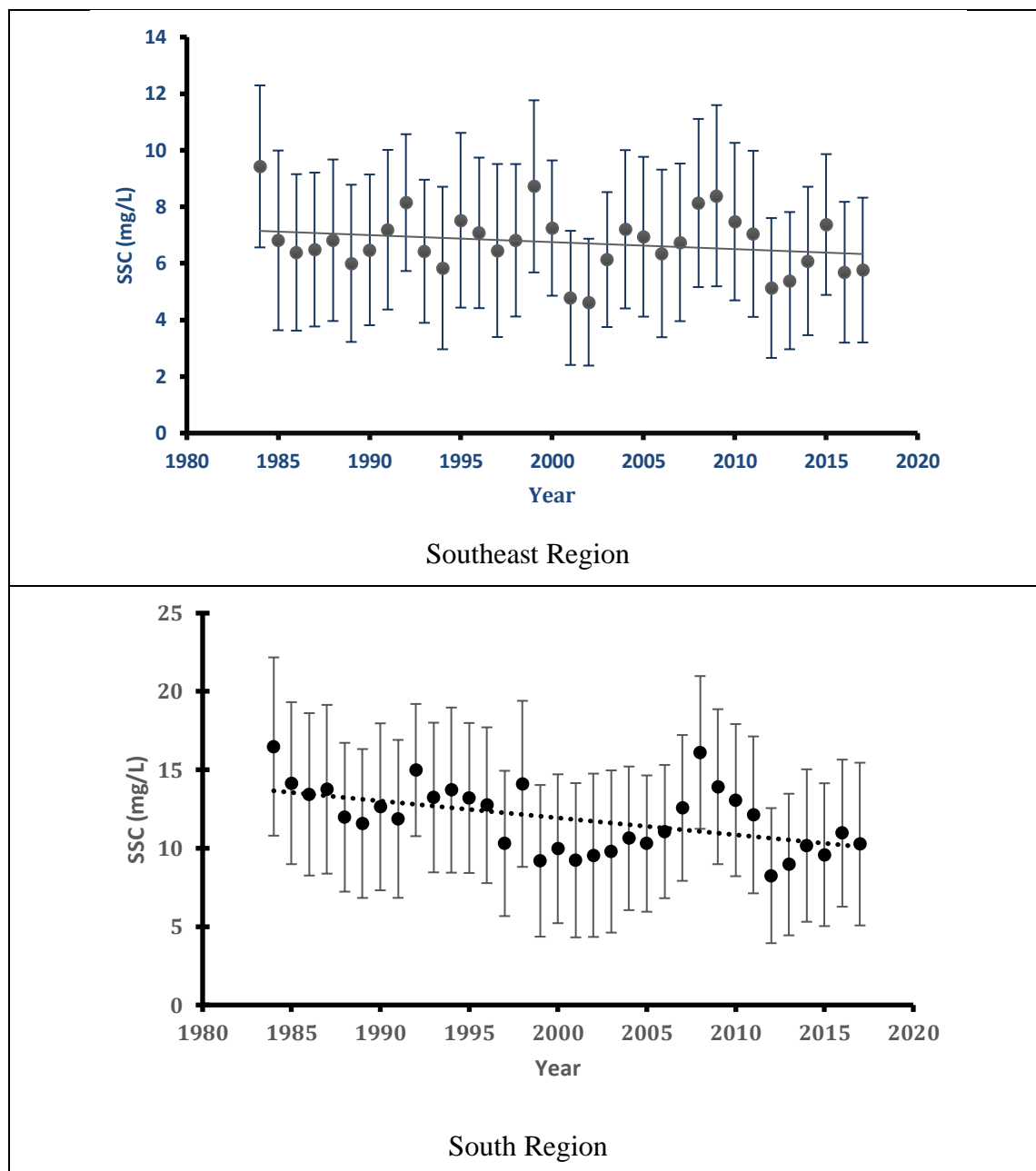


Figure 11 - Mean SSC values per year for the different coastal regions of Brazil.

Based on the graphs shown in figure 11, we noticed that practically all the regions showed a tendency of decreasing in the average value of SSC, except for the northeast region, which practically did not present any variation, being the trendline for this region practically flat. This may be due to the fact that few large hydropower plants or reservoirs were built there after 1984, and in other regions the construction of power plants and reservoirs remained over the years after 1984.

4. CONCLUSION

In this paper, we explored the potentiality of the Google earth engine platform in providing data and processing power, achieving an innovative framework for SSC estimation for great areas and along the decades since 1984.

The method presented in this article proved to be a great tool being very effective and practical for the determination of areas in which SSC increased over the years, as well as the determination of areas where there was increase or decrease of water surface. The method can be used in different areas of interest or countries in order to verify the dynamics of SSC over the years.

As a conclusion we can affirm that the method developed in the present work enabled the deduction of factors pertinent to the concentration of suspended sediments SSC for the entire Brazilian coast. Important factors such as the trend of decreasing SSC values for practically all coastal regions, except for the northeast region, were verified. Allowing to conclude that such behavior is mainly due to the constant construction of hydroelectric power plants and water reservoirs along the great Brazilian rivers that in flow into the coast. A similar result corroborating such result for the Amazon basin can be found at (Latrubesse et al., 2017). Finally, we can state that the technique developed here can be applied to other bodies of water, and it is also possible to use other relevant indices such as chlorophyll, suspended organic matter etc.

5. REFERENCES

- Aber, James S. 2011. Landsat Image Processing.
http://academic.emporia.edu/aberjame/remote/landsat/landsat_proc.htm
- Binding, C. E., D. G. Bowers, and E. G. Mitchelson-Jacob. "Estimating suspended sediment concentrations from ocean colour measurements in moderately turbid waters; the impact of variable particle scattering properties." *Remote sensing of Environment* 94.3 (2005): 373-383.
- Chen, Zhimin, Paul J. Curran, and Jim D. Hansom. "Derivative reflectance spectroscopy to estimate suspended sediment concentration." *Remote Sensing of Environment* 40.1 (1992): 67-77.

- Doxaran, D., J-M. Froidefond, and P. Castaing. "A reflectance band ratio used to estimate suspended matter concentrations in sediment-dominated coastal waters." *International Journal of Remote Sensing* 23.23 (2002): 5079-5085.
- Doxaran, David, et al. "Dynamics of the turbidity maximum zone in a macrotidal estuary (the Gironde, France): Observations from field and MODIS satellite data." *Estuarine, Coastal and Shelf Science* 81.3 (2009): 321-332.
- Feng, M., Sexton, J. O., Channan, S. & Townshend, J. R. A global, high-resolution (30-m) inland water body dataset for 2000: first results of a topographic– spectral classification algorithm. *Int. J. Digit. Earth* 9, 113–133 (2015).
- FIUZA, B. et al. Detection of suspended sediments in Grande River and Ondas River-Bahia. Brazil, Federal University of Bahia Institute of Environment Sciences and Sustainable Developments, Brazil, 2011. Montalvo, I., 2010. Spectral analysis of suspended material in coastal waters: A comparison between band math equations. gers.uprm.edu/geol6225/pdfs/I_montalvo.pdf.
- Foga, Steve, et al. "Cloud detection algorithm comparison and validation for operational Landsat data products." *Remote Sensing of Environment* 194 (2017): 379-390.
- Gorelick, N., Hancher, M., Dixon, M., Ilyushchenko, S., Thau, D., & Moore, R., 2017. Google Earth Engine: Planetary-scale geospatial analysis for everyone. *Remote Sensing of Environment*.
- Harrington, John A., Frank R. Schiebe, and Joe F. Nix. "Remote sensing of Lake Chicot, Arkansas: Monitoring suspended sediments, turbidity, and Secchi depth with Landsat MSS data." *Remote Sensing of Environment* 39.1 (1992): 15-27.
- Hossain, A.K.M; Chao, Xiaobo; Jia, Yafei. 2006. Development of Remote Sensing based Index for estimating/mapping Suspended Sediment Concentration in River and Lake Environments, The University of Mississippi.
- Latrubesse, Edgardo M., et al. "Damming the rivers of the Amazon basin." *Nature* 546.7658 (2017): 363.
- Montalvo, I. "Spectral analysis of suspended material in coastal waters: A comparison between band math equations." (2010).
- Okumura, Hirofumi, and Tetsuya Sumi. "Reservoir Sedimentation Management in Hydropower Plant Regarding Flood Risk and Loss of Power Generation." *International Symposium on Dams For A Changing World ICOLD 2012*, Kyoto, Japan. 2012.

- Qu, Liqin. "Remote sensing suspended sediment concentration in the Yellow River." (2014).
- Ritchie, Jerry C., Charles M. Cooper, and Jiang Yongqing. "Using Landsat multispectral scanner data to estimate suspended sediments in Moon Lake, Mississippi." *Remote Sensing of Environment* 23.1 (1987): 65-81.
- Ritchie, Jerry C., and Charles M. Cooper. "Comparison of measured suspended sediment concentrations with suspended sediment concentrations estimated from Landsat MSS data." *Title REMOTE SENSING* 9.3 (1988): 379-387.
- Ritchie, Jerry C., Charles M. Cooper, and Frank R. Schiebe. "The relationship of MSS and TM digital data with suspended sediments, chlorophyll, and temperature in Moon Lake, Mississippi." *Remote Sensing of environment* 33.2 (1990): 137-148.
- Topliss, B. J., C. L. Almos, and P. R. Hill. "Algorithms for remote sensing of high concentration, inorganic suspended sediment." *International Journal of Remote Sensing* 11.6 (1990): 947-966.
- Wulder, M. A. et al. The global Landsat archive: status, consolidation, and direction. *Remote Sens. Environ.* 185, 271–283 (2016).
- Yuming, You, and Hou Min. "Remote sensing analysis of the suspended sediment transport in Lingdingyang." *China Ocean Engineering* 6 (1992): 331-331.